A REACTOR-CONTROLLED
VARIABLE-SPEED INDUCTION MOTOR DRIVE

A Thesis

Presented to

the Faculty of Graduate Studies and Research

of the University of Manitoba

In Partial Fulfillment

of the Requirements for the Degree

Master of Science in

Electrical Engineering

---

by

Leon Liffmann

May 1962

ABSTRACT

This dissertation describes the development of a reactor-controlled, variable-speed, induction motor drive. Symmetrical component analysis is used to evaluate the effect of an asymmetrical reactor circuit on the induction motor performance characteristics. Motor torque-current characteristics are predicted, showing the amount of phase asymmetry introduced by the saturable reactor circuit. Experimental results are given for the transient and steady-state response of the drive.

PREFACE

The subject of this thesis is the development of a reactor-controlled, variable-speed, induction motor drive. Chapter I, the review of the past work, is included to provide a background on induction motor drives. Chapter II describes the basic theory of a feedback control system. In the third chapter, the block diagram form of the drive is considered, and certain induction motor relations are derived. The power modulator and certain other components of the drive are presented in the fourth and fifth chapters respectively. In Chapter VI various results are presented which are indicative of open and closed-loop performance of the drive. Conclusions are presented in Chapter VII. Data compiled from induction motor tests are presented in Appendix A. Appendix B describes the design of certain elements of the drive, and Appendix C contains information relating to the tachometer used in the feedback portion of the closed-loop drive.

Superscripts found in the text refer to references which have been placed in the bibliography.

The author wishes to acknowledge the kind guidance and assistance rendered by Professor W. Shepherd through all phases of this project. In addition thanks are extended to Miss Laura Walker for her invaluable work in typing the manuscript. Appreciation is also extended to the University of Manitoba for its financial assistance received from the President's National Research Council Fund under Grant No. G 710.

TABLE OF CONTENTS

CHAPTER PAGE

LIST OF TABLES

LIST OF FIGURES

CHAPTER I

REVIEW OF THE PAST WORK

1.1 INTRODUCTION

The problem of continuous control of the speed of induction motors is as old as the motors themselves.[1.1] Since the end of the last century numerous control schemes have been developed and successfully applied. During the first quarter of the century, the use of direct current motors was regarded as essential; the main objection to the use of alternating current induction motors being inadequate methods of speed control. The increasing availability of alternating current power supplies eventually resulted in an extensive use of slip-ring induction motors employing secondary-resistance speed control.[1.2]

Many of the schemes that have been developed are relatively efficient but require auxiliary machines. A brief summary of the work done on problems very closely related to the present problem will be given.

1.2 HISTORY OF DEVELOPMENT

Electrically controlled mechanical braking systems operating against the driving motor have provided control at high values of slip. Possibly, the most widely used mechanical braking system is the d.c. dynamic brake.[1.3] Schmitz[1.4] and others[1.5] have given much attention to a.c. dynamic braking methods which avoid completely the need of a d.c. supply. These methods employ asymmetrical primary connections[1.6,1.7] or asymmetrical terminal

voltages of the motor.

Where the torque developed by the motor has been appreciable and in the same direction as the mechanical rotation, speed control has been effected with moderate success by the use of adjustable resistance in the secondary or rotor circuit.[1.8] Special consideration in control design has been required where the torque must be opposite to the direction of rotation at less than synchronous speed. A combination of adjustable rotor resistance along with the use of d.c. dynamic braking has made it possible to obtain subsynchronous speed control provided the torque has been in excess of approximately 35% of full-load torque. Where the counter-torque has been less than 50% normal, or absent altogether, satisfactory speed control has been provided by application of asymmetrical voltages (a.c. dynamic braking) to the motor primary.

Neither of the aforementioned systems has proven itself to be entirely satisfactory for the complete speed-torque range. The system employing d.c. dynamic braking along with adjustable rotor resistance does not provide control of low torque at high speeds. The system employing asymmetrical voltages to the secondary does not provide control of torque at slow speeds.

Both of the above systems require, for their operation, a greater input current than the motor would require in order to develop an equivalent counter-torque with balanced polyphase voltages applied.

Recent developments have occurred which still adhere to the open-loop principle.[1.2] Independent and simultaneous a.c. motoring or plugging and d.c. dynamic braking torques have been

made possible by the provision on the common magnetic circuit of a single motor of two electromagnetically separate stator windings, each of which reacts exclusively with only one of two electromagnetically separate rotor windings.[1.9] In yet another development the special single machine of the latter control method is avoided. Two directly coupled standard a.c. machines provide simultaneous torques, as well as permitting both machines to be connected as a.c. motors.[1.10]

More recently, techniques employing static components such as saturable reactors and magnetic amplifiers to control the primary voltage of high-slip induction motors, have been developed. The speed-torque curves resemble those of Ward-Leonard drives with smooth speed control extending down to about 1% of synchronous speed.[1.1] The application is normally restricted to intermittent slow-speed duty since the efficiency is low at reduced speed.

It is of historic interest to note that Alexanderson developed a non-reversing reactor-controlled induction motor drive to trim the speed of a 200 kw high-frequency alternator in his transoceanic radio-communication system.*

Most recently, arrangements of saturable reactors with or without transformers to control the primary voltage of high-slip induction motors have been given by Bolt, Simeon and Shepherd,[1.11] Zollinger,[1.12] Leonhard,[1.1] and Foote.[1.13] The proposed arrangements introduce some degree of terminal-voltage asymmetry, in general, whilst providing static reversible control of the speed and torque of the motor. The connection proposed by L. R. Foote maintains very nearly symmetrical voltages at the motor terminals.

---

* Alexanderson, E. F. W. "The Electric Plant of Transocean Radio Telegraphy", Transactions of The American Institute of Electrical Engineers, vol. 42 (1923), p.p. 707-717.

Hausen, Biringer, and Slemon have described a drive in which a wound-rotor induction motor is supplied with power from a static power modulator.[1.14] The drive incorporates the closed-loop principle in which a signal dependent upon the speed of the load is compared with a reference or control signal. The difference is fed back to the drive to maintain speed within close limits of that corresponding to the reference signal, irrespective of the magnitude of the load or of extraneous disturbances.

CHAPTER II

BASIC THEORY

2.1 DESCRIPTION OF THE FEEDBACK CONTROL SYSTEM

Regulator and servomechanism are terms that have been applied to feedback control systems. Though equipments of the two types may be similar if not identical in their physical appearance, the difference in name arises primarily from the different nature of the inputs. These two types of control systems exhibit a close functional similarity which has resulted in their recently being given the common title of feedback control system.

Fig. 2.1 is a block diagram representation of a simplified feedback control system. An actuating error E(s) which is the difference between the reference input R(s) and some function of the controlled variable B(s) is obtained at the summing point. The amplified actuating error signal E(s) is such that it tends to reduce to zero the difference between the reference input R(s) and the feedback signal B(s). To provide amplification at one or more points in the feedback control system a supplemental source of power is available.

Since the control system endeavours continually to correct any error that exists, the basic principle of feedback control or closed-loop operation tends to make for accurate performance. When control elements having a large amount of amplification and significant delays in their time response are used, this corrective action can give rise to a dangerous condition of unstable operation.[2.1] With high amplification more corrective action on the controlled variable C(s)

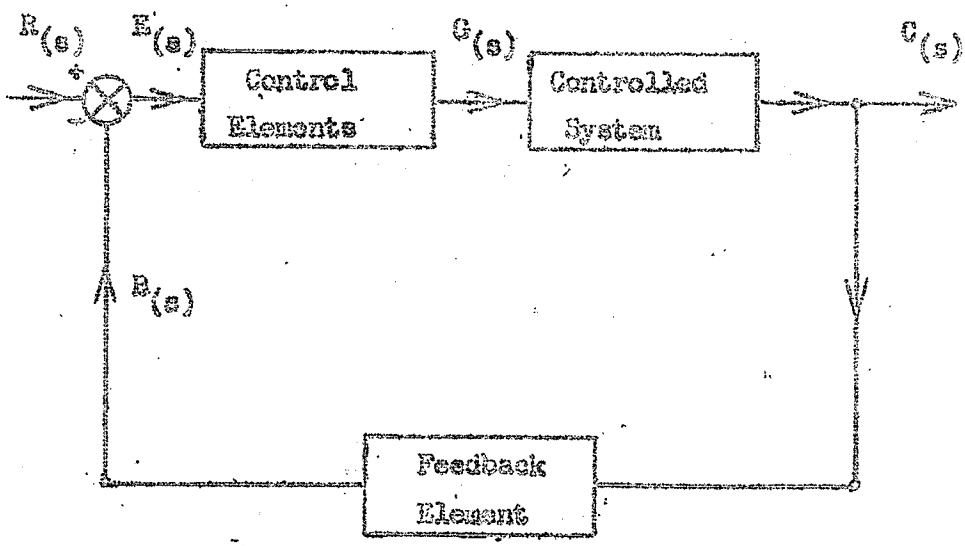

Figure 2.1

BLOCK DIAGRAM OF A SIMPLIFIED FEEDBACK CONTROL SYSTEM

can take place for a given error, and the time during which corrective action is required can be decreased. After the corrective action is initiated and the need for correction ceased, an overshoot by the controlled variable C(s) may occur. This may be attributed to the inherent time delay of the system elements which regulate the action of the control elements. The process of continued corrective action, building up to violent oscillations, is started if the overshoot is greater than that which initiated the control motion.

Qualitatively then, it can be seen that the time delays present in the control elements cause the instability.

CHAPTER III

CONSIDERATION OF THE DRIVE IN BLOCK DIAGRAM FORM

3.1 COMPONENTS OF THE CLOSED-LOOP DRIVE

Fig. 3.1 shows a block diagram of a proposed variable-speed reversible drive using an induction motor. The functions of the various elements of the drive are discussed in this chapter.

A 3-phase supply of standard voltage and frequency supplies the power modulator. The power modulator components consist of saturable transformers. The output of the power modulator is a 3-phase supply having a constant frequency which is that of the supply frequency. The relative phase and magnitude of the output is a function of (and ideally proportional to) direct-control current I_c of the power modulator.

The output of the power modulator is applied to the stator windings of a standard 3-phase wound-rotor induction motor. For control purposes it is desirable to have the torque produced by the induction motor vary in proportion to the applied control current I_c. Since the characteristics of induction motors do not lend themselves directly to regulated speed operation, it is necessary to alter the basic speed-torque characteristics of the wound-rotor motor. This is accomplished by the insertion of a network into the rotor circuit consisting of fixed resistive and inductive elements connected to the rotor terminals. For purpose of identification these elements will be referred to as the rotor network.

Another unit of the system is a permanent-magnet tachometer generator that is mechanically coupled to a rotating unit of the

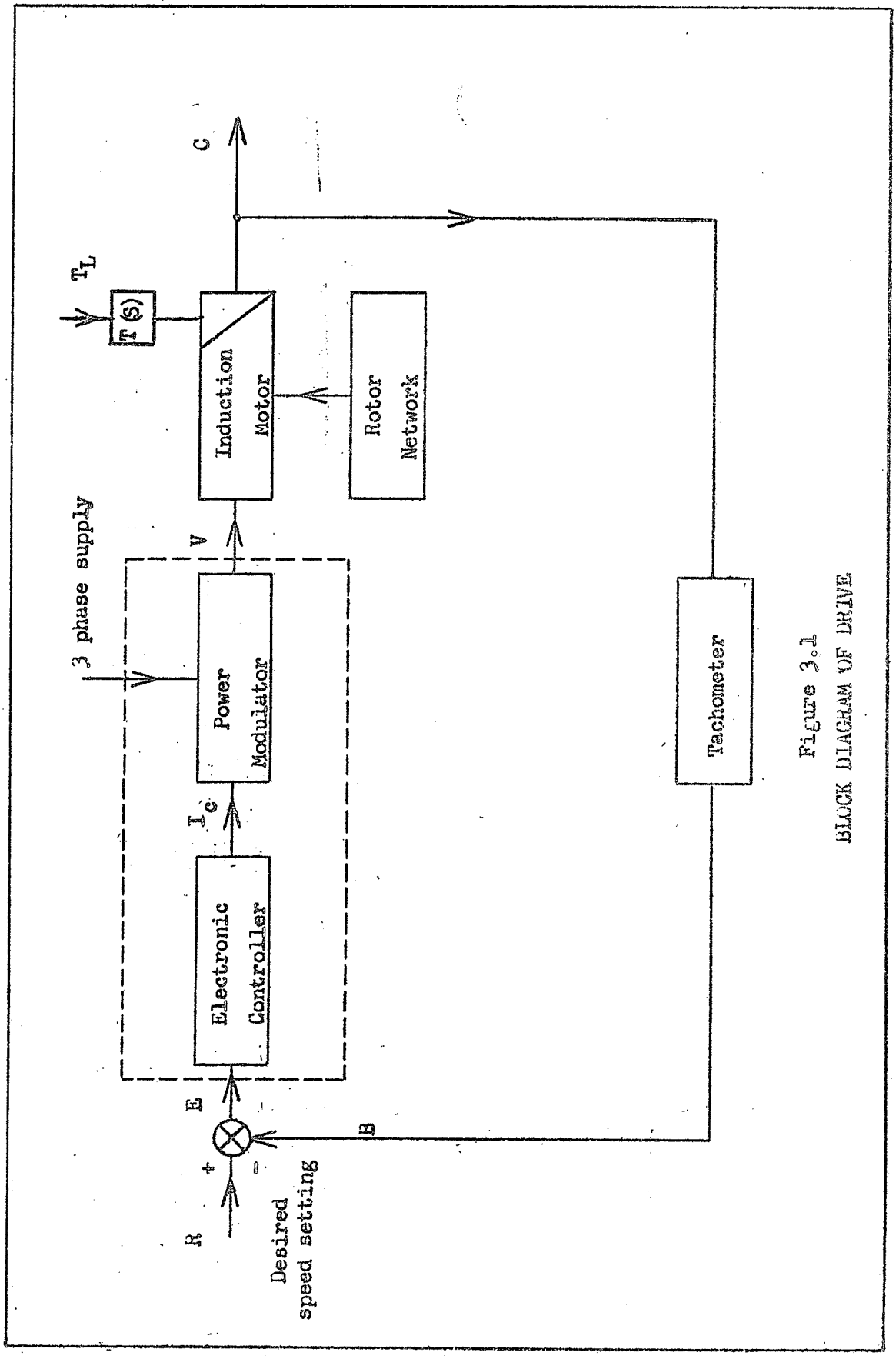

Figure 3.1
BLOCK DIAGRAM OF DRIVE

mechanical drive such that its speed of rotation is proportional to motor speed. This tachometer generator provides the feedback signal used to obtain speed regulation in the system. The output voltage B of this tachometer is compared with a voltage R representing the desired speed. The error E is amplified to produce a proportional value of control current I_c which acts upon the power modulator.

3.2 IDEALIZED PERFORMANCE OF THE DRIVE

There are three main factors to consider in designing a regulating system for a variable speed drive:

1. Steady-state stability must be present.
2. At any setting of the desired speed, the motor speed should be relatively independent of load torque up to the rated torque of the drive.
3. The drive should respond rapidly to changes in the setting of the desired speed, that is, the transient response must be relatively fast.

The ideal speed-torque curve for an induction motor in a variable-speed drive is shown in figure 3.2(a). This curve is drawn for a constant control current I_c supplied to the power modulator. The ideal relationship between the output torque and the control voltage of the power modulator will then be of the form shown in figure 3.2(b) at any value of forward or reversed speed.[1.14] If the drive elements are ideal the following relationships will hold:[1.14]

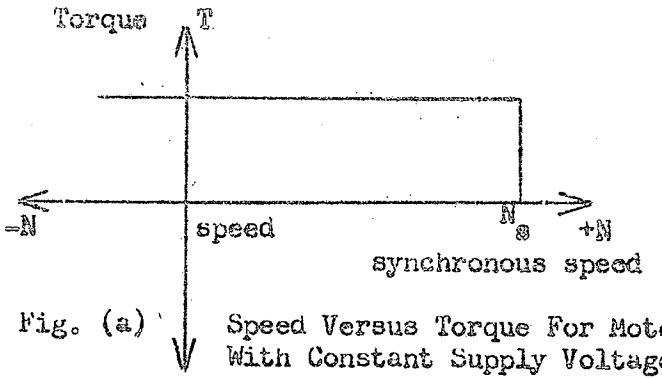

Fig. (a) Speed Versus Torque For Motor With Constant Supply Voltage

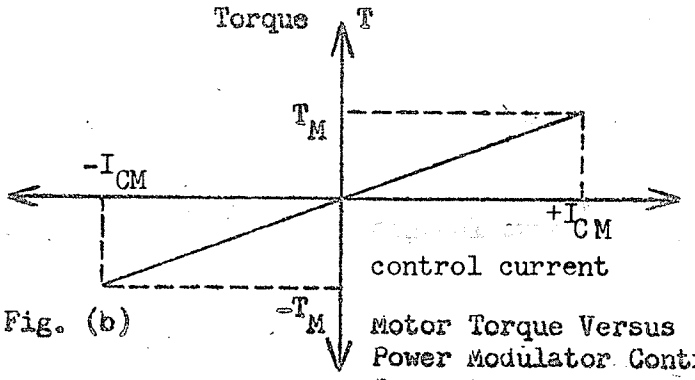

Fig. (b) Motor Torque Versus Power Modulator Control Current.

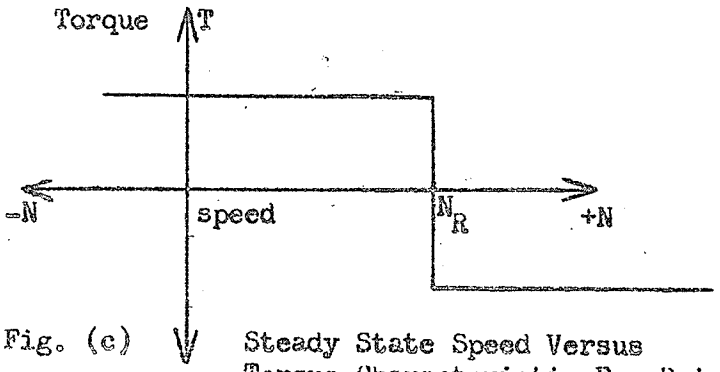

Fig. (c) Steady State Speed Versus Torque Characteristic For Drive

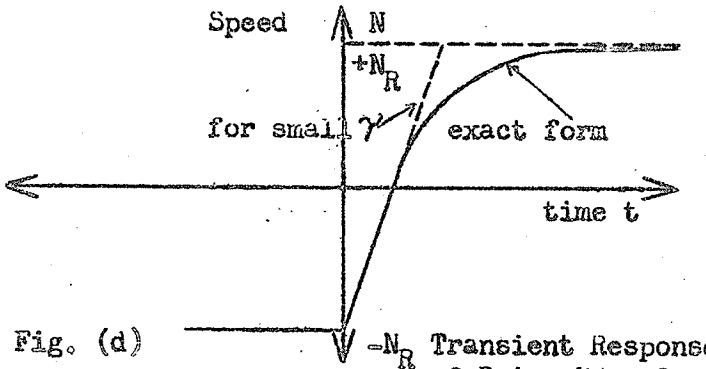

Fig. (d) Transient Response of Drive Upon Speed Reversal

FIGURE 3.2 IDEALIZED RELATIONSHIP FOR MOTOR AND DRIVE

With reference to Fig. 3.1, 3.2(a), and 3.2(b):

$$I_c = K_1 E \qquad 3.1$$

$$T = K_2 I_c \qquad 3.2$$

$$B = K_T N \qquad 3.3$$

where K_1 is a constant of the amplifier (electronic controller)

K_2 is a constant of the power modulator and motor

K_T is a constant of the tachometer

and T is the total output torque of the drive in appropriate units. From the foregoing equations the steady-state speed N of the drive with a load torque T_L may be determined as follows:

From equation 3.3 $N = \frac{B}{K_T}$

Reference to Fig. 3.1 shows $B = R - E$.

Substitution into equation 3.3 yields:

$$N = \frac{R}{K_T} - \frac{E}{K_T} \qquad 3.4$$

Applying equation 3.1 and 3.2 for an intersection of drive and load T/N curves at speed N yields:

$$N = \frac{R}{K_T} - \frac{T_L}{K_1 K_2 K_T} \qquad 3.5$$

or $$N = N_R - \frac{T_L}{K_1 K_2 K_T} \qquad 3.6$$

where $$N_R = \frac{R}{K_T}$$

A torque limit T_M may be imposed on the drive by constraining the control current to the power modulator to a maximum value of I_{CM}.

From equations 3.1 and 3.2 it is seen that:

$$T_M = K_1 K_2 E_M \qquad 3.7$$

Substitution into equation 3.6 where $T_L = T_M$ yields:

$$N = N_R - \frac{K_1K_2E_M}{K_1K_2K_T} = N_R - \frac{E_M}{K_T} \qquad 3.8$$

whence $$N = N_R - N_M \qquad 3.9$$

where $$N_M = \frac{E_M}{K_T} .$$

Within the limits on T_L, it is shown in equation 3.6 that the slope of the speed-torque curve is $\frac{-1}{K_1K_2K_T}$. If the product $K_1K_2K_T$ is sufficiently large, i.e.

$$\frac{T_L}{K_1K_2K_T} \ll N_R$$

the steady-state speed of the drive will be independent of the load torque T_L. The steady-state characteristic of the drive will be shown as in Fig. 3.2(c).

The torque limit dominates the transient response of the idealized drive. If the drive is connected to a pure inertia load with a polar moment of inertia J (including the inertia of the motor), and if the time constants of the amplifier and power modulator can be neglected, (in this case they may because the mechanical time constant of the induction motor is much larger than that of the associated equipment), the speed transient can be described by a simple first order differential equation

$$J K \frac{dN}{dt} = T \qquad 3.10.$$

Here K is a constant dependent on the units used for torque, speed, and inertia.

If the speed is reversed from a value $-N_R$ to a value $+N_R$ the error E during most of the transient duration, will be greater than that required to produce the maximum control current I_{CM}. The motor will therefore

have a constant torque T_M during this transient. Combining equations 3.7 and 3.10 it is seen that

$$J K \frac{dN}{dt} = T_M = K_1 K_2 E_M \qquad 3.11$$

and $$J K \frac{dN}{dt} = K_1 K_2 K_T (N_R - N) \qquad 3.12.$$

Setting $\frac{JK}{K_1 K_2 K_T} = \gamma$ (a time constant),

it follows that $\frac{dN}{dt} = \frac{1}{\gamma} (N_R - N)$.

Solving for transient and steady state conditions 3.12 becomes

$$N = Pe^{-t/\gamma} + N_R \qquad 3.13$$

where P is a constant such that at time $t = 0$, $N = -N_R$

therefore, at $t = 0$, $-N_R = P + N_R$

and $P = -2N_R$

thence $N = -2N_R e^{-t/\gamma} + N_R$

$$= N_R (1 - 2 e^{-t/\gamma}) \qquad 3.14$$

The speed will therefore approach the set value N_R in a simple exponential manner with a time constant γ. The idealized transient response will then be of the form shown in Fig. 3.2(d).

If, as stated earlier, the product $K_1 K_2 K_T$ is sufficiently large, accurate steady-state response can be achieved. This product may be made large by employing high values of gain in the design of the amplifier and power modulator.

If equation 3.14 is expanded in a simple Maclaurin series and γ is small, then to good approximation

$$N = -2N_R \left(1 - \frac{t}{\gamma}\right) + N_R \qquad 3.15$$

or $$N = \frac{2N_R}{\gamma} t - N_R .$$

The approximation is shown in Fig. 3.2(d).

3.3 THE INDUCTION MOTOR.

Fig. 3.3(a) represents the equivalent circuit on a per phase basis of an induction motor.[3.1] The induction machine is seen to be a generalized electromechanical transformer. The symbols used to refer to this diagram are generally accepted and only brief reference will be made to them here. The stator resistance and leakage reactance are referred to as r_1 and x_1. The exciting current I_m can be accounted for by means of a shunt branch, formed by core-loss conductance g_c and magnetizing susceptance b_m in parallel as shown in the figure. Both g_c and b_m are usually determined at rated stator frequency and are assumed to remain constant over the range of operation of the rotor. The voltages, currents, and impedances in the equivalent rotor are represented by their values referred to the stator. The normalizing factors are ratios of effective turns and are the same in essence as in transformer theory. It is shown in the literature[3.2] that the secondary resistance (i.e. rotor resistance) referred to the stator is $\frac{r_2}{S}$ where S is defined as the per unit slip. Thus the rotor resistance appears as a reflected resistance which is a function of slip and therefore a function of mechanical load. The secondary reactance x_2 is proportional to rotor frequency and therefore to slip. Thus x_2 is defined as the value that the referred rotor leakage reactance would have at stator frequency. It should be noted that when rotor currents and voltages are reflected into the stator, their frequency is also changed to stator frequency. It thus becomes possible to make an analysis of the equivalent circuit using established circuit theory techniques.

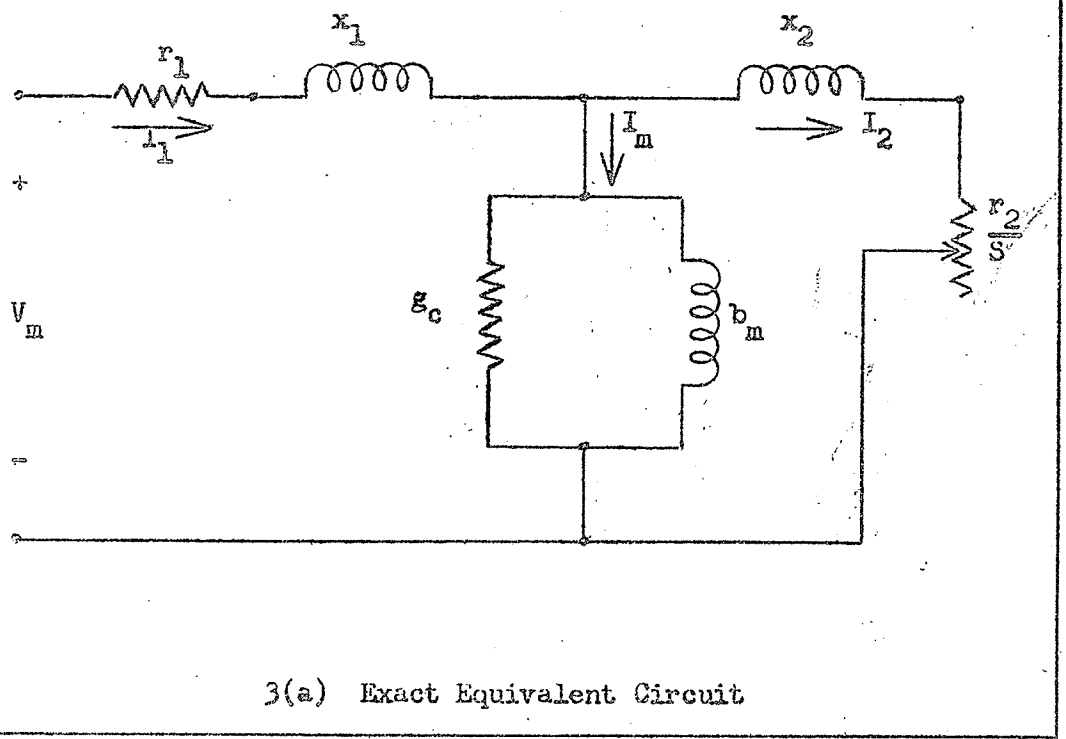

3(a) Exact Equivalent Circuit

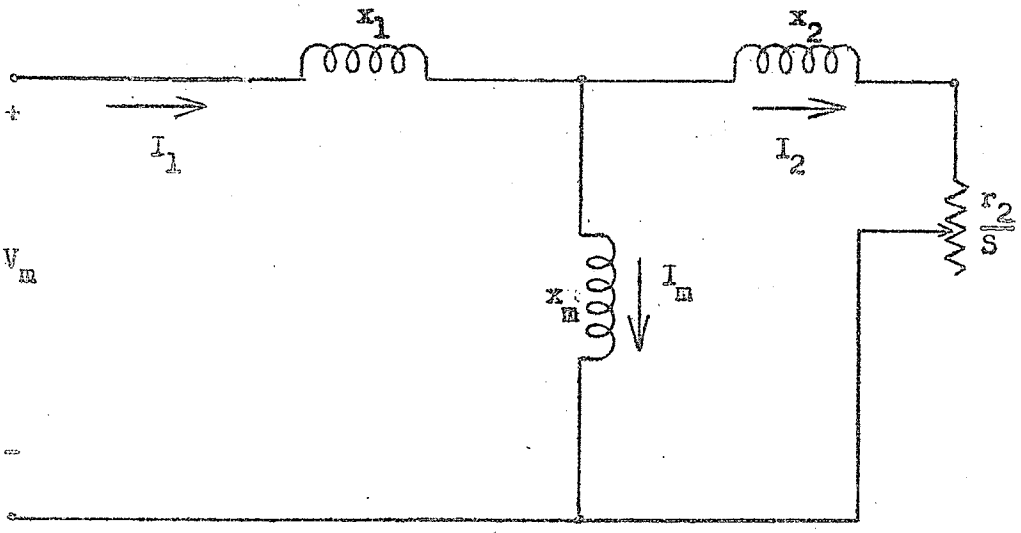

3(b) Simplified Equivalent Circuit

FIGURE 3.3

THE PER PHASE EQUIVALENT CIRCUIT OF AN INDUCTION MOTOR

A simplified per phase analysis of an induction motor follows, the results of which will be applied in section 4.4 of Chapter IV.

Fig. 3.3(b) shows a simplified per phase equivalent of an induction motor. The core-loss susceptance, primary winding resistance, and friction losses are neglected. The primary-leakage reactance and magnetizing reactance are x_1 and x_m respectively, at line frequency. The reflected secondary-leakage reactance and total rotor resistance per phase are x_2 and r_2 respectively. The slip of the rotor for positive sequence operation is S.

In matrix form the equations of the network shown in Fig. 3.3(b) are:

$$\begin{vmatrix} V_m \\ 0 \end{vmatrix} = \begin{vmatrix} j(x_1 + x_m) & -j x_m \\ -j x_m & \frac{r_2}{S} + j(x_2 + x_m) \end{vmatrix} \begin{vmatrix} I_1 \\ I_2 \end{vmatrix} \qquad 3.16$$

where V_m is the per phase motor voltage applied to the stator

I_1 is the stator current,

and I_2 is the rotor current.

The determinant $\triangle$ of the system may be written in the form

$$\triangle = \frac{r_2}{S}(x_1 + x_m) - (x_1 + x_m)(x_2 + x_m) + x_m^2 \qquad 3.17.$$

Define a leakage factor, α such that

$$\alpha = \left[1 - \frac{x_m}{(x_1 + x_m)(x_2 + x_m)} \right] \qquad 3.18.$$

This is a reasonable definition in that for $x_1 = x_2 = 0$, $\alpha = 0$.

Further rearrangement of equations 3.17 and 3.18 yields

$$\Delta = (x_1 + x_m)(x_2 + x_m)\alpha\left[\frac{j\, r_2}{\alpha S(x_2 + x_m)} - 1\right] \qquad 3.19$$

Set $$\frac{r_2}{\alpha(x_2 + x_m)} = S_m . \qquad 3.20$$

It will be shown that $S = S_m$ when the motor torque is a maximum.

From equations 3.19 and 3.20 it follows that

$$\Delta = -(x_1 + x_m)(x_2 + x_m)\,\alpha\,(1 - j\,\frac{S_m}{S}) \qquad 3.21.$$

Using equations 3.16 and 3.21 it may be shown that

$$Z_{a1} = \frac{V_m}{I_1} = \frac{j(x_1 + x_m)\;\;(1 + j\,S/S_m)}{(1 + \frac{j\,S}{\alpha\,S_m})} \qquad 3.22$$

where Z_{a1} is the motor input impedance per phase to positive sequence current.

If $Z_{oc} = j(x_1 + x_m)$ is defined as the no-load motor input impedance per phase, then the normalized motor input impedance per phase to positive sequence current is

$$\frac{Z_{a1}}{Z_{oc}} = \frac{(1 + j\,S/S_m)}{(1 + \frac{j\,S}{\alpha\,S_m})} \qquad 3.23.$$

It follows from equation 3.23 that the normalized motor input impedance per phase to negative sequence current is

$$\frac{Z_{a2}}{Z_{oc}} = \frac{1 + j\frac{(2 - S)}{S_m}}{1 + j\frac{(2 - S)}{\alpha\,S_m}} \qquad 3.24.$$

The developed internal torque T of an induction motor on a per phase basis is[3.3]

$$T = \frac{1}{w_S}\left|I_2\right|^2\,\frac{r_2}{S} \qquad 3.25.$$

where T is in synchronous watts.

W_s is the synchronous speed in mechanical radians per second. If W_s is arbitrarily set as 1 pu (1 per unit) then equation 3.25 becomes

$$T = \left|I_2\right|^2 \frac{r_2}{S} \qquad 3.26$$

The combination of equations 3.16 and 3.26 yields

$$T = \frac{-x_m^2 V_m^2 S_m^2 S}{(x_1 + x_m)^2 (S^2 + S_m^2) r_2} \qquad 3.27$$

The stator terminal per phase voltage as used in equation 3.16 is not necessarily the rated motor per phase voltage. If $V_m = V_p$, where V_p is the rated per phase motor voltage then equation 3.27 becomes:

$$T = \frac{-x_m^2 V_p^2 S_m^2 S}{(x_1 + x_m)^2 (S^2 + S_m^2) r_2} \qquad 3.28.$$

Now taking the derivative $\frac{dT}{dS}$ of equation 3.28 and evaluating the result at $\frac{dT}{dS} = 0$, it is found that $\frac{dT}{dS}$ is a maximum at $S = S_m$ as stated in conjunction with equation 3.20. The maximum torque T_{max} when $V_m = V_p$ is from equation 3.28

$$T_{max} = \frac{-x_m^2 V_p^2 S_m}{2(x_1 + x_m)^2 r_2} \qquad 3.29$$

The combination of equations 3.27 and 3.29 yields:

$$T = \left[\frac{V_m}{V_p}\right]^2 \left[\frac{2 T_{max}}{\frac{S}{S_m} + \frac{S_m}{S}}\right] \qquad 3.30$$

Where T is the torque per phase in synchronous watts.

If an overload capacity [3.4] $T_{max} = 2.75\ T_r$ is assumed, where T_r is the rated motor torque per phase, then, equation

3.30 may be written as follows:

$$\frac{T}{T_r} = \left[\frac{V_m}{V_p}\right]^2 \left[\frac{5.5}{\frac{S}{S_m} + \frac{S_m}{S}}\right] \qquad 3.31$$

The results of equations 3.23, 3.24, and 3.31 will be applied in section 4.4 of Chapter IV.

3.4 THE ROTOR NETWORK

Fig. 3.4 shows a typical torque versus slip characteristic[3.5] for a 3-phase induction motor. It was shown in equation 3.29 that the slip at maximum torque is directly proportional to the total rotor resistance r_2. Expansion of equation 3.29 shows that the value of maximum internal torque is independent of r_2. The speed at which maximum internal torque occurs may therefore be directly controlled by inserting external resistance in the rotor circuit of a wound-rotor motor, while the maximum internal torque remains unaffected. This external resistance control is made possible by use of a rotor network which forms an integral part of the closed-loop drive and will now be briefly described.

Ideally, if the drive is to have uniform accuracy and transient response at all speed settings, the torque must be independent of the speed as shown in Fig. 3.2(a).

Shepherd and Slemon[3.6] have suggested an analytical method for the synthesis of a rotor network to obtain prescribed torque-speed characteristics with induction motors. Through the manipulation of rotor impedance it is shown that the torque-speed characteristics required of a stable variable speed drive can be synthesized.

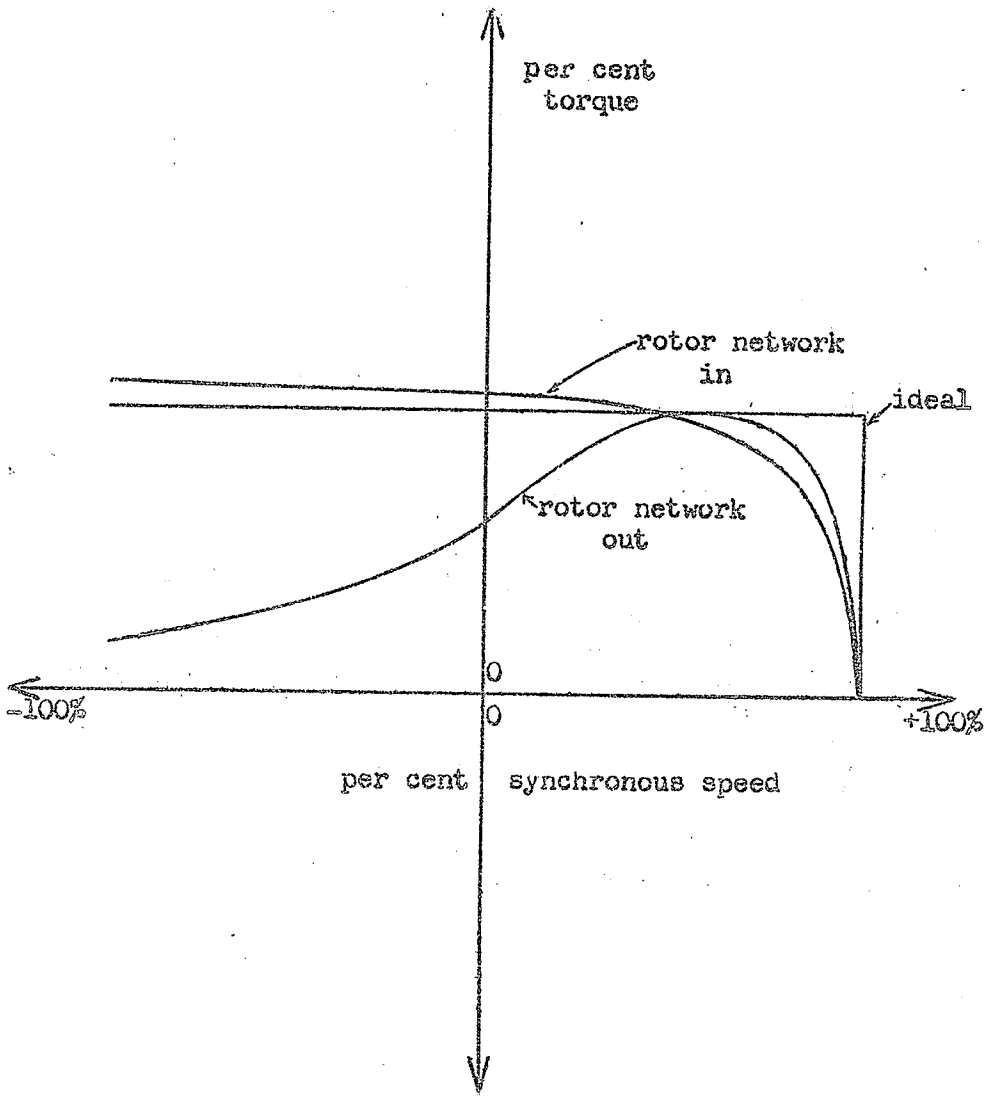

FIGURE 3.4
SPEED-TORQUE CURVES FOR A 3-PHASE MACHINE

The proposed network consists of a coil having resistance and inductance, connected in parallel with a resistor and inserted in each phase of the rotor circuit and is shown in Fig. 3.5(a)

The form of the network is justified on the following grounds:

To develop constant internal torque it is necessary to have constant air-gap power in the motor. To maintain a constant air-gap power it is therefore necessary to have a relatively constant effective total value of rotor circuit resistance as seen from the air-gap. This is achieved by having the rotor current transfer from the low resistance path through the coil at low values of slip to the high resistance path at high values of slip. In order to achieve this behaviour a reactive network which has a real **frequency locus (since the only current of interest in torque** production is the in-phase component) which increases with frequency is needed. With reference to Fig. 3.5(a) it is seen that the following equations apply:

$$\left[\frac{Z_{(s)}}{S}\right] = \frac{\left[\frac{R_1}{S} + j X_3\right]\left[\frac{R_o}{S}\right]}{\frac{R_1 + R_o}{S} + j X_3} \qquad 3.32.$$

When $\frac{Z_{(s)}}{S}$ is separated into real and imaginary components,

$$R_e\left[\frac{Z_{(s)}}{S}\right] = \frac{R_o}{S}\left[\frac{R_1(R_1 + R_o) + S^2X^2_3}{(R_1 + R_o)^2 + S^2X^2_3}\right] \qquad 3.33$$

$$\text{Imag.} \left[\frac{Z_{(s)}}{S}\right] = \frac{X_3 R_o^2}{\left[(R_1 + R_o)^2 + S^2X^2_3\right]} \qquad 3.34.$$

A plot of real $\left[\frac{Z_{(s)}}{S}\right]$ versus imaginary $\left[\frac{Z_{(s)}}{S}\right]$ for all values of S results in a curve of the form shown in Fig. 3.5(b).

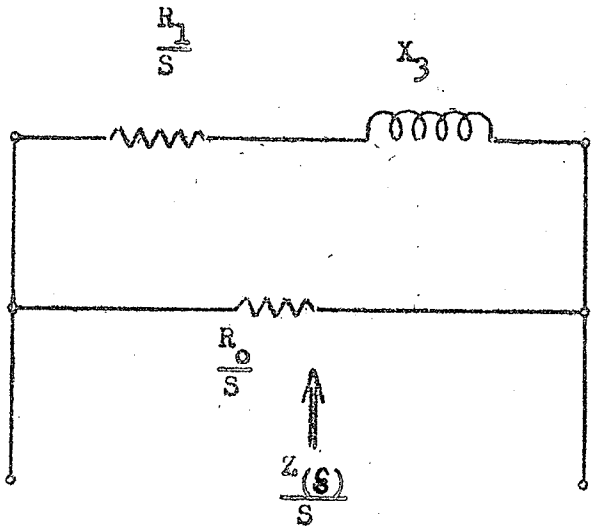

All Quantities Referred to Stator Frequency

FIGURE 3.5(a) ROTOR NETWORK

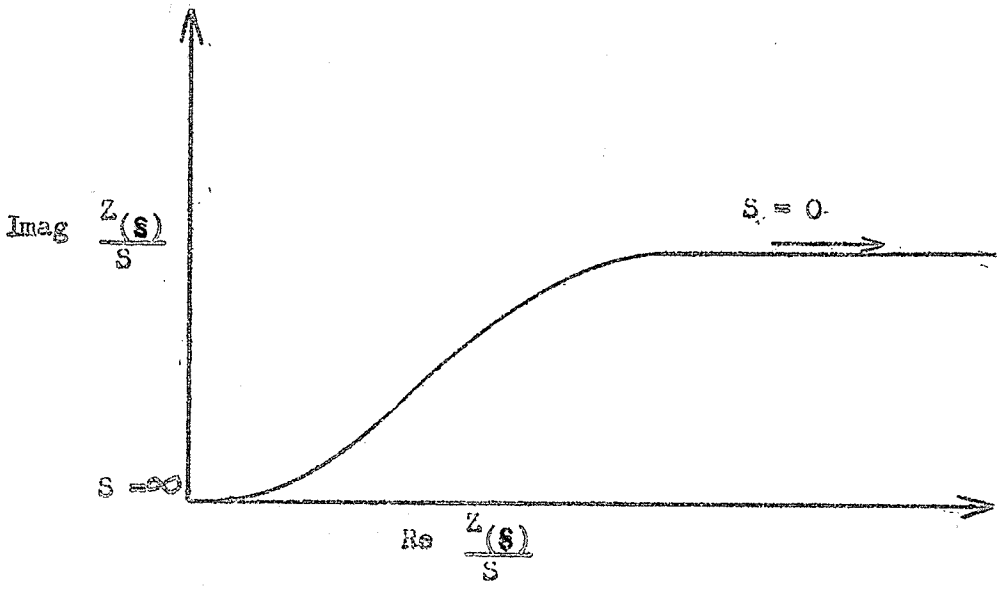

All Quantities Referred to Stator Frequency

FIGURE 3.5(b) LOCI OF ROTOR NETWORK IMPEDANCE

The synthesis of the rotor network as suggested in reference 3.6 will be carried out in Chapter V for the particular machine used by the present author. Reference 3.6 showed that performance characteristics of a polyphase machine incorporating a rotor network can be modified so that a rising torque can be obtained throughout both the driving range and counter torque range. With rated voltage applied to the motor, the effect of this rotor combination is shown in Fig. 3.4 , where it can be compared with the conventional curve of the wound rotor motor. As the voltage applied to the primary of the motor is reduced, this curve will move downward. Thus for various values of reduced primary voltage a family of speed-torque curves will be produced. It has been shown that a reasonably constant torque from about 80% forward speed to full reversed speed i.e. from a slip of .2 to a slip of 2.0 per unit can be attained with the use of a rotor network.[3.7]

CHAPTER IV

THE POWER MODULATOR

4.1 CHOICE OF CIRCUIT.

The power modulator used in this project utilised an arrangement of two saturable transformers. Each winding of a saturable transformer may be thought of as a saturable reactor.

The impedance of a fixed reactor is invariant, whereas the impedance of a saturable reactor can be controlled. A saturable reactor has one a.c. primary winding, and a second d.c. control winding. A decrease in the a.c. winding impedance may be effected by increasing the d.c. control current.

Zollinger [1.12] has given typical saturable reactor characteristic curves for a simplified saturable reactor circuit. The circuit and characteristic curves are shown in Fig. 4.1. With small d.c. excitation most of the voltage drop is across the reactor, with little across the load. If the control current is increased to 50% of the reactor rating, the voltage across the a.c. winding is reduced, with a resulting increase of a.c. current through the load. The voltage drop across the reactor is low if the load impedance limits the current to 50% of the full load alternating current. If an increase in load current is required, the d.c. control current must be increased in order to reduce the voltage drop across the a.c. primary winding.

The reactors in the power modulator may have the form of self-saturating magnetic amplifiers or the form of d.c. controlled saturable reactors. Both circuits have non-linear average voltage-current characteristics, and both produce harmonics. The non-

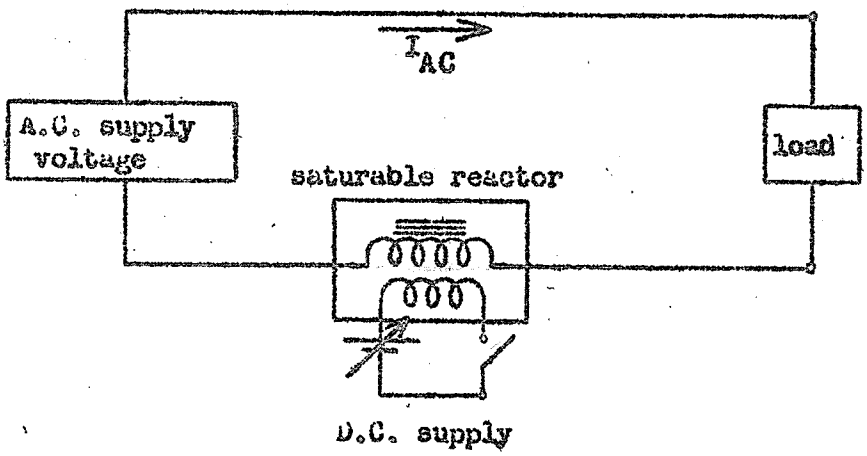

Simplified Saturable Reactor Circuit

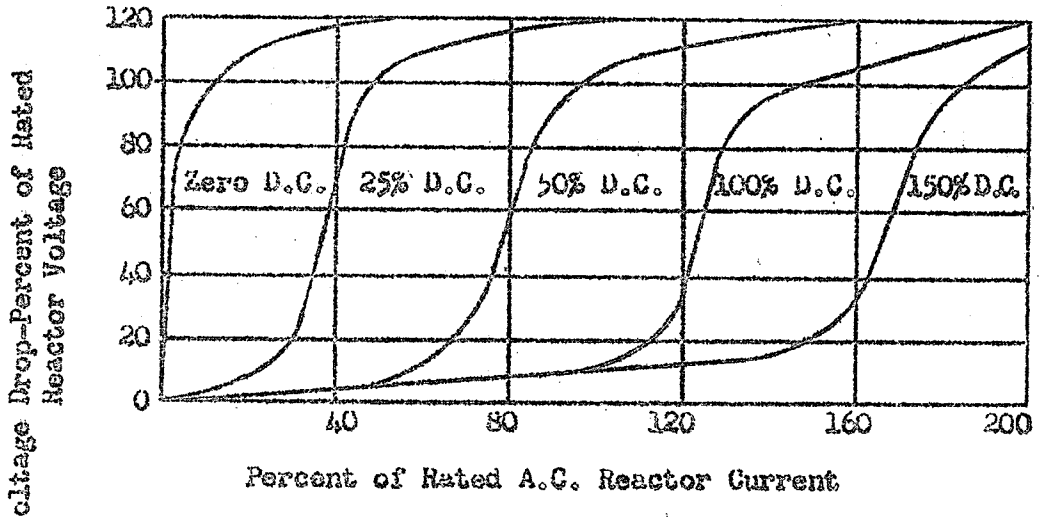

FIGURE 4.1 TYPICAL SATURABLE REACTOR CHARACTERISTIC CURVES[1.12]

linear voltage-current characteristics may be qualitatively discussed with reference to Fig. 4.2(a) and (b). These figures depict the idealized output characteristics of a saturable reactor and a self-saturating magnetic amplifier. Fig. 4.2(a) shows that the saturable reactor has high incremental impedance in the operating region. If reactors are used to control the current input to an induction motor, distorted speed-torque characteristics may result. At speeds close to synchronism, the motor impedance is high; correspondingly, most of the supply voltage appears across the motor, while the reactors, operating in their initial low impedance region, have little voltage. The torque therefore approaches that obtained with rated motor voltage. The motor impedance decreases when the slip increases and the current through the a.c. primary winding of the saturable reactor rises. The voltage across the reactor rises sharply at a certain value of primary current determined by the reactor control current. Subsequently, the motor voltage decreases and the torque falls off rapidly.

Examination of Fig. 4.2(b) indicates that the self-saturating magnetic amplifier exhibits a low output impedance. If such an amplifier were used to control the stator current of an induction motor, the motor speed-torque characteristics would approach those obtained when the motor stator was directly excited by an a.c. supply source. However, the use of self-saturating magnetic amplifiers introduces the need for rectifiers with relatively low short-time overload capacity into the power circuit. This problem was resolved by the use of saturable reactors within the power modulator and the use of a rotor network to maintain a relatively constant motor impedance throughout the slip range.

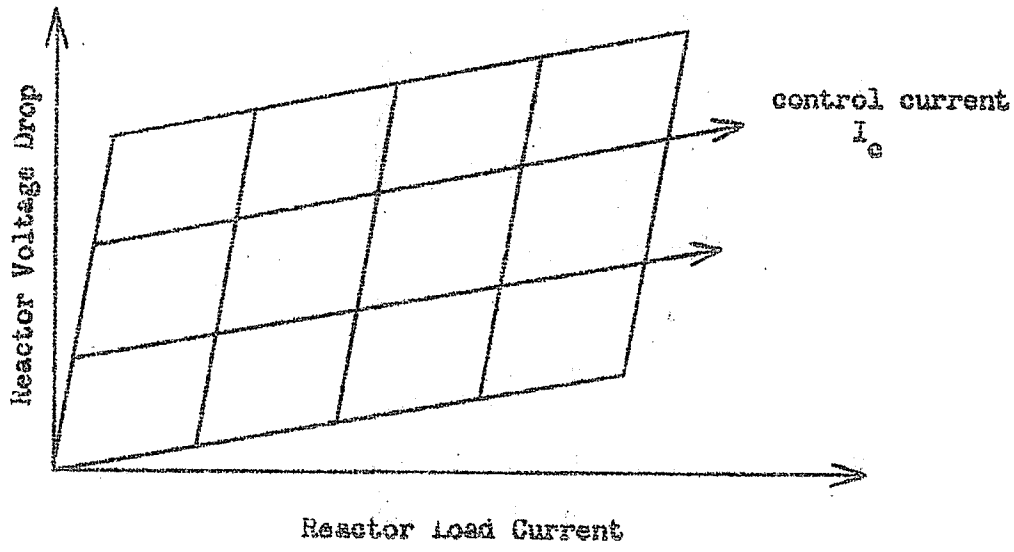

Figure (a)

Saturable Reactor

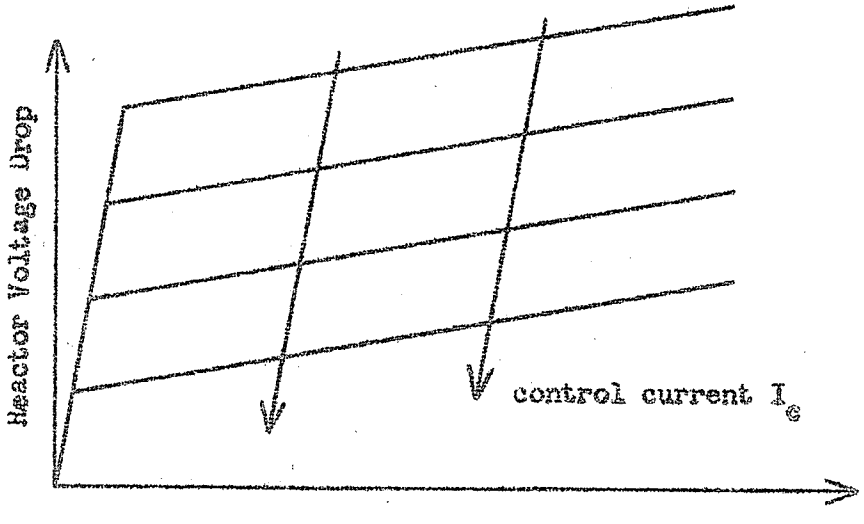

Figure (b)

Self-Saturating Magnetic Amplifier

FIGURE 4.2 VOLTAGE-CURRENT CHARACTERISTICS OF CONTROL COMPONENTS

4.2 ANALYSIS OF A SATURABLE REACTOR CIRCUIT

A schematic circuit diagram of the power modulator is shown in Fig. 4.3. The arrangement has been described in a paper by Bolt, Simeon, and Shepherd,[1.11] and uses two saturable transformers SX_1 and SX_2. Each saturable transformer has identical load or gate windings. The d.c. control windings are omitted for the sake of clarity. Load impedances are denoted as Z_L and the magnetic polarity is indicated by the dots. The results of the analysis performed in reference 1.11, and the assumptions made will now be outlined.

For the purpose of analysis the reactors are assumed to be ideal, lossless, and have no leakage flux. When this ideal magnetic coupling has unity turns ratio, the self inductances of each power winding and the mutual inductance between them are equal. The mutual reactance is symbolized by X in Fig. 4.3 and is a function of the reactor control current.

It is assumed that the reactor core has an idealized magnetization characteristic of the type shown in Fig. 4.1 . It is apparent that reactance X is then variable from almost zero at saturation to almost infinity in the unsaturated region and has different finite values corresponding to every point on the curved transitional region of the magnetization characteristic. The assumptions of reference 1.11 permit the analysis of this circuit to be carried out by conventional steady-state, sinusoidal circuit analysis techniques.

The power modulator of Fig. 4.3 possesses the basic property that its output voltages are capable of controlled phase inversion.

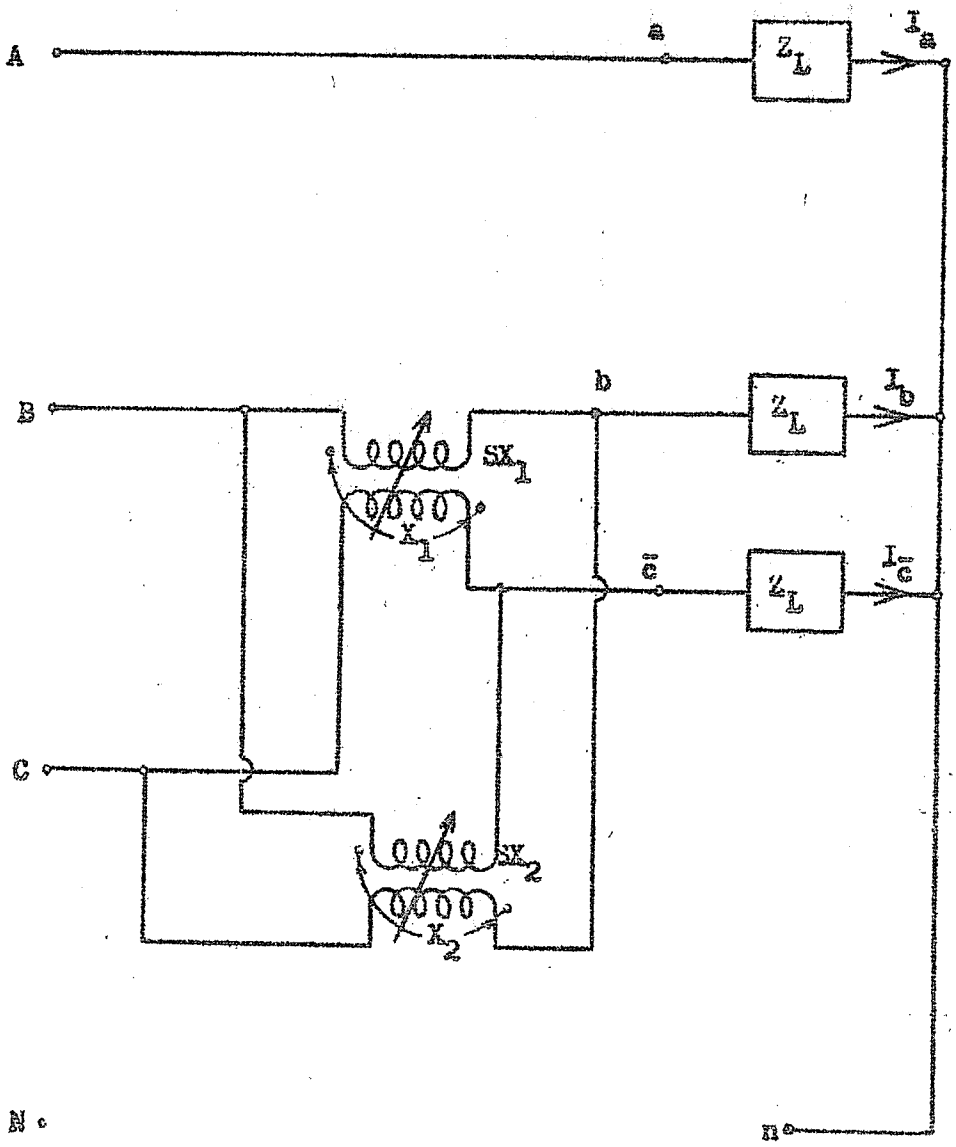

FIGURE 4.3 SYMMETRICAL SATURABLE REACTOR INTERPHASE CONNECTION 1.11

This property is an axiomatic requirement of a variable speed drive, in that the driving motor must be reversible.

The authors of reference 1.11 found that the theoretical load voltage characteristics had a locus as shown in Fig. 4.4 when the load impedance Z_L is arbitrarily set to equal a pure resistance R, such that $Z_L = R$. An examination of this figure indicates a phase inversion point at $\frac{V_{CB}}{2}$.

The relative symmetrical component load voltages for the circuit of Fig. 4.3 are shown in Fig. 4.5. The torque-speed characteristics of a polyphase induction motor to which are applied unbalanced voltages, may be considered as the algebraic sum of two separate characteristics. These two characteristics are due to the positive sequence and negative sequence components of applied voltage acting independently. The analysis of reference 1.11 did not preclude an induction motor load for the balanced impedance Z_L. Fig. 4.5 was plotted for $Z_L = R$ and for $Z_L = j\,WL$. The authors [1.11] found the theoretical characteristic for a pure resistance load to consist of two elliptical sections intersecting at the phase inversion point. The characteristic for a purely inductive load was found to be linear. The theoretical locus for any Z_L and hence any induction motor will therefore lie within the shaded area of Fig. 4.5.

The measured performance of the power modulator was found to approach its ideal theoretical performance fairly closely.

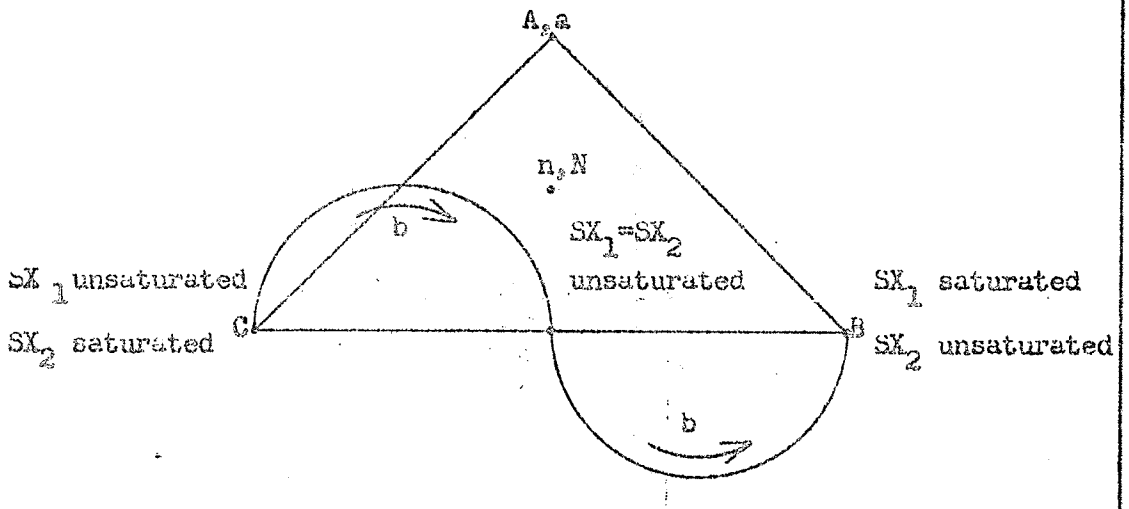

FIGURE 4.4 THEORETICAL LOAD VOLTAGE LOCI WITH RESISTIVE LOAD

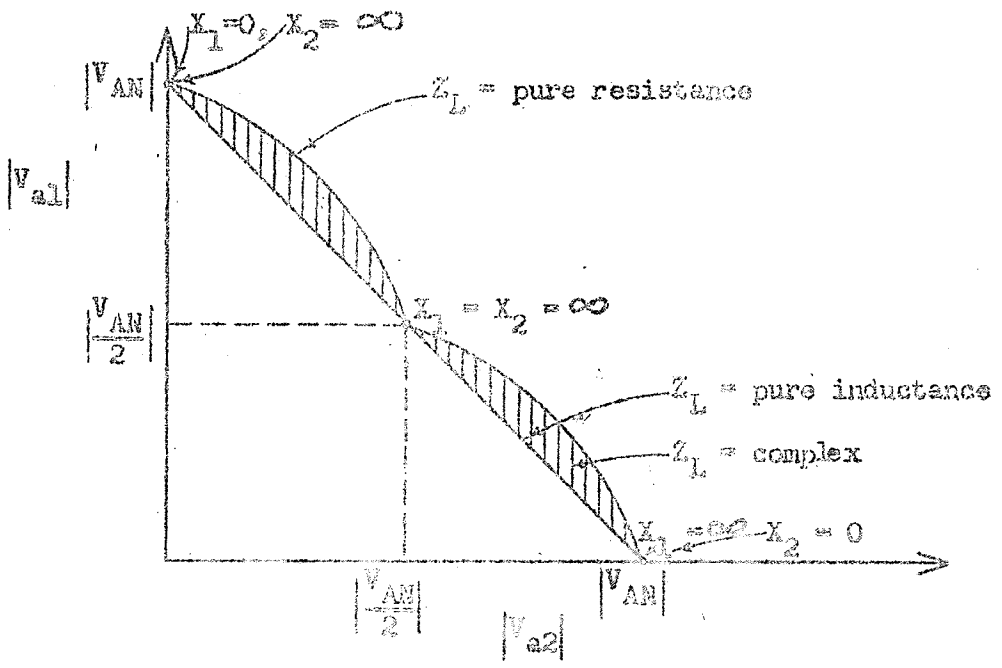

FIGURE 4.5 SYMMETRICAL COMPONENT LOAD VOLTAGES

4.3 ANALYSIS OF THE POWER MODULATOR WITH AN INDUCTION MOTOR LOAD.

The power modulator is now analyzed for the case of an induction motor load. Such an analysis gives information as to the nature of the motor currents under asymmetrical operating conditions and the motor torque developed under these conditions. It is shown that reactor control current may be represented as a function of motor torque and that torque-slip curves may be thereby predicted. Motor currents predicted with the use of the power modulator will be compared with those currents which would occur in the symmetrical case (i.e. with the impedance of $SX_1 = 0$, the impedance of $SX_2 = \infty$). For simplicity the effect of the rotor network will be neglected. This simplification is justified on the grounds that symmetrical and asymmetrical operation will be compared for the same machine.

The circuit under consideration is shown in Fig. 4.6. The assumptions made for the saturable reactors in section 4.2 will apply here.

It was found that an explicit solution for the currents I_b and I_c of Fig. 4.6 could not readily be made in terms of the fixed line voltages, the motor terminal voltages, and the modulator parameters. Elementary circuit theory dictated that such a circuit must have a unique solution for the currents I_b and I_c if the proper independent equations could be written. However, it was found impossible to choose proper equations to solve the circuit uniquely. This was evidenced by the fact that any set of equations chosen had a zero determinant, and hence constituted a dependent set.

It was therefore decided to solve a circuit such as shown in Fig. 4.7. This circuit has resistances "R" placed in series with the reactor power windings. Such a circuit readily yielded independent equations which were solvable for I_b and $I_{\bar{c}}$ in terms of the fixed line voltages, motor terminal voltages, and modulator parameters. In the final result the resistances "R" were allowed to approach zero.

It was assumed that the motor rotor circuit was wye connected and had no neutral return connection.

Let X_1 and X_2 be the self inductance of saturable transformers SX_1 and SX_2 respectively. With the assumptions made in section 4.2, the mutual inductance of each transformer is equal to the self inductance of the power windings. For purposes of analysis let X = jX. With reference to Fig. 4.7 the following system equations may be written.

$$V_{AB} + V_{ba} = -I_1(R + X_1) + I_2X_1 \qquad 4.1$$

$$V_{BC} + V_{\bar{c}b} = I_1(R + 2X_1) - I_2(R + 2X_1) \qquad 4.2$$

$$V_{BC} = I_1(R + X_1) - I_2X_1 + I_3X_2 - I_4(R + X_2) \qquad 4.3$$

$$V_{BC} = I_1X_1 - I_2(R + X_1) + I_3(R + X_2) - I_4X_2 \qquad 4.4$$

where I_1, I_2, I_3, and I_4 are the currents indicated in Fig. 4.7, V_{AB}, V_{BC}, V_{ba}, and $V_{\bar{c}b}$ are the voltages existing across the terminals shown in Fig. 4.7.

These equations may be written in matrix form as follows:

$$\begin{vmatrix} V_{AB} + V_{ba} \\ V_{BC} + V_{\bar{c}b} \\ V_{BC} \\ V_{BC} \end{vmatrix} = \begin{vmatrix} -(R + X_1) & X_1 & 0 & 0 \\ (R + 2X_1) & -(R + 2X_1) & 0 & 0 \\ (R + X_1) & -X_1 & X_2 & -(R + X_2) \\ X_1 & -(R + X_1) & (R + X_2) & -X_2 \end{vmatrix} \begin{vmatrix} I_1 \\ I_2 \\ I_3 \\ I_4 \end{vmatrix} \qquad 4.5$$

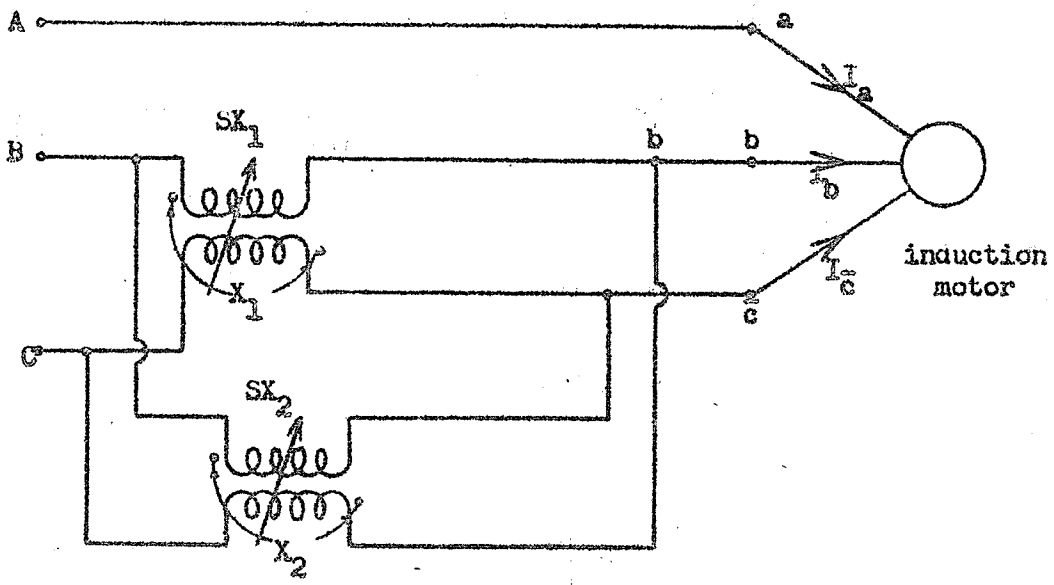

FIGURE 4.6 POWER MODULATOR WITH INDUCTION MOTOR LOAD

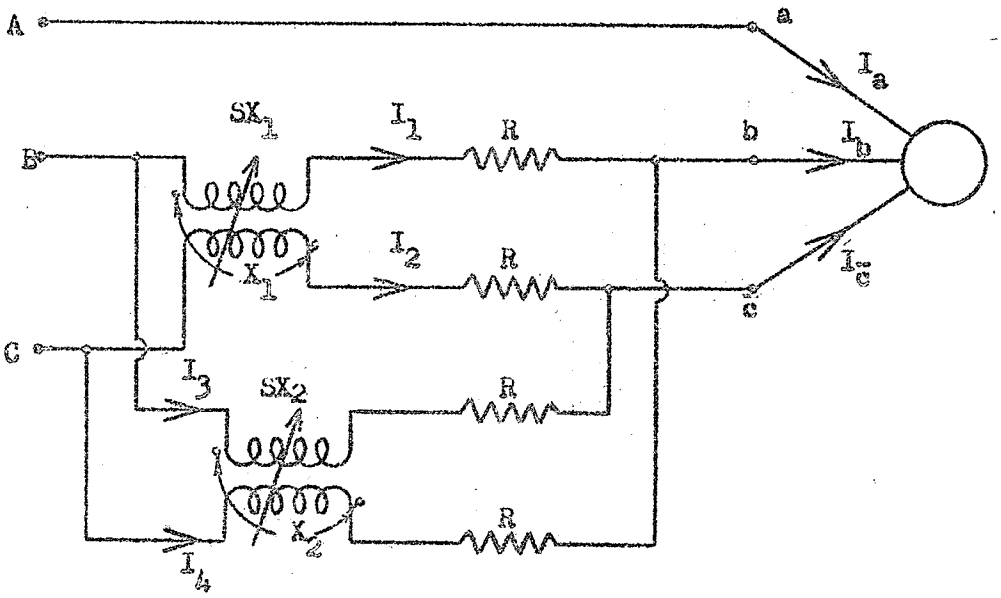

FIGURE 4.7

POWER MODULATOR WITH RESISTANCE AND INDUCTION MOTOR LOAD

Solutions for currents I_1, I_2, I_3, I_4, are as follows:

$$I_1 = - \frac{(V_{AB}+V_{ba})(R+2X_1)+X_1(V_{BC}+V_{\bar{c}b})}{R(R+2X_1)} \qquad 4.6$$

$$I_2 = - \frac{(V_{BC}+V_{\bar{c}b})(R+X_1)+(R+2X_1)(V_{AB}+V_{ba})}{R(R+2X_1)} \qquad 4.7$$

$$I_3 = - \frac{(V_{AB}+V_{ba}+V_{BC})X_2+(R+X_2)(V_{AB}+V_{ba}+V_{\bar{c}b})}{R(R+2X_2)} \qquad 4.8$$

$$I_4 = - \frac{(V_{AB}+V_{ba}+V_{\bar{c}b})X_2+(R+X_2)(V_{AB}+V_{ba}+V_{BC})}{R(R+2X_2)} \qquad 4.9$$

The motor phase currents I_b and $I_{\bar{c}}$ may readily be found from,

$$I_b = I_1 + I_4 \qquad 4.10$$

$$I_{\bar{c}} = I_2 + I_3 \qquad 4.11$$

Define the following quantities:

$$A = (V_{AB} + V_{ba})$$

$$B = (V_{BC} + V_{\bar{c}b})$$

$$C = (V_{AB} + V_{ba} + V_{\bar{c}b})$$

$$D = (V_{AB} + V_{ba} + V_{BC})$$

Equations 4.10, 4.11 may now be written in the following form:

$$I_b = \frac{-(R+2X_2)\left[AR+X_1(2A+B)\right] \quad -(R+2X_1)\left[RD+X_2(D+C)\right]}{R(R+2X_1)(R+2X_2)} \qquad 4.12$$

$$I_{\bar{c}} = \frac{-(R+2X_2)\left[R(B+A)+X_1(B+2A)\right] \quad -(R+2X_1)\left[RC+X_2(C+D)\right]}{R(R+2X_1)(R+2X_2)} \qquad 4.13$$

Fig. 4.8 shows a vector diagram of a symmetrical set of phase voltages applied to the motor terminals of Fig. 4.7. Voltage vector V_{an} is taken as the reference vector and arbitrarily assigned an angle of zero degrees. The vector V_{an} leads vector V_{bn} by 120° in time and lags vector $V_{\bar{c}n}$ by 120° in time. If a vector operator "a" is defined such that $a = \exp(j\frac{2\pi}{3}) = 1 \angle +120°$ then

the phase voltages may be written in terms of their symmetrical component voltages as follows:[4.1]

$$\begin{aligned} V_{an} &= V_{a0} + V_{a1} + V_{a2} \\ V_{bn} &= V_{a0} + a^2 V_{a1} + a\, V_{a2} \\ V_{cn} &= V_{a0} + a\, V_{a1} + a^2 V_{a2} \end{aligned} \qquad 4.14$$

where V_{a0}, V_{a1}, and V_{a2} are the zero sequence, positive sequence, and negative sequence symmetrical component phase voltages respectively.

Although equations 4.14 are in the form most commonly used in practice they do not lend themselves to the analysis at hand.

Fig. 4.9 shows the vector diagram of Fig. 4.8 rotated in such a manner that the line voltage V_{bc} becomes the reference voltage vector. Re-define the vector "a" so that $a = e^{-j2\pi/3} = 1/\underline{-120^\circ}$. With the aid of Fig. 4.9 and equations 4.14 the motor terminal voltages are now defined in terms of the positive and negative symmetrical component sequence voltages V_{b1} and V_{b2} of line voltage V_{bc}.

$$\begin{aligned} V_{bc} &= V_{b1} + V_{b2} \qquad \text{by definition} \\ V_{ca} &= a\, V_{b1} + a^2 V_{b2} \\ V_{ab} &= a^2 V_{b1} + a\, V_{b2} \end{aligned} \qquad 4.15$$

In a three wire wye connection with balanced impedances there is no zero sequence component of load voltage.[4.2] Since a three phase induction motor constitutes a balanced load impedance no zero sequence component voltage appears in equations 4.15.

The motor line currents may be written in terms of their positive and negative symmetrical component sequence currents I_{a1} and I_{a2} in a form similar to equations 4.15. The line currents

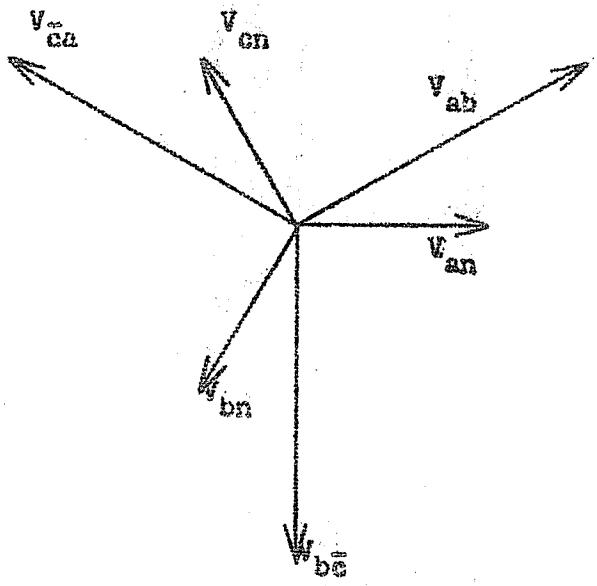

FIGURE 4.8 BALANCED 3-PHASE VOLTAGES WITH V_{an} AS REFERENCE

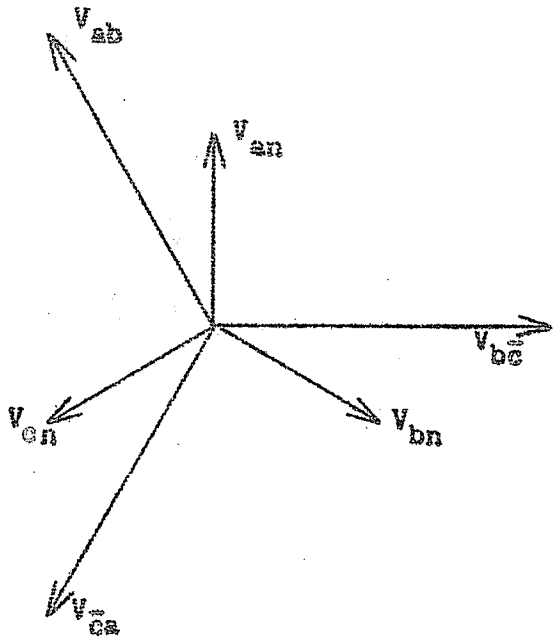

FIGURE 4.9

BALANCED 3-PHASE VOLTAGES WITH $V_{b\bar{c}}$ AS REFERENCE

are referred to the current I_a and are as follows:

$$I_a = I_{a1} + I_{a2} \qquad \text{by definition}$$
$$I_b = aI_{a1} + a^2 I_{a2} \qquad 4.16$$
$$I_c = a^2 I_{a1} + aI_{a2}$$

The three line input voltages to the power modulator are applied at terminals A, B, and C as shown in Fig. 4.7.

For a phase sequence ABC,

$$\text{Let} \quad V_{BC} = V_o$$
$$\text{Then} \quad V_{CA} = a\,V_o \qquad 4.17$$
$$\text{and} \quad V_{AB} = a^2\,V_o$$

where V_o is a constant.

Solving for I_{a1} and I_{a2} in 4.16 in terms of I_b and I_c results in the equations:

$$I_{a1} = \frac{I_b - aI_c}{(a-1)}$$
$$I_{a2} = \frac{aI_b - I_c}{(a-1)} \qquad 4.18$$

Equations 4.18 may now be solved with the use of equations 4.12, 13, 15, and 17.

$$I_{a1} = \frac{(R+2X_2)\left[RBa+RA(a-1)+X_1(B+2A)(a-1)\right] + (R+2X_1)\left[R(Ca-D)+X_2(C+D)(a-1)\right]}{(a-1)R(R+2X_1)(R+2X_2)} \qquad 4.19$$

$$I_{a2} = \frac{(R+2X_2)\left[RB+RA(1-a)+X_1(B+2A)(1-a)\right] + (R+2X_1)\left[R(C-aD)+X_2(C+D)(1-a)\right]}{(a-1)R(R+2X_1)(R+2X_2)} \qquad 4.20$$

where $A = a(aV_o - aV_{b1} - V_{b2})$

$B = (V_o - V_{b1} - V_{b2})$

$C = a^2 V_o - V_{b1}(1 + a^2) - V_{b2}(1 + a)$

and $D = V_o(1 + a^2) - a^2 V_{b1} - a\,V_{b2}$.

Equations 4.19 and 4.20 express I_{a1} and I_{a2} in terms of V_{b1}, V_{b2}, V_o, the circuit parameters X_1, X_2, and R.

With reference to Fig. 4.8, it may be shown that[4.3]

$$V_{a1} = I_{a1} Z_{a1}$$
$$V_{a2} = I_{a2} Z_{a2} \qquad 4.21$$

where Z_{a1} and Z_{a2} are the impedance per phase to positive sequence and negative sequence currents respectively. V_{a1} and V_{a2} are the positive sequence and negative sequence voltages per phase respectively, where V_{an} is taken as a reference vector.

However, equations 4.19 and 4.20 are written in terms of V_{b1} and V_{b2}. Reference to equations 4.15 will show that the voltages V_{b1} and V_{b2} are the positive and negative symmetrical component sequence voltages of line voltage V_{bc}.

Equations 4.21 may be modified so that

$$V_{b1} = -j\sqrt{3}\ I_{a1} Z_{a1}$$
$$V_{b2} = j\sqrt{3}\ I_{a2} Z_{a2} \qquad 4.22$$

Substitution of equations 4.19 and 4.20 into equations 4.22 yields the following results:

$$V_{b1} = \frac{-j\sqrt{3}Z_{a1}(R+2X_2)\left[RBa+RA(a-1)+X_1(B+2A)(a-1)\right]+(R+2X_1)\left[R(Ca-D)+X_2(C+D)(a-1)\right]}{(a-1)R(R+2X_1)(R+2X_2)}$$

(equation No. 4.23)

$$V_{b2} = \frac{j\sqrt{3}Z_{a2}(R+2X_2)\left[RB+RA(1-a)+X_1(B+2A)(1-a)\right]+(R+2X_1)\left[R(C-aD)+X_2(C+D)(1-a)\right]}{(a-1)\ R(R+2X_1)(R+2X_2)}$$

(equation No. 4.24)

Equations 4.23 and 4.24 may be rearranged in the following form:

$$E V_o = K V_{b1} + P V_{b2} \qquad 4.25$$
$$G V_o = F V_{b2} + M V_{b2} \qquad 4.26$$

The parameters E, K, P, G, F, and M are functions of X_1, X_2, R, Z_{a1}, Z_{a2}, and "a", all of which are known. Solving equations 4.25 and 4.26 for the ratios $\frac{V_{b1}}{V_o}$, $\frac{V_{b2}}{V_o}$, and allowing R to approach

zero (in the limit) yield the following results:

$$\frac{V_{b1}}{V_o} = \frac{Z_{a1}\, Z_{a2}\, X_2 + Z_{a1}\, X_1\, X_2}{Z_{a1}\, Z_{a2}\, X_1 + Z_{a1}\, Z_{a2}\, X_2 + Z_{a1}\, X_1\, X_2 + Z_{a2}\, X_1\, X_2} \qquad 4.27$$

$$\frac{V_{b2}}{V_o} = \frac{-(Z_{a1}\, Z_{a2}\, X_1 + Z_{a2}\, X_1\, X_2)}{Z_{a1}\, Z_{a2}\, X_1 + Z_{a1}\, Z_{a2}\, X_2 + Z_{a1}\, X_1\, X_2 + Z_{a2}\, X_1\, X_2} \qquad 4.28$$

Equations 4.27 and 4.28 permit the analysis of the induction motor operation to be carried forward as a function of the power modulator parameters X_1 and X_2.

4.4 EFFECTS OF THE POWER MODULATOR ON INDUCTION MOTOR OPERATION.

The per phase analysis of the equivalent circuit of an induction motor was carried out in section 3.3 of Chapter III. The following equations were derived:

$$\frac{Z_{a1}}{Z_{oc}} = \frac{1 + j\, S/S_m}{1 + \frac{jS}{\alpha S_m}} \qquad 3.23 \text{ (reprise)}$$

$$\frac{Z_{a2}}{Z_{oc}} = \frac{1 + j\,\frac{(2 - S)}{S_m}}{1 + j\,\frac{(2 - S)}{\alpha S_m}} \qquad 3.24 \text{ (reprise)}$$

$$\frac{T}{T_r} = \left[\frac{V_m}{V_p}\right]^2 \frac{5.5}{\frac{S}{S_m} + \frac{S_m}{S}} \qquad 3.31 \text{ (reprise)}$$

where the parameters have been defined in section 3.3.

With reference to equation 3.31, the quantities V_m and V_p have been defined as per phase voltages where V_m is arbitrary, and V_p is the rated per phase motor voltage. Equation 3.31 may be modified as follows:

$$\frac{T}{T_r} = \left[\frac{\sqrt{3}\,V_m}{\sqrt{3}\,V_p}\right]^2 \quad \frac{5.5}{\frac{S}{S_m} + \frac{S_m}{S}} \qquad 4.29$$

rated motor line to line voltage has been defined as V_o in section 4.3. From elementary considerations

$$|V_o| = \sqrt{3}\,|V_p|$$

also, set $\sqrt{3}\,|V_m| = |V_L|$.

Equation 4.29 may now be written as follows:

$$\frac{T}{T_r} = \left[\frac{V_L}{V_o}\right]^2 \quad \frac{5.5}{\frac{S}{S_m} + \frac{S_m}{S}} \qquad 4.30$$

where V_L and V_o are line to line motor and modulator terminal voltages.

When both positive and negative sequence voltages are applied simultaneously to the motor stator terminals, the total developed internal torque is as follows:[4.4]

$$T = T' - T'' \qquad 4.31$$

where T' is the torque produced by the presence of positive sequence voltage, and T'' is the torque produced by the presence of negative sequence voltage.

If superposition is applied to equation 4.30 the following relations may be written:

$$\left[\frac{T}{T_r}\right]' = \left[\frac{V_{b1}}{V_o}\right]^2 \quad \frac{5.5}{\frac{S}{S_m} + \frac{S_m}{S}} \qquad 4.32$$

$$\left[\frac{T}{T_r}\right]'' = \left[\frac{V_{b2}}{V_o}\right]^2 \quad \frac{5.5}{\frac{(2-S)}{S_m} + \frac{S_m}{(2-S)}} \qquad 4.33$$

where $\left[\frac{T}{T_r}\right]'$ is the normalized positive sequence torque, and $\left[\frac{T}{T_r}\right]''$ is the normalized negative sequence torque.

Incorporating the results of equations 4.32 and 4.33 into equation 4.31 yields:

$$\left[\frac{T}{T_r}\right]=\left[\frac{V_{b1}}{V_o}\right]^2\left[\frac{5.5}{\frac{S}{S_m}+\frac{S_m}{S}}\right]-\left[\frac{V_{b2}}{V_o}\right]^2\left[\frac{5.5}{\frac{(2-S)}{S_m}+\frac{S_m}{(2-S)}}\right] \quad 4.34$$

Equation 4.34 expresses the normalized motor torque per phase as a function of motor slip, motor parameters, and power modulator parameters.

The normalized per phase motor stator current may be defined as I/I_r, where I is any current per phase and I_r is the rated phase current.

In order to find the ratio I/I_r it is necessary to define a new quantity $\frac{Z_{ar}}{Z_{oc}}$ which will be called normalized rated stator impedance per phase. For the symmetrical case when either X_1 or X_2 is zero, the power modulator is bypassed, and the motor stator terminals are directly connected to the supply source. This cannot be verified by simultaneous substitution of $X_1 = X_2 = 0$ into equations 4.27 and 4.28 since the equations then become indeterminate. Equations 4.27, 4.28 can be verified as being consistent with Fig. 4.5 by letting X_1, X_2 approach zero independently.

For example

when $X_1 = 0$, X_2 = finite

$$\text{then } \frac{V_{b1}}{V_o} = 1, \frac{V_{b2}}{V_o} = 0 \quad 4.35$$

In order to determine $\frac{Z_{ar}}{Z_{oc}}$ it will be necessary to define a quantity $\frac{S_r}{S_m}$ where S_r is the rated motor slip which occurs when X_1 or $X_2 = 0$, and torque T is equal to rated motor torque T_r (i.e. $T/T_r = 1$). The quantity S_m has been defined in equation 3.20

of section 3.3. Substitution of equations 4.35 into equation 4.34 yields the following results:

when $\frac{T}{T_r} = 1$,

then $1 = (1)^2 \frac{5.5}{\frac{S_r}{S_m} + \frac{S_m}{S_r}}$.

This result gives

$$\frac{S_r}{S_m} = 0.19 \qquad 4.36$$

The quantity $\frac{Z_{ar}}{Z_{oc}}$ may now be found by application of equation 3.23 which states

$$\frac{Z_{al}}{Z_{oc}} = \frac{1 + j\, S/S_m}{1 + \frac{jS}{\alpha S_m}}.$$

Clearly, if $S = S_r$,

then $\frac{Z_{al}}{Z_{oc}} = \frac{Z_{ar}}{Z_{oc}}$.

If the leakage factor α is taken to be .1 (a reasonable value), and the result of equation 4.36 is substituted into equation 3.23, then it follows that:

$$\frac{Z_{ar}}{Z_{oc}} = \frac{1 + j\ .19}{1 + j\ \frac{.19}{.1}} \qquad 4.37$$

whence $\frac{Z_{ar}}{Z_{oc}} = .467\ \angle -51°30'$

It was shown in equations 4.35 that $V_{b2} = 0$ when $X_1 = 0$ (i.e. conditions of symmetrical motor operation). Reference to equation 4.22 yields:

$$V_{b2} = j\sqrt{3}\ I_{a2}\ Z_{a2}$$

but $V_{b2} = 0$ as shown in equations 4.35.

Therefore, when $I_1 = 0$, the negative sequence current $I_{a2} = 0$, since Z_{a2} is not necessarily zero. Reference to equations 4.16 shows that

$$I_a = I_{a1} + I_{a2}$$

but $$I_{a2} = 0$$

whence $$I_a = I_{a1} \qquad 4.38$$

Further reference to equations 4.16 indicates

$$|I_{a1}| = |I_a| = |I_b| = |I_{\bar{c}}| \text{ , when } I_{a2} = 0.$$

The above indicates symmetrical motor operation. It was shown in equations 4.22 that

$$V_{b1} = -j\sqrt{3}\ I_{a1} Z_{a1}$$

From equations 4.15 it is seen that

$$V_{b\bar{c}} = V_{b1} + V_{b2}$$

but $$V_{b2} = 0$$

whence $$V_{b\bar{c}} = V_{b1} \qquad 4.39$$

Substitution of equations 4.38 and 4.39 into equation 4.22 yields:

$$V_{b\bar{c}} = -j\sqrt{3}\ I_a Z_{a1} \qquad 4.40$$

with reference to Fig. 4.7 it is seen that the voltage $V_{b\bar{c}}$ is in phase with the voltage V_{BC} when $I_1 = 0$. The voltage V_{BC} has been defined such that $V_{BC} = V_o$ in section 4.3, where V_o is the rated motor line to line voltage.

By definition it may be stated that

$$V_o = \sqrt{3}\ I_r\ Z_{ar} \qquad 4.41$$

where V_o is the rated motor line to line stator voltage

and I_r is the rated motor per phase stator current,

Z_{ar} is the rated motor per phase stator impedance.

Division of equation 4.40 by equation 4.41 yields:

$$\frac{\bar{V}_{bc}}{V_o} = \frac{-j\sqrt{3}\, I_a\, Z_{al}}{\sqrt{3}\, I_r\, Z_{ar}} \qquad 4.42$$

whence $$\frac{I_a}{I_r} = j\left[\frac{\bar{V}_{bc}}{V_o}\right]\left[\frac{Z_{ar}}{Z_{al}}\right]$$

Since the voltages $\bar{V}_{bc}$ and V_o are vector quantities that are in phase when $X_1 = 0$, it is seen that their ratio is not complex. Substitution of equation 4.39 into equation 4.42 and multiplication of the right hand side of equation 4.42 by $\frac{Z_{oc}}{Z_{oc}}$ yields upon rearrangement:

$$\frac{I_a}{I_r} = j\left[\frac{V_{bl}}{V_o}\right]\left[\frac{Z_{ar}}{Z_{oc}}\right]\left[\frac{Z_{oc}}{Z_{al}}\right] \qquad 4.43$$

For given values of $\frac{V_{bl}}{V_o}$ and assumed values of S, S_m, and α, a set of normalized induction motor torque-current characteristics may be derived by application of equations 4.34 and 4.43. It has been shown that under conditions of symmetrical operation $|I_a| = |I_b| = |\bar{I}_c|$. Hence, equation 4.43 is equally valid for all phases of the three phase machine.

For the case of asymmetrical operation when $X_1 \neq X_2 \neq 0$, a different procedure must be followed in order to deduce a set of torque-current characteristics.

Equation 4.22 may be written in the form

$$\frac{V_{bl}}{V_o} = \frac{-j\sqrt{3}\, I_{al}\, Z_{al}}{V_o}$$

But from equation 4.41, $V_o = \sqrt{3}\, I_r\, Z_{ar}$

Therefore $$\frac{V_{bl}}{V_o} = \frac{-j\sqrt{3}\, I_{al}\, Z_{al}}{\sqrt{3}\, I_r\, Z_{ar}}$$

Therefore $$\frac{I_{a1}}{I_r} = j\left[\frac{V_{b1}}{V_o}\right]\left[\frac{Z_{ar}}{Z_{oc}}\right]\left[\frac{Z_{oc}}{Z_{a1}}\right] \qquad 4.44$$

It follows from equation 4.22 that

$$\frac{I_{a2}}{I_r} = -j\left[\frac{V_{b2}}{V_o}\right]\left[\frac{Z_{ar}}{Z_{oc}}\right]\left[\frac{Z_{oc}}{Z_{a2}}\right] \qquad 4.45$$

In order to utilize equations 4.44 and 4.45 a minor change of form must be introduced into equations 4.27 and 4.28. If the numerator and denominator of the aforementioned equations are divided by Z_{oc}^3 the result is as follows:

$$\frac{V_{b1}}{V_o} = \frac{\frac{Z_{a1}}{Z_{oc}}\frac{Z_{a2}}{Z_{oc}}\frac{X_2}{Z_{oc}} + \frac{Z_{a1}}{Z_{oc}}\frac{X_1}{Z_{oc}}\frac{X_2}{Z_{oc}}}{\frac{Z_{a1}}{Z_{oc}}\frac{Z_{a2}}{Z_{oc}}\frac{X_1}{Z_{oc}} + \frac{Z_{a1}}{Z_{oc}}\frac{Z_{a2}}{Z_{oc}}\frac{X_2}{Z_{oc}} + \frac{Z_{a1}}{Z_{oc}}\frac{X_1}{Z_{oc}}\frac{X_2}{Z_{oc}} + \frac{Z_{a2}}{Z_{oc}}\frac{X_1}{Z_{oc}}\frac{X_2}{Z_{oc}}} \qquad 4.46$$

$$\frac{V_{b2}}{V_o} = \frac{-\left[\frac{Z_{a1}}{Z_{oc}}\frac{Z_{a2}}{Z_{oc}}\frac{X_1}{Z_{oc}} + \frac{Z_{a2}}{Z_{oc}}\frac{X_1}{Z_{oc}}\frac{X_2}{Z_{oc}}\right]}{\frac{Z_{a1}}{Z_{oc}}\frac{Z_{a2}}{Z_{oc}}\frac{X_1}{Z_{oc}} + \frac{Z_{a1}}{Z_{oc}}\frac{Z_{a2}}{Z_{oc}}\frac{X_2}{Z_{oc}} + \frac{Z_{a1}}{Z_{oc}}\frac{X_1}{Z_{oc}}\frac{X_2}{Z_{oc}} + \frac{Z_{a2}}{Z_{oc}}\frac{X_1}{Z_{oc}}\frac{X_2}{Z_{oc}}} \qquad 4.47$$

With reference to equations 4.46 and 4.47 it must be recalled that the parameters X_1 and X_2 were defined as $X_1 = j\,X_1$, and $X_2 = j\,X_2$ in section 4.1 of Chapter IV to facilitate analysis. The parameter Z_{oc} was defined as $Z_{oc} = j(x_1 + x_m)$ in section 3.3 of Chapter III. It is therefore evident that the ratio X/Z_{oc} is real.

For assumed values of S, S_m, α, X_1/Z_{oc}, X_2/Z_{oc}, and with the use of equations 4.44, 45, 46, and 47, the values of $\frac{I_{a1}}{I_r}$ and $\frac{I_{a2}}{I_r}$ may be found.

A further application of equations 4.16 permits the evaluation of the asymmetrical normalized induction motor per phase stator currents $\frac{I_a}{I_r}$, $\frac{I_b}{I_r}$, and $\frac{I_c}{I_r}$.

Solution of equation 4.34 under the same conditions assumed for evaluation of $\frac{I_{a1}}{I_r}$ and $\frac{I_{a2}}{I_r}$ will yield the normalized per phase induction motor torque in synchronous watts.

A normalized set of torque-current induction motor characteristics may now be plotted for any value of motor slip S and any arbitrary normalized power modulator impedance $\frac{X_1}{Z_{oc}}$ and $\frac{X_2}{Z_{oc}}$.

Table 4.1 has been compiled for the case of symmetrical induction motor operation (i.e. $\frac{X_1}{Z_{oc}} = 0$). Equations 4.43 and 4.34 have been used to compute values of I_a/I_r and T/T_r for three different values of motor slip S and for various values of $\frac{V_{b1}}{V_o}$.

Table 4.2 has been compiled for the case of asymmetrical induction motor operation (i.e. $\frac{X_1}{Z_{oc}} \neq \frac{X_2}{Z_{oc}} \neq 0$). For the sake of simplicity it has been assumed that saturable transformer SX_2 has no d.c. excitation applied to the control winding, while saturable transformer SX_1 has control winding excitation. These assumptions imply that the normalized saturable transformer impedances take on the following values:

$$\frac{X_2}{Z_{oc}} \longrightarrow \infty$$

$$0 < \frac{X_1}{Z_{oc}} < \infty$$

The case where $\frac{X_1}{Z_{oc}} \to \infty$, and $0 < \frac{X_2}{Z_{oc}} < \infty$ need not be considered. It may be shown that the results in this latter case are identical to the results of Table 4.2, except that the direction of rotation of the induction motor is reversed. The data of Tables 4.1 and 4.2 when set out in graphical form displays the effect of the power modulator on induction motor operation.

Table 4.1

Symmetrical Motor Operation

Leakage factor α = .1 $\quad S_m = \frac{r_2}{\alpha (x_2 + x_m)} = 4 \quad \frac{X_1}{Z_{oc}} = 0$

S	$\left\|\frac{V_{b1}}{V_o}\right\|$	$\left\|\frac{I_a}{I_r}\right\|$	$\left\|\frac{T}{T_r}\right\|$
.500	1.00	.742	.677
.500	0.75	.562	.382
.500	0.50	.372	.169
.500	0.25	.187	.042
1.00	1.00	1.22	1.30
1.00	0.75	.915	.732
1.00	0.50	.610	.325
1.00	0.25	.305	.081
1.50	1.00	1.70	1.81
1.50	0.75	1.28	1.02
1.50	0.50	.850	.453
1.50	0.25	.425	.113

In Table 4.1 the following terminology applies:

S is the induction motor slip,

$\left\|\frac{V_{b1}}{V_o}\right\|$ is the absolute value of the normalized positive symmetrical component voltage of the line voltage V_{bc}.

$\left\|\frac{I_a}{I_r}\right\|$ is the absolute value of the normalized line current I_a.

$\left\|\frac{T}{T_r}\right\|$ is the absolute value of the normalized per phase motor torque T.

Table 4.2

Asymmetrical Motor Operation

Leakage factor $\alpha = .1 \quad S_m = \frac{r_2}{\alpha(x_2 + x_m)} = 4 \quad \frac{X_2}{Z_{oc}} \to \infty \quad 0 < \frac{X_1}{Z_{oc}} < \infty$

S	$\frac{X_1}{Z_{oc}}$	$\left\|\frac{V_{b1}}{V_o}\right\|$	$\left\|\frac{V_{b2}}{V_o}\right\|$	$\left\|\frac{I_{a1}}{I_r}\right\|$	$\left\|\frac{I_{a2}}{I_r}\right\|$	$\left\|\frac{I_a}{I_r}\right\|$	$\left\|\frac{I_b}{I_r}\right\|$	$\left\|\frac{I_{\bar{c}}}{I_r}\right\|$	$\left\|\frac{T}{T_r}\right\|$
.500	0.00	1.00	0.00	.742	0.00	.742	.742	.742	.667
.500	0.10	.910	.114	.675	.194	.832	.737	.500	.530
.500	0.25	.812	.190	.603	.323	.900	.679	.368	.375
.500	0.50	.735	.266	.545	.384	1.00	.619	.340	.232
.500	∞	.698	.305	.518	.518	1.04	.516	.516	.158
1.00	0.00	1.00	0.00	1.22	0.00	1.22	1.22	1.22	1.30
1.00	0.10	.835	.190	1.02	.232	1.22	1.10	.800	.863
1.00	.467	.660	.370	.805	.451	1.22	.904	.550	.390
1.00	1.00	.560	.440	.683	.542	1.22	.723	.528	.152
1.00	∞	.500	.500	.611	.611	1.22	.611	.611	0.00
1.5	0.00	1.00	0.00	1.70	0.00	1.70	1.70	1.70	1.81
1.5	0.25	.641	.443	1.09	.328	1.38	1.15	.818	.611
1.5	0.30	.595	.468	.935	.348	1.28	1.00	.735	.492
1.5	0.50	.500	.634	.850	.470	1.07	.544	.538	.179
1.5	∞	.505	.698	.518	.518	1.04	.516	.516	.158

In Table 4.2, the following terminology applies:

S is the induction motor slip

$\left|\frac{V_{b1}}{V_o}\right|$ is the absolute value of the normalized positive symmetrical component voltage of line voltage $V_{b\bar{c}}$.

$\left|\frac{V_{b2}}{V_o}\right|$ is the absolute value of the normalized negative symmetrical component voltage of line voltage $V_{b\bar{c}}$.

$\left|\frac{I_{a1}}{I_r}\right|$ is the absolute value of the normalized positive symmetrical component of current of the line current I_a.

$\left|\frac{I_{a2}}{I_r}\right|$ is the absolute value of the normalized negative symmetrical component of current of the line current I_a.

$\left|\frac{I_a}{I_r}\right|$, $\left|\frac{I_b}{I_r}\right|$, and $\left|\frac{I_{\bar{c}}}{I_r}\right|$ are the absolute values of the per phase motor currents I_a, I_b, and $I_{\bar{c}}$.

$\left|\frac{T}{T_r}\right|$ is the absolute value of the normalized per phase motor torque T.

4.5 THEORETICAL PERFORMANCE CHARACTERISTICS OF THE MODULATOR AND INDUCTION MOTOR COMBINATION.

The motor current-torque characteristics compiled in Tables 4.1 and 4.2 are reproduced in Figures 4.10, 4.11, and 4.12. The current-torque characteristics have been plotted for motor slips of 0.5, 1.0, and 1.5 for the conditions

$$\frac{X_2}{Z_{oc}} \longrightarrow \infty \qquad ,0 < \frac{X_1}{Z_{oc}} < \infty$$

Examination of Figures 4.10, 4.11, and 4.12 shows a marked unbalance of motor phase currents for asymmetrical motor operation. However, it is seen that at higher values of normalized per phase torque, the motor phase currents approach balance.

For the case of symmetrical operation it is seen that the motor phase currents approach zero when $\left|\frac{T}{T_r}\right|$ approaches zero. However, this is not necessarily true of asymmetrical operation. Examination of Figs. 4.10, 4.11, and 4.12 indicates the following consequences of asymmetrical motor operation:

(1) For low values of $\left|\frac{T}{T_r}\right|$ the motor currents are not balanced, and may be quite large.

(2) Values of normalized torque $\left|\frac{T}{T_r}\right|$ may not approach zero, but some finite value different from zero.

Fig. 4.11 is drawn for the standstill condition (i.e. S = 1). For the case of asymmetrical operation where $\frac{X_1}{Z_{oc}} = \frac{X_2}{Z_{oc}} = \infty$ (i.e. no d.c. excitation on either SX_1 or SX_2 in Fig. 4.6) it is apparent

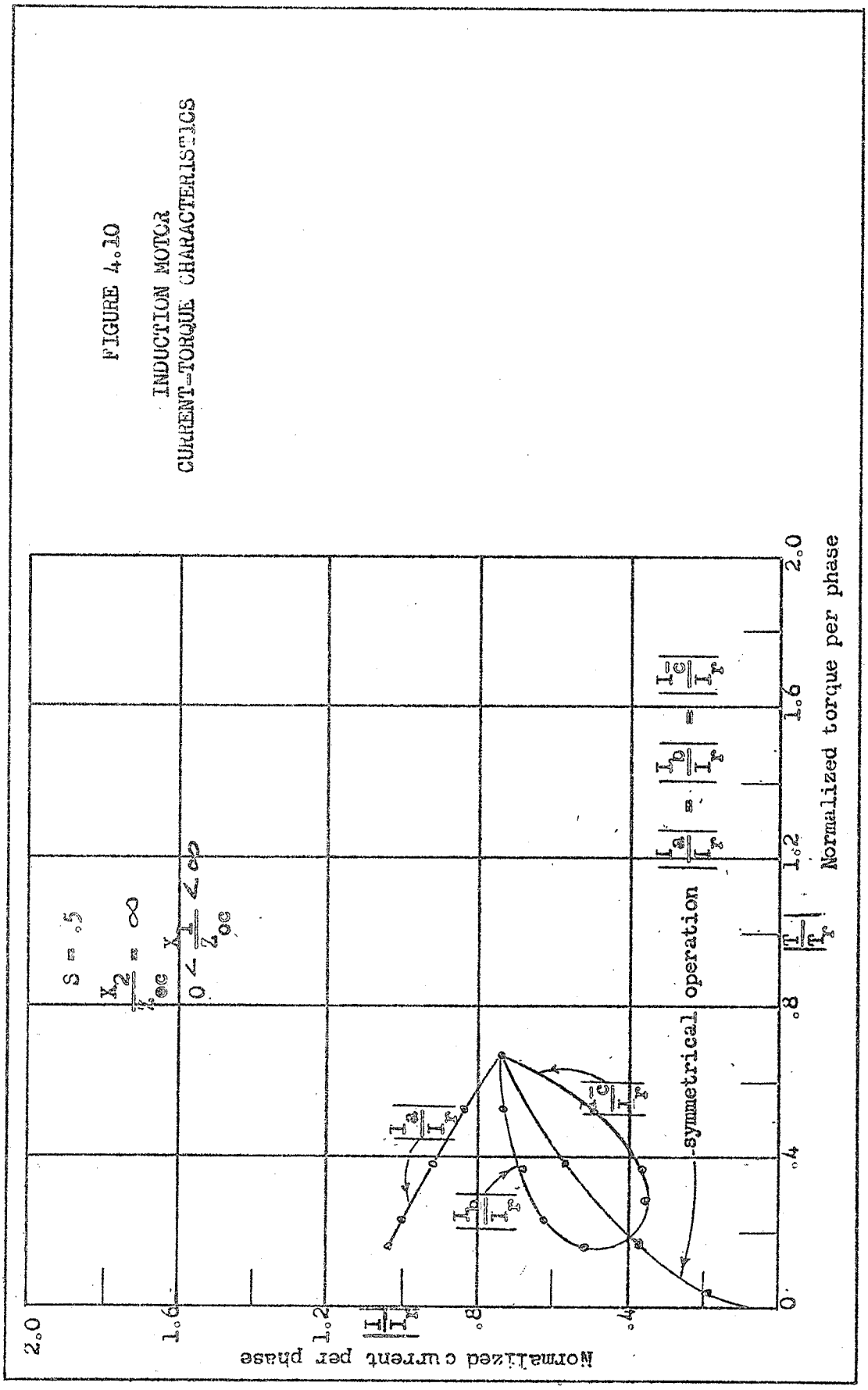

FIGURE 4.10

INDUCTION MOTOR
CURRENT-TORQUE CHARACTERISTICS

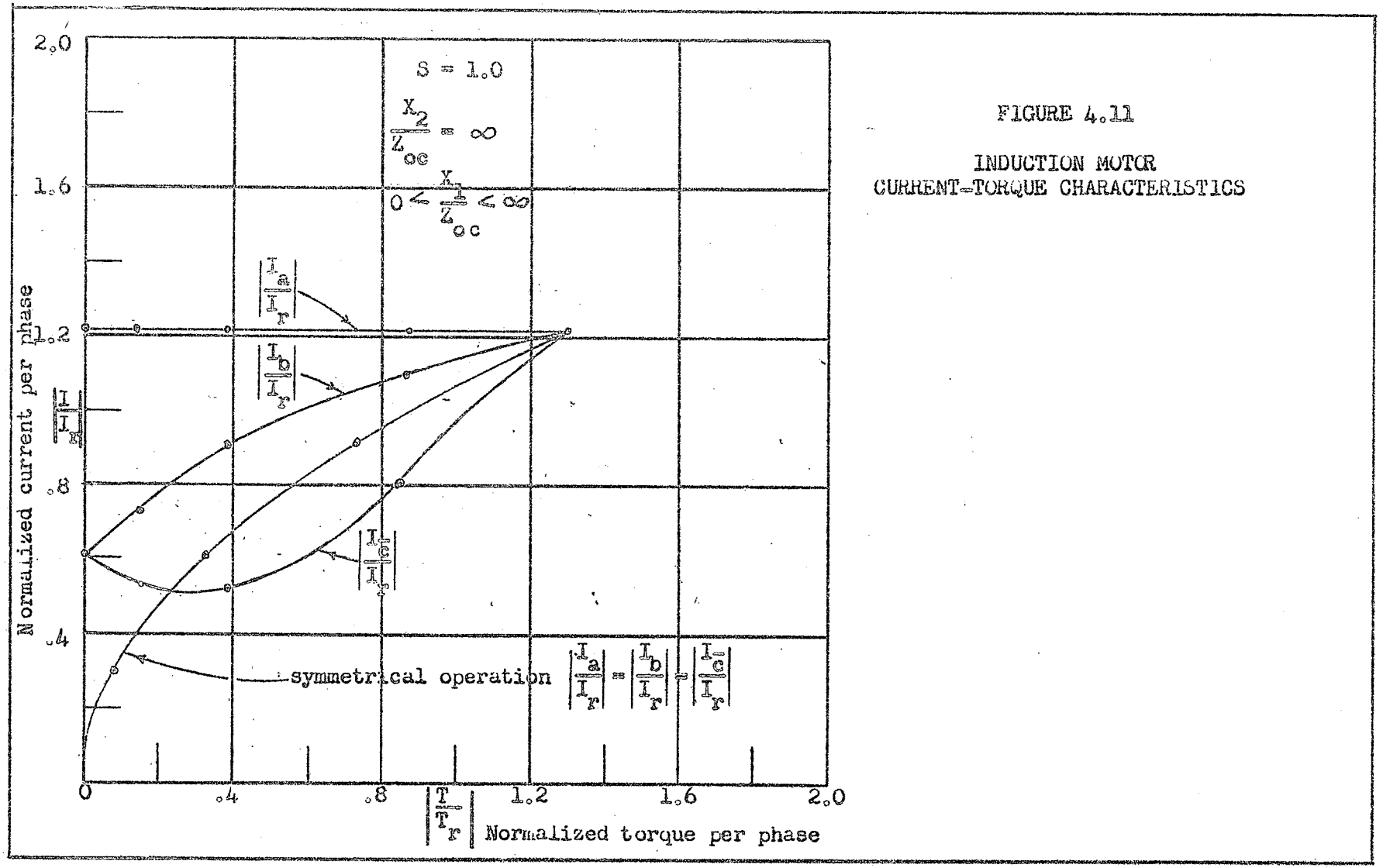

FIGURE 4.11

INDUCTION MOTOR
CURRENT-TORQUE CHARACTERISTICS

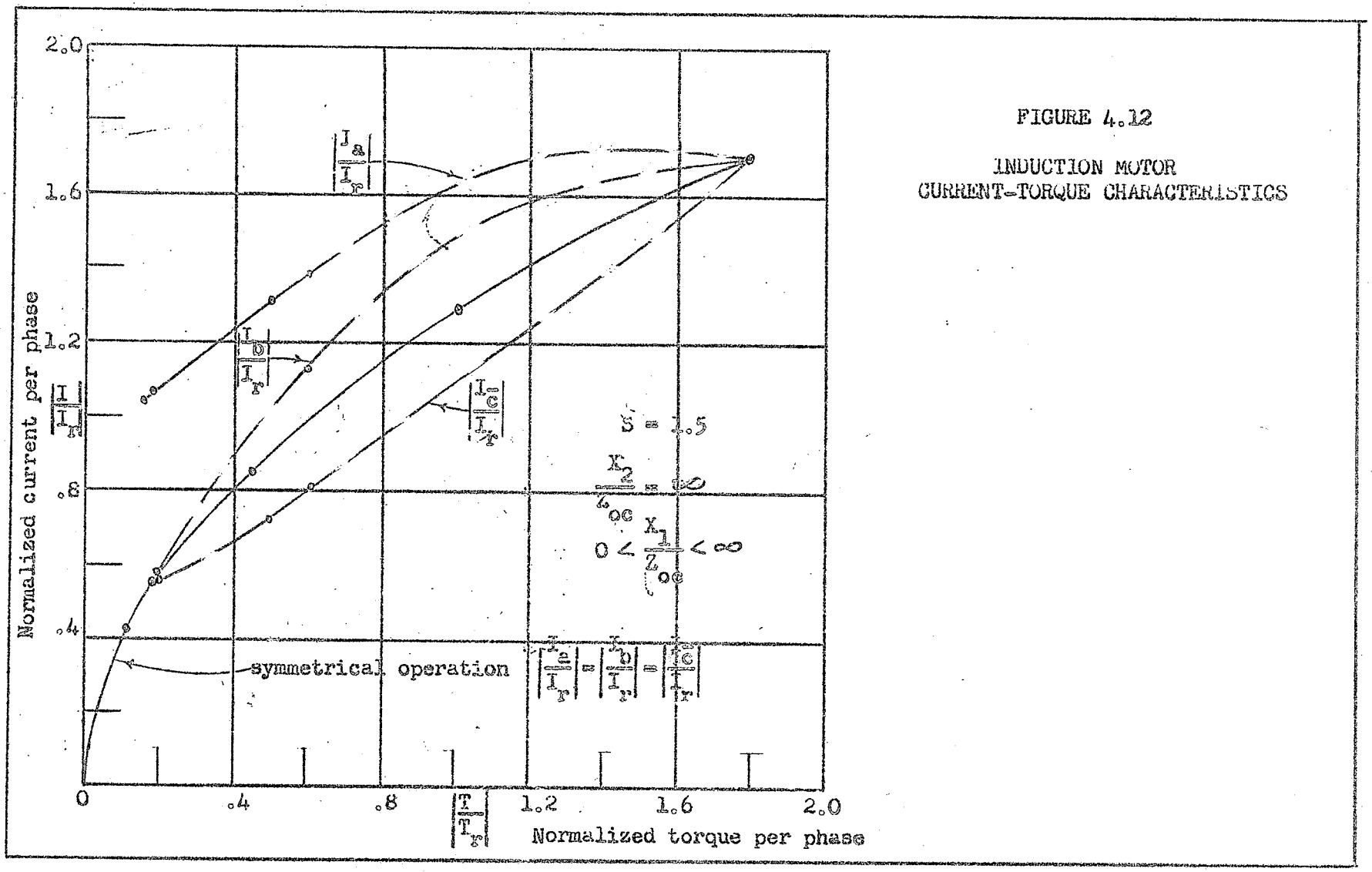

FIGURE 4.12

INDUCTION MOTOR
CURRENT-TORQUE CHARACTERISTICS

that the phase carrying current I_a is subjected to maximum excitation while $\left|\frac{T}{T_r}\right| = 0$. This result is indicative of single-phase operation. That this is in fact the case, may be borne out by substituting the parameters $\frac{X_1}{Z_{oc}} = \frac{X_2}{Z_{oc}} = \infty$ into equations 4.27 and 4.28. Subsequent solution of these equations yields $\frac{V_{b1}}{V_{b2}} = \frac{-Z_{a1}}{Z_{a2}}$. This result is characteristic of single-phase operation.[4.5]

Due to single-phase excitation, torque becomes immediately available when one of the saturable reactor d.c. control currents is increased. This situation is very undesirable, since at standstill ($S = 1$, $\left|\frac{T}{T_r}\right| = 0$) the motor currents cannot be interrupted by d.c. control of the saturable transformers, and a line contactor is necessary.

It has been stated that for asymmetrical motor operation the motor phase currents for small values of $\left|\frac{T}{T_r}\right|$ are high. Table 4.3 shows a comparison between symmetrical motor currents (i.e. the case when $\frac{X_1}{Z_{oc}} = 0$) and the currents incurred for the asymmetrical case $\frac{X_2}{Z_{oc}} \to \infty$, $0 < \frac{X_1}{Z_{oc}} \leqslant \infty$. For asymmetrical motor operation the three phase currents at a given torque are combined to an equivalent per phase symmetrical motor current which would result in the same secondary resistance losses. The following is a sample calculation:

With reference to Fig. 4.11, the motor current for symmetrical operation at $\left|\frac{T}{T_r}\right| = 1$, is $\left|\frac{I_a}{I_r}\right| = 1.08$. If the secondary motor resistance is r_2 then the secondary resistance loss is

$$(1.08)^2 r_2 = 1.17\, r_2 \text{ normalized watts per phase.}$$

For conditions of asymmetrical operation at $\left|\frac{T}{T_r}\right| = 1$, $\left|\frac{I_a}{I_r}\right| = 1.22$, $\left|\frac{I_b}{I_r}\right| = 1.15$, $\left|\frac{I_c}{I_r}\right| = 1.0$

Therefore, total secondary resistance loss for the three phases is as follows:

$$\left[(1.22)^2 + (1.15)^2 + (1.0)^2\right] r_2 = 3.81\ r_2 \text{ normalized watts.}$$

The average loss per phase is $\frac{3.81}{3} = 1.27\ r_2$ normalized watts per phase. The secondary resistance loss under conditions of symmetrical operation has been found to be $1.17\ r_2$ normalized watts per phase. This corresponds to a normalized current $\left|\frac{I_a}{I_r}\right| = \sqrt{1.17} = 1.08$ as shown above. Similarly, for the case of asymmetrical operation, a normalized current $\left|\frac{I}{I_r}\right| = \sqrt{1.27} = 1.13$ is found.

Table 4.3 is now compiled as follows:

Table 4.3

Comparison of Motor Phase Currents Under Conditions of Symmetrical and Asymmetrical Operation

All data compiled from Fig. 4.11

$\left\|\frac{T}{T_r}\right\|$	$\left\|\frac{I_a}{I_r}\right\|$	$\left\|\frac{I}{I_r}\right\|$
0	0	.86
.5	.65	.96
1	1.08	1.13

In Table 4.3 the following terminology applies:

$\left|\frac{T}{T_r}\right|$ is the absolute value of the normalized per phase motor torque T.

$\left|\frac{I_a}{I_r}\right|$ is the absolute value of the per phase motor current I_a under conditions of symmetrical operation.

$\left|\frac{I}{I_r}\right|$ is the absolute value of the equivalent per phase motor current under conditions of a symmetrical operation.

Inspection of Table 4.3 shows that for low values of $\left|\frac{T}{T_r}\right|$, motor currents under conditions of asymmetrical operation are much larger than the currents which would result under conditions

of symmetrical operation. Hence, Table 4.3 confirms the fact that a high degree of asymmetry is introduced by the power modulator at low motor loads. As load increases the currents become more nearly equal, and relatively symmetrical motor operation is possible with the power modulator.

It may be concluded that a criterion for machine heating due to current asymmetry must be considered if the power modulator is to be useful in control of the induction motor.

Fig. 4.13 shows the relative magnitudes of the two positive and negative sequence voltages for slip values of .5, 1.0, and 1.5. The characteristics of Fig. 4.13 confirm the results obtained by Bolt, Simeon, and Shepherd[1.11] which are shown in Fig. 4.5. The characteristics of Fig. 4.13 differ from those of Fig. 4.5 in that the former are plotted for an induction motor load, whereas the latter are plotted for a general load impedance Z_L.

Fig. 4.14 shows a plot of normalized motor torque versus normalized reactor impedance at three different values of slip. The absolute value of slope at any point on a given characteristic of Fig. 4.14 may be found by evaluating

$$\left.\frac{\partial\left|\frac{T}{T_r}\right|}{\partial\left|\frac{X_1}{X_{oc}}\right|}\right| \quad S = \text{constant}.$$

Examination of Fig. 4.14 shows that for a constant value of slip the slope of the torque-reactor impedance curve is small for light loads and large for higher values of torque. It is recognized that when the motor is to be controlled by a velocity-feedback loop, the loop gain will be substantially affected, causing the response

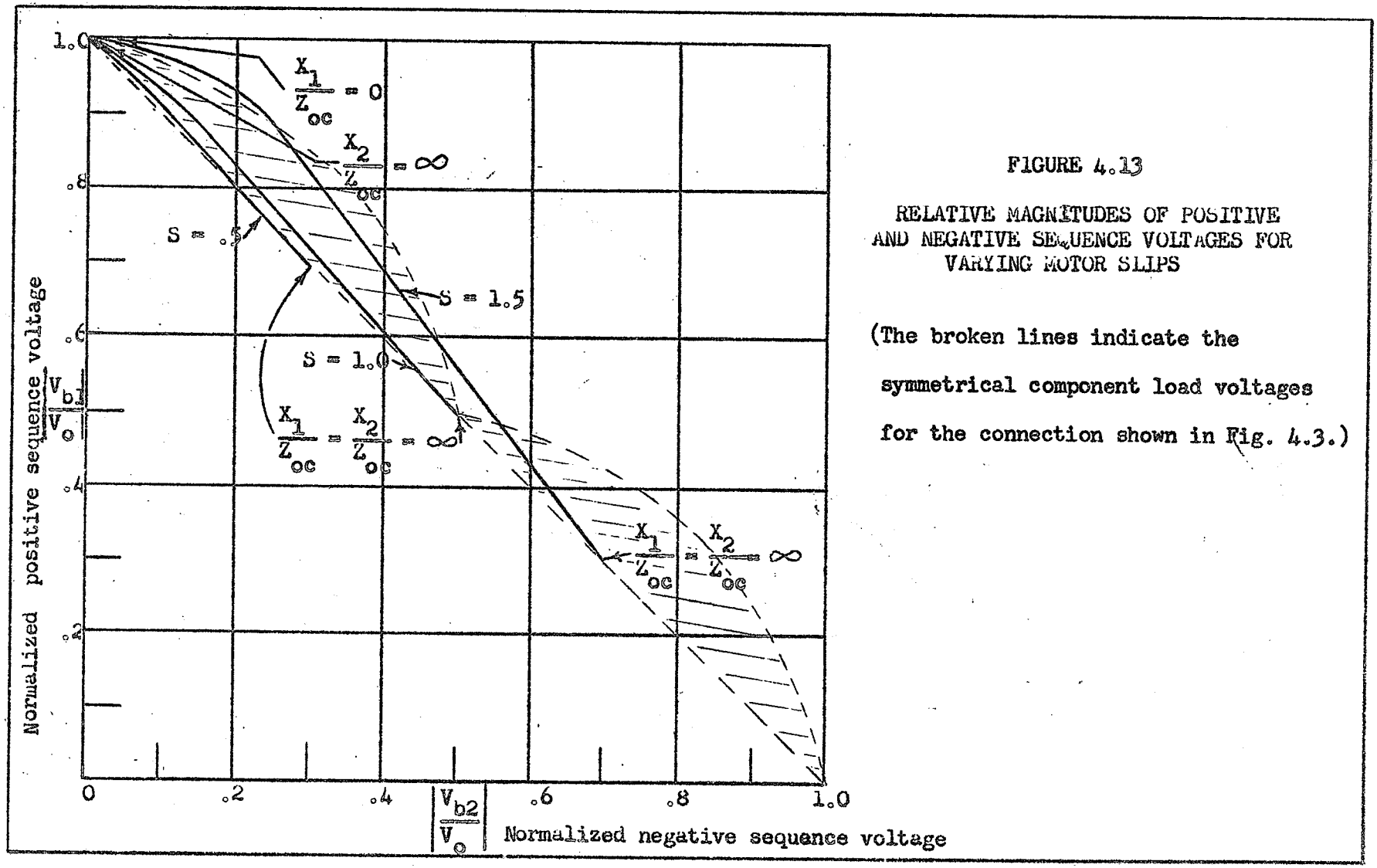

FIGURE 4.13

RELATIVE MAGNITUDES OF POSITIVE AND NEGATIVE SEQUENCE VOLTAGES FOR VARYING MOTOR SLIPS

(The broken lines indicate the symmetrical component load voltages for the connection shown in Fig. 4.3.)

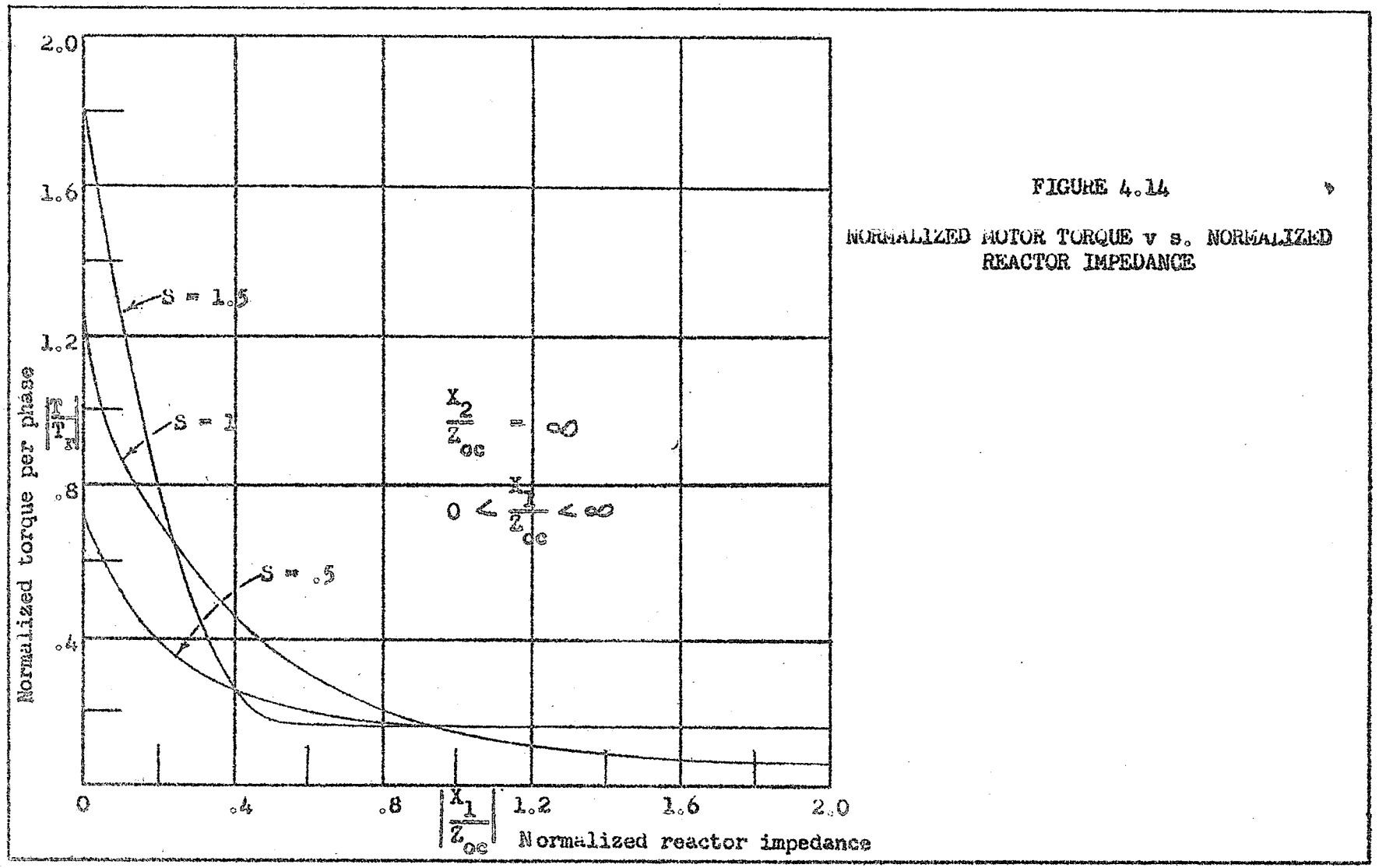

FIGURE 4.14

NORMALIZED MOTOR TORQUE v s. NORMALIZED REACTOR IMPEDANCE

of the system to vary at various operating points.

Fig. 4.14 also shows that reactor impedance does not vary linearly with normalized motor torque for the chosen values of motor slip. To show that this is true in general the following procedure may be carried out:

The substitution of equations 4.46 and 4.47 for the case of $\frac{X_2}{Z_{oc}} \longrightarrow \infty$ and $0 < \frac{X_1}{Z_{oc}} < \infty$ into equation 4.34 yields equation 4.48 as follows:

$$\frac{T}{T_r} = \frac{5.5}{\left[\frac{Z_{a1}}{Z_{oc}}\frac{Z_{a2}}{Z_{oc}} + \left[\frac{Z_{a1}}{Z_{oc}} + \frac{Z_{a2}}{Z_{oc}}\right]\frac{X_1}{Z_{oc}}\right]^2} \left[\frac{\left[\frac{Z_{a1}}{Z_{oc}}\frac{Z_{a2}}{Z_{oc}} + \frac{Z_{a1}}{Z_{oc}}\frac{X_1}{Z_{oc}}\right]^2}{\frac{S}{S_m} + \frac{S_m}{S}} - \frac{\left[\frac{Z_{a2}}{Z_{oc}}\frac{X_1}{Z_{oc}}\right]^2}{\frac{2-S}{S_m} + \frac{S_m}{2-S}}\right] \qquad 4.48$$

Inspection of equation 4.48 shows that:

$$\left|\frac{T}{T_r}\right| = f\left(\frac{Z_{a1}}{Z_{oc}}, \frac{X_1}{Z_{oc}}, \frac{Z_{a2}}{Z_{oc}}\right).$$

In order to substantiate the results shown in Fig. 4.14 it is necessary to perform the following operation:

$$\left.\frac{\partial\left|\frac{T}{T_r}\right|}{\partial\left|\frac{X_1}{Z_{oc}}\right|}\right|_{S = \text{constant}}. \qquad 4.49$$

Due to the complexity involved, this operation will not be carried forward.

Since $\frac{X_1}{Z_{oc}}$ is not a function of $\frac{Z_{a1}}{Z_{oc}}$ or $\frac{Z_{a2}}{Z_{oc}}$, where $\frac{Z_{a1}}{Z_{oc}}$ and $\frac{Z_{a2}}{Z_{oc}}$ are complex numbers, the following operation may be performed by differentiating equation 4.48:

$$\left.\frac{\partial\left[\frac{T}{T_r}\right]}{\partial\left[\frac{X_1}{Z_{oc}}\right]}\right|_{S = \text{constant}}$$ 4.50.

It is also possible to find

$$\left.\frac{\partial\left[\frac{T}{T_r}\right]}{\partial\left[\frac{S}{S_m}\right]}\right|_{\frac{X_1}{Z_{oc}} = \text{constant}}$$ 4.51

by differentiating equation 4.48. Since Z_{a1} and Z_{a2} are both complex functions of "S" this operation would entail considerable difficulty.

The incremental expression of torque may be written as follows:

$$\Delta\left[\frac{T}{T_r}\right] = \left.\frac{\partial\left[\frac{T}{T_r}\right]}{\partial\left[\frac{X_1}{Z_{oc}}\right]}\right|_{S = \text{const.}} \Delta\left[\frac{X_1}{Z_{oc}}\right] + \left.\frac{\partial\left[\frac{T}{T_r}\right]}{\partial\left[\frac{S}{S_m}\right]}\right|_{\frac{X_1}{Z_{oc}} = \text{const.}} \Delta\left[\frac{S}{S_m}\right]$$ 4.52

Quazza[4.6] has pointed out that, although crude, the approximation that reactor impedance is proportional to reactor control current I_c may be made. Since all quantities of equation 4.52 are normalized, let the normalized reactor control current be $\frac{I_c}{I_o}$. Define the following quantities:

$$\left.\frac{\partial\left[\frac{T}{T_r}\right]}{\partial\left[\frac{I_c}{I_o}\right]}\right|_{S = \text{const.}} = K_1, \qquad \left.\frac{\partial\left[\frac{T}{T_r}\right]}{\partial\left[\frac{S}{S_m}\right]}\right|_{\frac{X_1}{Z_{oc}} = \text{const.}} = K_2$$

Then equation 4.52 may be written as follows:

$$\frac{T}{T_r} = K_1 \Delta\left[\frac{i_c}{i_o}\right] + K_2 \Delta\left[\frac{S}{S_m}\right]$$

The values of K_1, K_2 and their variation for varying operating points are of basic interest for transient and stability analysis.

Quazza[4.6] has also shown that the transfer function of the power modulator and induction motor may be represented by a linear transfer function for small perturbations. The transfer function is dependent upon the coefficients "K_1" and "K_2" and may be satisfactory for stability and frequency response considerations around a given operating point. Quazza has also suggested the use of phase plane analysis.

A third alternative analysis would be that of a so-called "black box" analysis. The power modulator and motor transfer functions could be separately described graphically and an attempt could then be made to describe the over-all transfer function. However, this method of analysis would be extremely difficult in that the power modulator has three separate outputs. Alternatively, it might be argued that the overall transfer function of motor and power modulator could be graphically determined. This method cannot be readily applied in that the overall transfer function of motor and power modulator is dependent on motor slip.

It was decided that the theoretical analysis of the reactor-motor transfer function was beyond the scope of this work, and only the results of closed-loop operation will be given in Chapter VI.

CHAPTER V

DETAILED CONSIDERATION OF CERTAIN COMPONENTS OF THE DRIVE

5.1 INTRODUCTION

Fig. 3.1 shows a block diagram of the drive. The theoretical behaviour of the power modulator and induction motor has been discussed in Chapter IV. The synthesis of the associated control equipment shown in Fig. 3.1 will now be carried out.

5.2 ROTOR NETWORK

It was pointed out in Chapter III that the performance characteristics of a polyphase machine incorporating a rotor network can be modified so that a rising torque can be obtained for all speeds in the driving range and counter torque range. The synthesis of the rotor network as suggested by W. Shepherd and G. R. Slemon[3.6] will now be carried out.

The per phase equivalent circuit of a polyphase induction motor with an external motor network $Z(S) = R(S) + j\,X(S)$ is shown in Fig. 5.1. All quantities in the rotor (secondary) circuit have been referred to the stator (primary) circuit, whence the external rotor impedance becomes $Z(S)/S$.

The authors of reference 3.6 made the following assumptions: Core loss, the effects of saturation, and space harmonics are neglected. The passive two-terminal frequency sensitive network $Z(S)$ is connected externally to each rotor phase. The rotor frequency is SW radians per second where S is the per unit slip, and W is the angular supply frequency in radians per second.

An application of Thevenin's theorem at the air-gap

as in Fig. 5.2 yields the following results:

$$V_e = \frac{V_1 \, j \, x_m}{r_1 + j \, (x_1 + x_m)} \qquad 5.1$$

where V_e is the open circuit voltage at the air-gap.

The short-circuit current at the air-gap is

$$I_{sc} = \frac{V_1}{(r_1 + j \, x_1)} \qquad 5.2$$

The Thevenin equivalent impedance is

$$\frac{V_e}{I_{sc}} = Z_{th} = \frac{j \, x_m (r_1 + j \, x_1)}{r_1 + j \, (x_1 + x_m)} \qquad 5.3$$

Equation 5.3 may be broken into two parts; the real part $R_e \left[Z_{th} \right] = r_e$, and the imaginary part Imag $Z_{th} = \left[x_e \right]$.

From equation 5.3

$$r_e = \frac{x_m^2 \, r_1}{r_1^2 + (x_1 + x_m)^2} \qquad 5.4$$

$$x_e = \frac{x_m r_1^2 + x_m x_1^2 + x_m^2 x_1}{r_1^2 + (x_1 + x_m)^2} \qquad 5.5$$

The internal electromagnetic torque T of an induction motor is determined by the power P_g crossing the air-gap and the synchronous speed. In MKS units, torque and speed have units such that

$$P_g = TW \qquad 5.6$$

where P_g = synchronous watts per phase, and T = torque in newton-meters per phase per pole pair and W = synchronous speed.

The air-gap power of equation 5.6 may be expressed in terms of rotor current and impedance as follows:

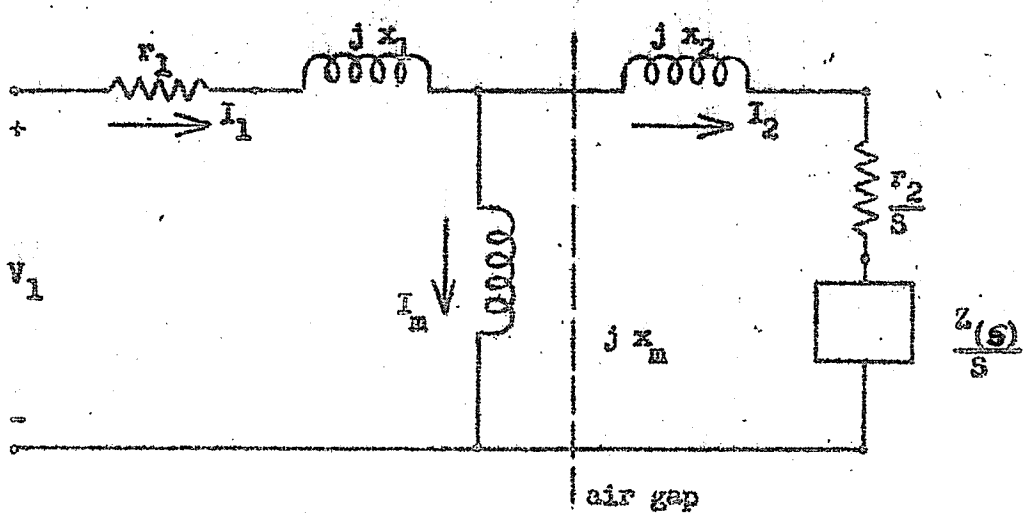

FIGURE 5.1

THE PER PHASE CIRCUIT OF A POLYPHASE INDUCTION MOTOR WITH A ROTOR NETWORK

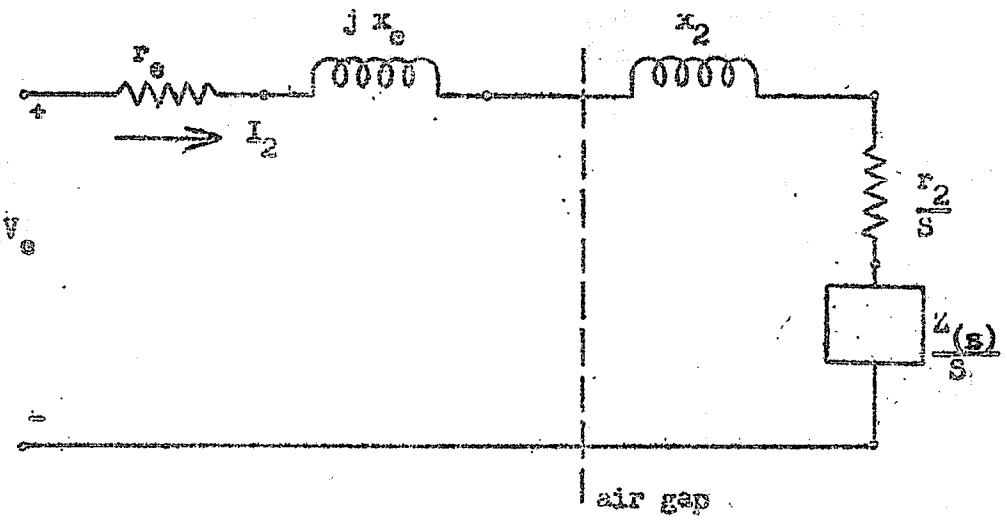

FIGURE 5.2 THEVENIN EQUIVALENT CIRCUIT

$$P_g = \left[\frac{r_2 + R_{(S)}}{S}\right] \left|I_2\right|^2 \qquad 5.7$$

where $R(S) = R_e \left[Z_{(S)}\right]$.

From Fig. 5.2, it is apparent that I_2 may readily be expressed as a function of V_e and the motor parameters.

It is expedient to state the following definitions:

$$R = \frac{r_2 + R_{(S)}}{S} \qquad 5.8$$

$$X = x_2 + \frac{X_{(S)}}{S} \qquad 5.9$$

where $X_{(S)} = \text{Imag} \left[Z_{(S)}\right]$

Combining equations 5.6, 5.7, 5.8, and 5.9, yields: 3.6

$$\left[R - \left[\frac{V_e^2}{2TW} - r_e\right]\right]^2 + \left[X + x_e\right]^2 = \left[\left[\frac{V_e^2}{2TW} - r_e\right]^2 - r_e^2\right] \qquad 5.10$$

Equation 5.10 is represented by a family of circles of constant torque in the R, X plane.

From equation 5.10, it is seen that the induction motor will deliver constant torque at constant applied voltage if the rotor impedance locus X versus R can be made to follow the circular constant torque locus.

The form of the rotor network has been discussed in Chapter III. Consider Fig. 3.5(a) where all quantities are referred to the stator:

$$\frac{Z_{(S)}}{S} = \frac{\left[\frac{R_1}{S} + j X_3\right]\left[\frac{R_o}{S}\right]}{\frac{(R_1 + R_o)}{S} + j X_3} \qquad 5.11$$

$$R_e \left[\frac{Z_{(S)}}{S}\right] = \frac{R_{(S)}}{S} = \frac{R_o\left[R_1(R_1 + R_o) + S^2 X_2^2\right]}{S\left[(R_1 + R_o)^2 + S^2 X_2^2\right]} \qquad 5.12$$

$$\text{Imag}\left[\frac{Z_{(S)}}{S}\right] = \frac{X_{(S)}}{S} = \frac{X_2 R_o^2}{\left[(R_1 + R_o)2 + S^2 X_2^2\right]} \qquad 5.13$$

The relationships expressed in equations 5.10, 5.12, and 5.13 allow the rotor network synthesis to be carried forward.

With reference to equation 5.10, the locus of the constant torque circle for TW = 1 p.u. and V_e = 1 p.u. may be drawn. The values of r_e and x_e may be found from the motor parameters. The motor parameters are given in Appendix A and are reproduced in Table 5.1:

Table 5.1

Per Phase Motor Parameters

(all quantities referred to stator)

r_1 = .060 p.u.

r_2 = .075 p.u.

x_1 = .114 p.u. at 60 cycles

x_2 = .114 p.u. at 60 cycles

x_m = 1.31 p.u. at 60 cycles.

Ratio of transformation a = 1.29

The following values of r_e and x_e were calculated from equations 5.4, 5.5, and table 5.1:

r_e = 0.51 p.u. per phase

x_e = .108 p.u. per phase at 60 cycles.

Equation 5.10 may now be written as

$$\left[R - .449\right]^2 + \left[X + .108\right]^2 \cong \left[.449\right]^2 \qquad 5.14$$

The locus of equation 5.14 is plotted in Fig. 5.3.

An attempt must now be made to fit the locus of $\frac{Z(s)}{S}$ to the locus of equation 5.14.

The authors of reference 3.6 stated that in order to obtain the proper shape of locus it is necessary to choose the proper ratios of $\frac{R_1}{R_o}$ and $\frac{R_o}{X_3}$. The reference suggested the following values:

$$\frac{R_1}{R_o} = .25$$

$$\frac{R_o}{X_3} = 1$$

An arbitrary, but reasonable value of X_3 must now be chosen. The values of R_1 and R_o are then determined and the locus of $\frac{Z(s)}{S}$ is plotted for various values of slip. The procedure is repeated several times until a value of X_3, R_1, and R_o is found that will give the proper shape of curve. Trial and error procedure indicates that X_3 = .28 ohms p.u. at 60 cycles is a good choice. This fixes the values of R_1 and R_o as follows:

X_3 = .28 ohms p.u.

$\frac{R_o}{X_3} = 1$ **therefore,** $R_o =$ .28 p.u.

$\frac{R_1}{R_o} = .25$ **therefore,** $R_1 =$ .07 p.u.

From equations 5.8, 5.9, 5.12, and 5.13, Table 5.2 is compiled:

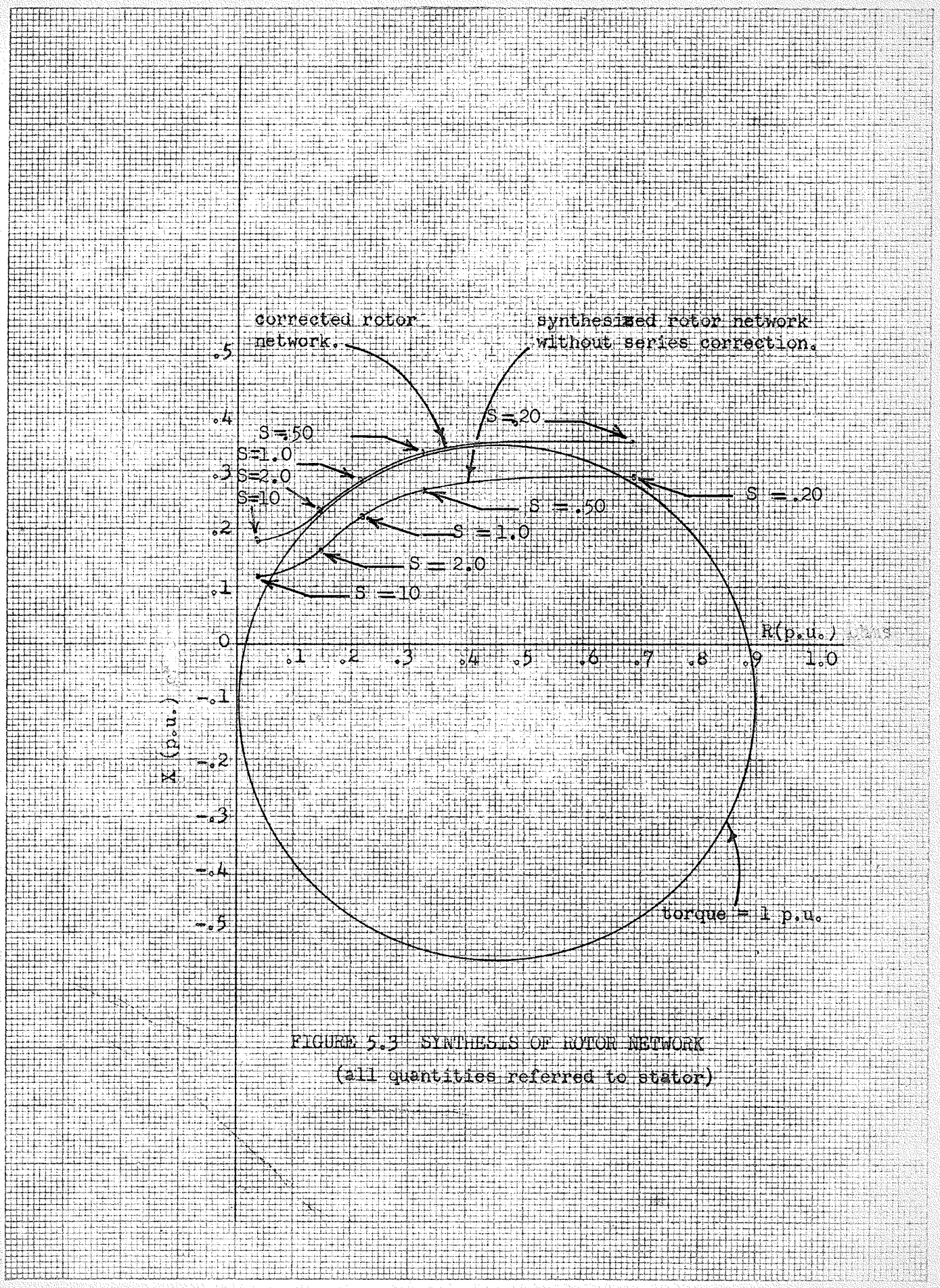

FIGURE 5.3 SYNTHESIS OF ROTOR NETWORK
(all quantities referred to stator)

Table 5.2

Components of the Rotor Circuit Impedance

(Per Phase, referred to stator circuit)

r_2 = .075 p.u.

x_2 = .114 p.u. at 60 cycles

X_3 = .28 p.u. at 60 cycles

R_1 = .07 p.u. at 60 cycles

R_o = .28 p.u. at 60 cycles.

Slip S	$\frac{R(s)}{S}$	$\frac{r_2}{S}$	R	$\frac{X_{(s)}}{S}$	x_2	X
10	.0276	.0075	.035	.00276	.114	.117
2.0	.109	.038	.147	.0503	.114	.164
1.0	.143	.075	.218	.109	.114	.223
.50	.174	.150	.324	.154	.114	.268
.20	.309	.375	.684	.176	.114	.290

The units of R and X are in p.u. referred to the stator circuit at 60 cycles.

The values in Table 5.2 are now used to plot X versus R as in Fig. 5.3. It is seen that the resulting locus does not fit the constant torque circle. To correct this an additional .06 ohms p.u. reactance at 60 cycles referred to the stator is placed in series with the rotor network. Let this additional series reactance be X_4. Table 5.2 is now altered to become Table 5.3 as follows:

Table 5.3

Modified Components of the Rotor Circuit Impedance

(Referred to stator circuit)

S	R	X	X_4	$X + X_4$
10	.035	.117	.06	.177
2.0	.147	.164	.06	.224
1.0	.218	.223	.06	.283
.50	.324	.268	.06	.328
.20	.684	.290	.06	.350

The values of R and $(X + X_4)$ obtained from Table 5.3 are plotted in Fig. 5.3. The result is a rotor network which results in a one per unit torque (within 5%) from a slip of 2 to a slip of approximately .2 per unit.

It must be recalled that the constant torque circle of Fig. 5.3 is based on equation 5.10. The Thevenin equivalent voltage V_e was taken to be 1 p.u. Reference to equation 5.1 shows that V_1 must be greater than 1 p.u. for V_e to equal 1 p.u. Consequently, the unity torque circle of Fig. 5.3 represents approximately 125% rated brake torque for this machine.

Fig. 5.4 shows the synthesized rotor network. All results are with reference to the stator.

The motor base impedance is 12 ohms and the ratio of transformation is 1.29:1 as found in Appendix A. Fig. 5.5 shows the rotor network with reference to the rotor circuit at 60 cycles.

Rotor network resistances were constructed of #18 nichrome wire which has a resistance of .424 ohms per lineal foot.

Since the current carrying capacity of the rotor network must equal the per phase current of the motor, physically large reactors were required in its construction. This, coupled with the

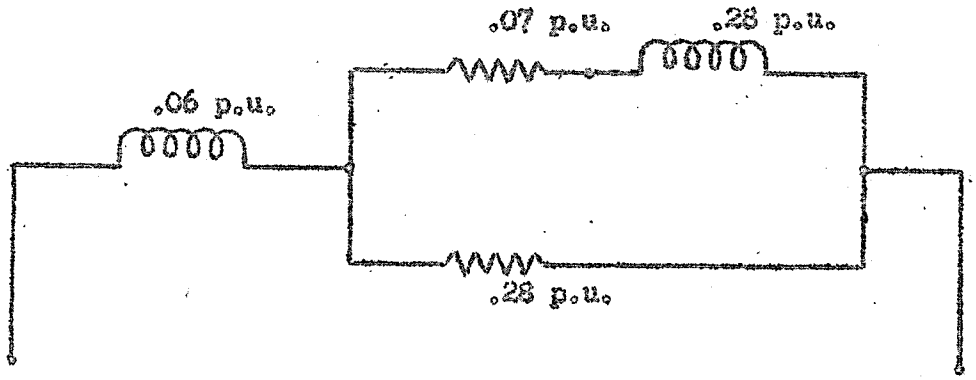

ROTOR NETWORK REFERRED TO STATOR AT 60 ~

FIGURE 5.4

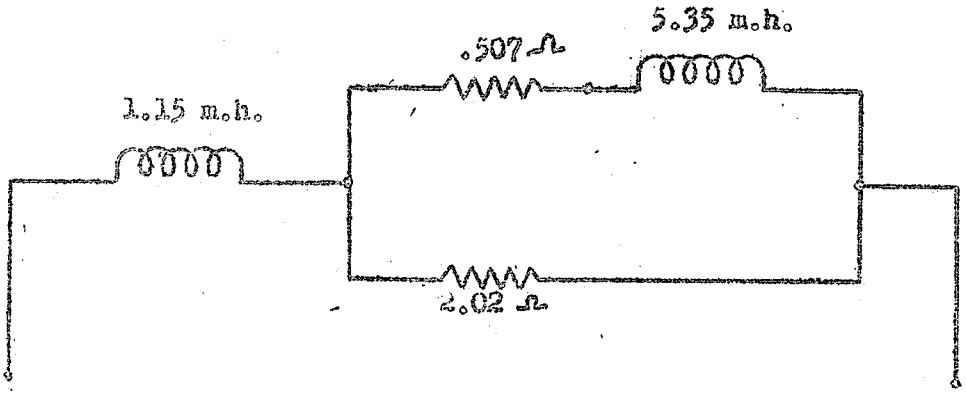

FIGURE 5.5 ACTUAL ROTOR NETWORK

fact that the required reactances were not available led to the decision to use the variable reactors in the A.C. Lab. Each individual reactor contains a number of coils which could be connected in either series or parallel, or both. With all coils in parallel it was found that the resistance measured with a "ducter" was negligible compared with the resistances present in the rotor network. The reactors were adjusted to have the required a.c. impedance at 60 cycles by use of a variac, ammeter, and voltmeter. The adjustment of the reactors was carried out at rated rotor current, and no appreciable saturation was noted.

5.3 SATURABLE REACTOR CONTROL WINDING VOLTAGE SUPPLY

As pointed out in Chapter IV, control of the power modulator is effected by variation of the d.c. control voltage to the control winding of a saturable transformer. The rating of the control winding was such that a control current of 1000 ma d.c. would fully saturate the transformer when the power windings carried no current. This magnitude of current can be readily supplied by grid controlled gas-filled rectifiers. Numerous circuits are available for supplying current to a resistive and inductive load (control winding of a saturable reactor) by controlled rectifiers. The one chosen for this purpose[5.1] is shown in Fig. 5.6.

The thyratrons selected were a type 3C23, with characteristics reproduced in Figs. 5.8 and 5.9. This selection was based on peak inverse voltage rating, tube current rating, reasonable cost, and availability. Theoretical voltage and current waveshapes are drawn in Fig. 5.7.

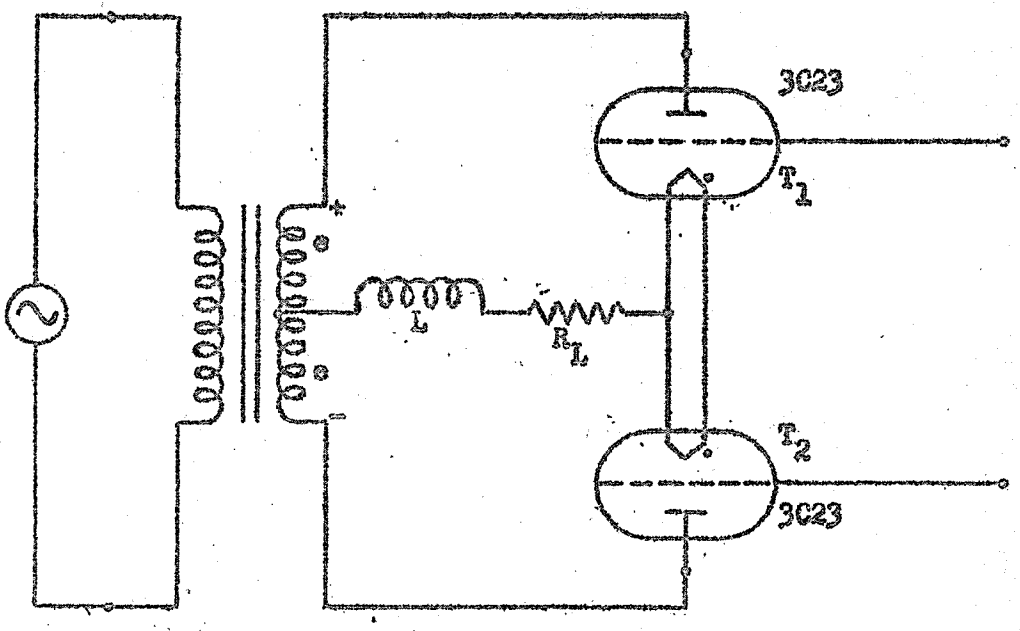

FIGURE 5.6 CONTROL OF SATURABLE REACTOR CONTROL WINDING CURRENT

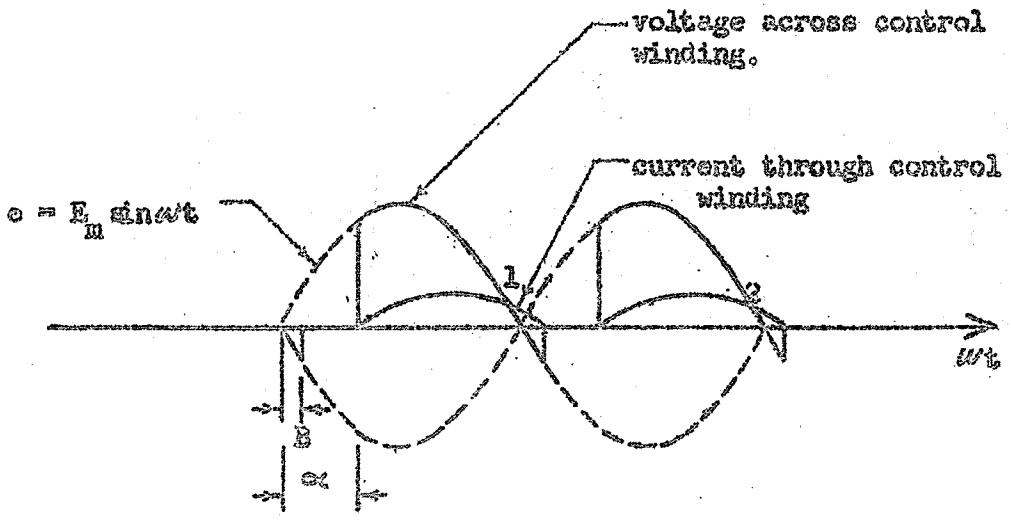

FIGURE 5.7

WAVE FORM OF CONTROLLED RECTIFIER IN DISCONTINUOUS OPERATION

3C23

3C23

GAS-AND-MERCURY-VAPOR THYRATRON

	Operating Condensed-Mercury Temperature Range -40° to +100°C	-50° to +80°C	
GRID VOLTAGE:			
Peak or DC, before tube conduction	-500 max.	-500 max.	volts
Average▲, during tube conduction	-10 max.	-10 max.	volts
ANODE CURRENT:			
Peak	6 max.	6 max.	amp
Average●	1.5 max.	1.5 max.	amp
Fault, for duration of 0.1 second max.	120 max.	120 max.	amp
GRID CURRENT:			
Average◆	+0.01 max.	+0.01 max.	amp

▲ Averaged over one conducting period.
● Averaged over any interval of 5 seconds maximum.
◆ Averaged over period of grid conduction.

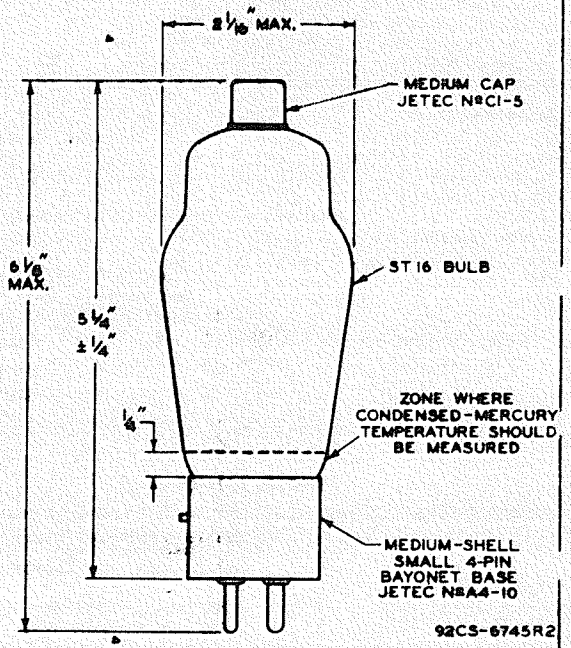

4-56 DATA

TUBE DIVISION
RADIO CORPORATION OF AMERICA, HARRISON, NEW JERSEY

FIGURE 5.8

THYRATRON CHARACTERISTICS

3C23

3C23

GAS-AND-MERCURY-VAPOR THYRATRON

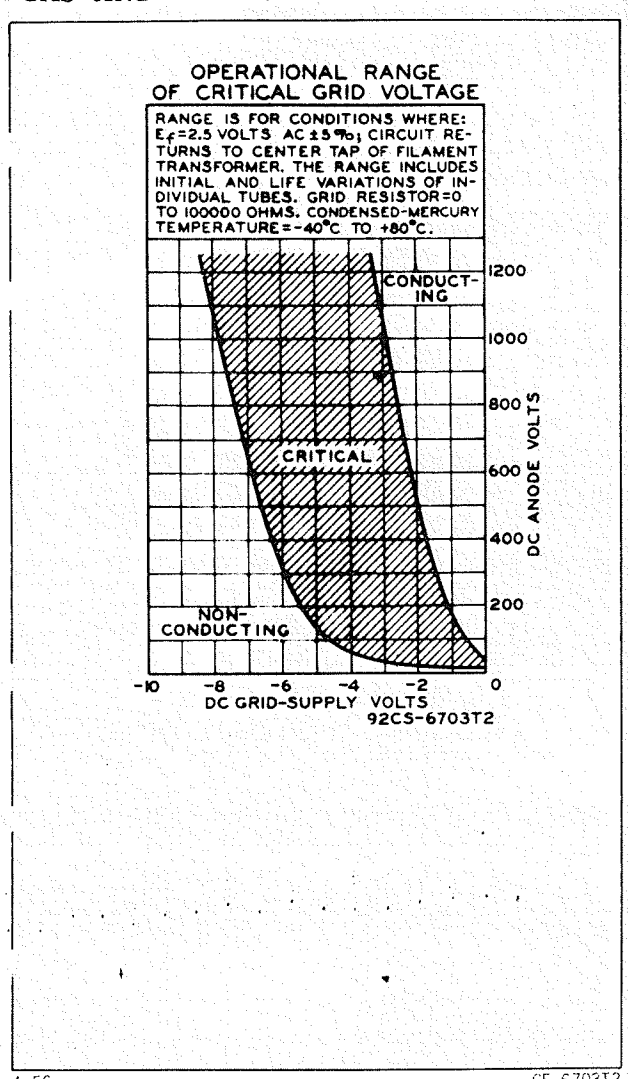

4-56

TUBE DIVISION
RADIO CORPORATION OF AMERICA, HARRISON, NEW JERSEY

CE-6703T2

FIGURE 5.9

THYRATRON CHARACTERISTICS

Reference to Fig. 5.7 will show that commutation from one tube to another does not necessarily take place as the supply voltage passes through zero. The tube "coming in" may be prevented from firing by a sufficiently negative grid voltage. As the supply voltage passes through zero the current through the conducting tube is not yet zero. Sufficient induced voltage is produced across the inductance by a negative current derivative to continue conduction. This conduction is possible only until the current reaches zero (assuming the tube voltage drop to be negligible), when conduction through the tube must stop.

If the conducting tube has already extinguished before the second tube fires, there is a period during each half cycle when neither tube conducts and the voltage across the load is zero.

Inspection of Fig. 5.7 shows that two angles are required to specify the operation. The angle α is measured in a particular half cycle at which the tube starts conduction. The angle β is the point in the same half cycle at which the preceding tube ceases conduction. It is not possible for $\beta > \alpha$ since the preceding tube is forced to cease conduction when a new tube starts if it has not already done so.

The values of average voltage and current are given as follows:[5.2]

$$E_{dc} = \frac{E_m}{\pi} (\cos\alpha + \cos\beta) \qquad 5.15$$

$$I_{dc} = \frac{E_m}{\pi R_L} (\cos\alpha + \cos\beta) \qquad 5.16$$

where E_m = peak value of rectified voltage

and R_L = control-coil resistance.

A saturable transformer was tested with the power windings open circuited. It was found that a potential difference of 100 volts d.c. applied across the control winding caused rated current to circulate through the winding. This indicated a control winding d.c. resistance of 100 ohms. Therefore, the thyratron supply must be capable of supplying d.c. voltages in the ranges $0 \leq V_{dc} \leq 100$ volts. Control voltages lying within this range will vary the output impedance of the saturable transformer between zero and infinity as discussed in section 4.1.

In providing 1000 ma to the control coil it would be undesirable to have the thyratron conduct for 180-degrees since control coil current would approach this value exponentially upon sudden loading, and the transient response of the over-all system would be relatively slow. In order to improve the transient response, the plate supply transformer was so chosen that for 180-degree conduction of the thyratron, the average load current would be 2000 ma. Under these conditions, the transient rise in load current would reach 1000 ma in a much shorter time.

If 2000 ma is selected as the load current under 180-degree conducting conditions, the secondary voltage rating for half the secondary of the plate transformer may be calculated by use of equation 5.16, as follows:

$$2 = \frac{E_m}{\pi 100} (\cos \alpha + \cos \beta)$$

but $\alpha = \beta = 0°$ for 180-degree conduction,

therefore

$$2 = \frac{E_m}{\pi 100} (1 + 1)$$

or $E_m = 314$ volts.

and $E_{r.m.s.} = \frac{314}{\sqrt{2}} = 222$ volts.

For a full wave rectifier with a R-L load, the utilization factor[5.3] is as follows:

$$VA = 1.11\ E_{dc}\ I_{dc}$$

where E_{dc} is the average load voltage

and I_{dc} is the average load current.

For full-load conditions $E_{dc}\ I_{dc} = 100 \times 1 = 100$ watts.

Therefore the transformer rating should be

$$1.11 \times 100 \simeq 110\ VA$$

A transformer conforming with calculated voltage and power requirements was not available, and a makeshift arrangement was undertaken as outlined in Appendix B.1.

5.4 THYRATRON TRIGGERING

Thyratron output is controlled by a combination of d.c. amplitude control and a.c. phase shift. A phase shifted alternating voltage which has the same frequency as the plate supply is superimposed on the unidirectional grid voltage as shown in Fig. 5.10(a) and (b). The alternating grid voltage lags the anode voltage by an angle θ. By varying the magnitude of the unidirectional grid voltage between fixed positive and negative values the tube current can be varied as shown in Fig. 5.10 (a) and (b).

The phase shifting network consists of the usual R-C combination found in standard circuit designs. Fig. 5.11(a) and (b) illustrates the schematic equivalent circuit of the network and the corresponding vector diagram. The network parameters are

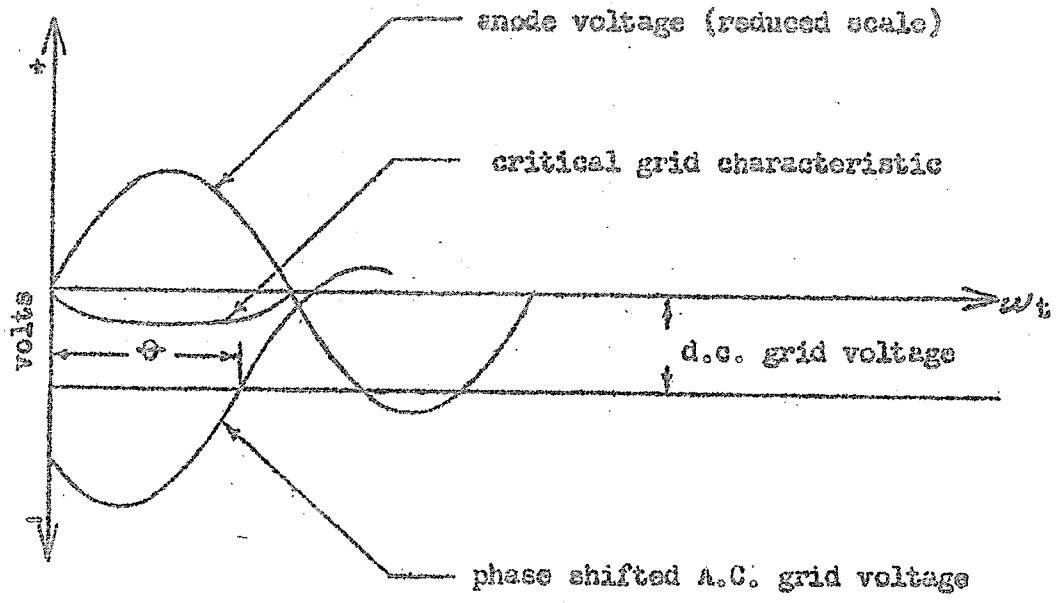

(a) Thyratron Extinguished

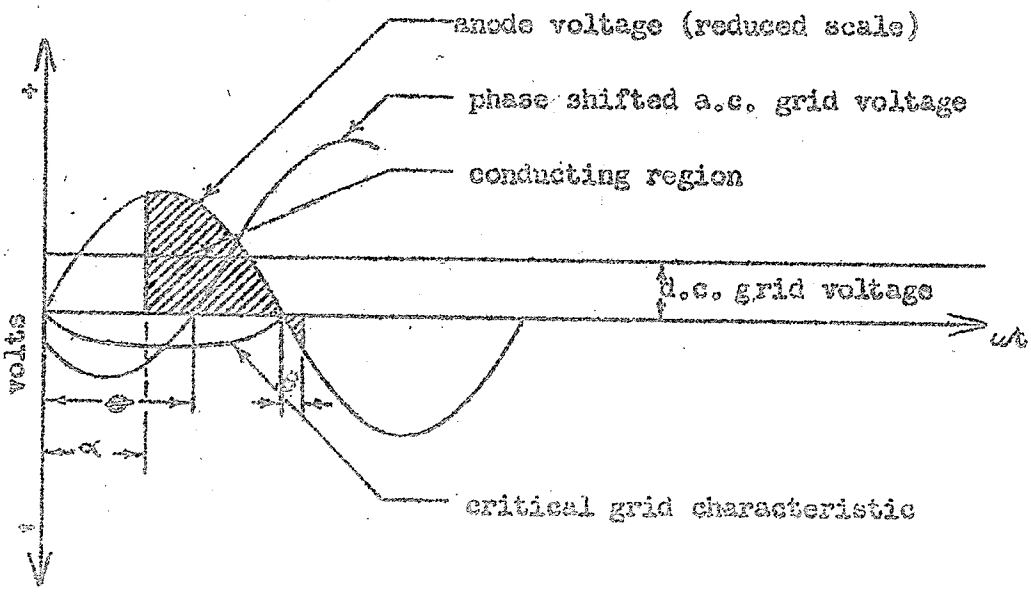

(b) Thyratron Conducting

FIGURE 5.10 THYRATRON TRIGGERING

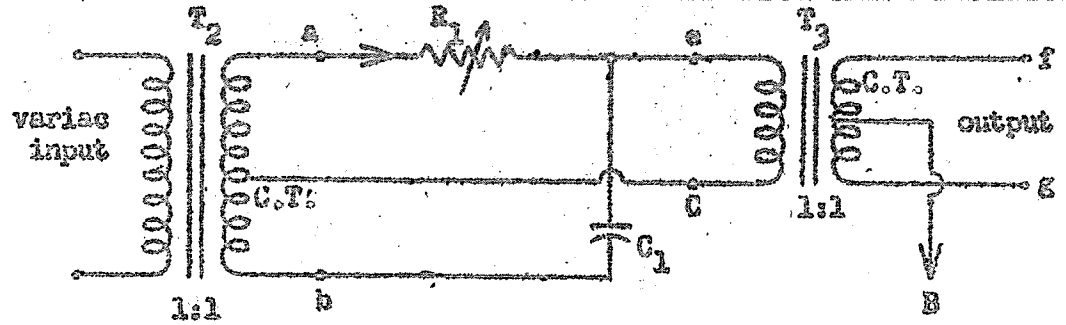

(a) Phase Shifting Circuit

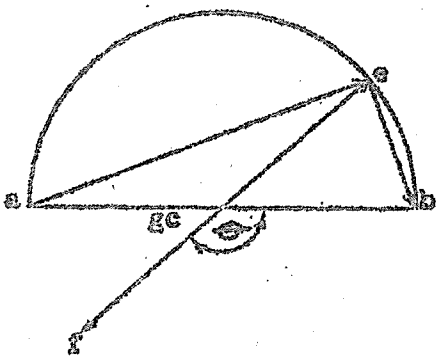

(b) Vector Diagram of Phase Shifting Circuit

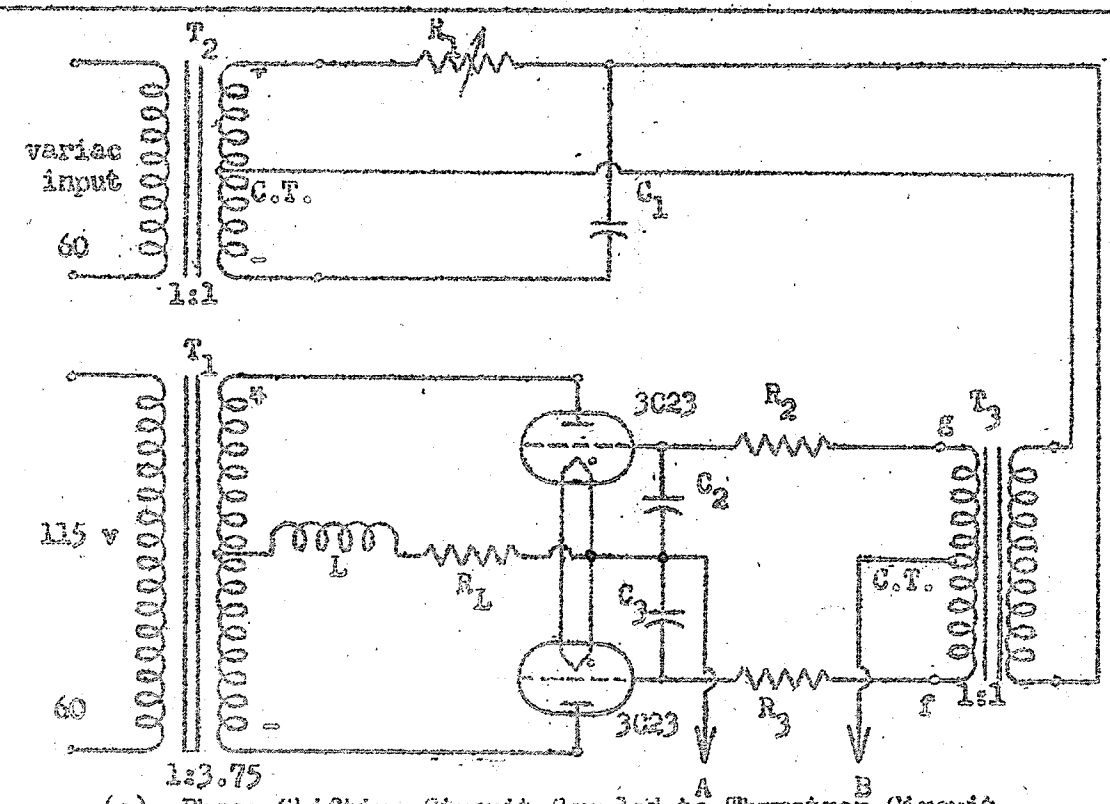

(c) Phase-Shifting Circuit Coupled to Thyratron Circuit

FIGURE 5.11 CONTROL OF THYRATRONS

obtained from Appendix B.2. In Fig. 5.11(b) the voltage V_{ce} leads voltage V_{ab} by 45°. Transformer T_3 is so connected that the secondary voltage V_{fg} lags voltage V_{ab} by 135°. (See the discussion in Appendix B.2).

The output voltage of the phase shifting circuit is coupled to the thyratron grids through protective resistors R_2 and R_3 as shown in Fig. 5.11(c). The resistors R_2 and R_3 have two purposes:

1. To limit the grid current before and after the tubes conduct.
2. To discharge from the grid capacitors any voltage accumulated on them because of surges in the anode circuits.

Selection of the resistors R_2 and R_3 requires a compromise. To perform the first function the resistor should be large, but to perform the latter they should be small. It is also necessary to avoid loading the phase shifting circuit. The tube characteristics reproduced in Fig. 5.8 and 5.9 indicate a choice of 0 to 100 K ohms for R_2 and R_3. It was decided to use approximately 50K ohms for each resistor.

The functions of capacitors C_2 and C_3 shown in Fig. 5.11(c) are to prevent the respective tubes from "shocking-over" or conducting if sudden voltage transients occur in the anode circuit. A pair of 600 pfd capacitors were found to function satisfactorily.

As mentioned previously, the tube current, and thus the load current, can be varied by varying the magnitude of the unidirectional tube grid voltage. This voltage is introduced between points "A" and "B" in Fig. 5.11.

It is shown in appendix B.4 that if the output voltage of

the phase shift network is 15 volts peak to peak, then the thyratron output can be controlled by varying the unidirectional voltage between points "A" and "B" between + 8 and -15 volts with reference to point "A". Fig. B.5 of Appendix B shows that zero to full load current is available for approximately half the firing range of the thyratrons.

5.5 AMPLIFIER

The system thus far developed has provided a means of varying the control-coil current in the power modulator by varying the magnitude of the d.c. component of the thyratron grid voltage.

This d.c. component of thyratron grid voltage was obtained by the use of a vacuum tube amplifier. The vacuum tube should have the following properties:

1. A high amplification factor (μ).
2. A normal current-carrying capacity of at least 10 ma.
3. Linear transfer characteristics in order to decrease steady-state error.

The amplifier circuit shown in Fig. 5.12 utilizes a 12AT7 duo-triode. All circuit parameters are obtained from Appendix B.5.

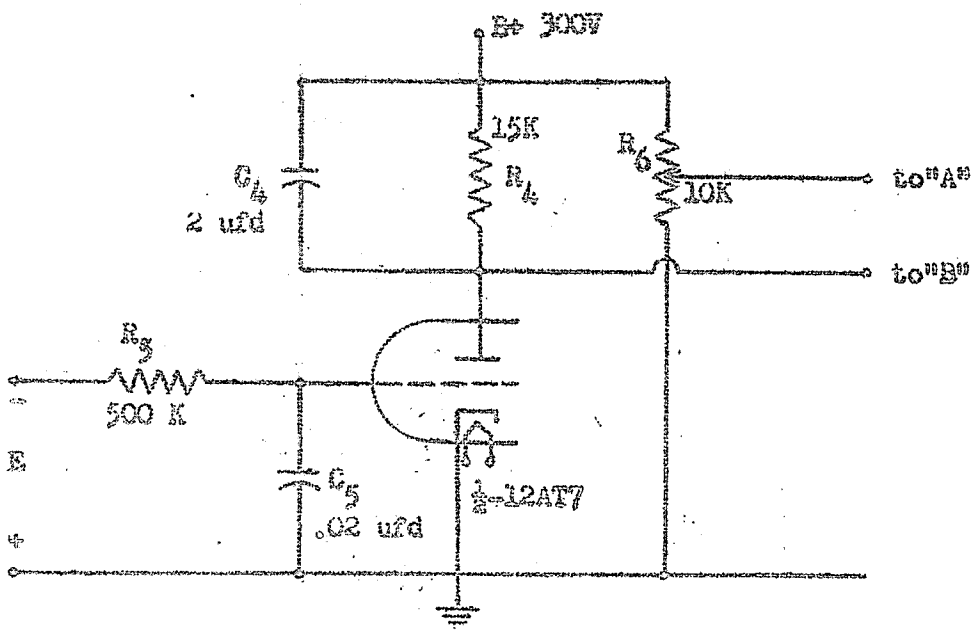

FIGURE 5.12 AMPLIFIER CIRCUIT

The potentiometer R_6 acts as a voltage divider which supplies a constant positive direct voltage to point "A" of the thyratron grid circuit shown in Fig. 5.11(c). A variable negative direct voltage is obtained across R_4 and is supplied to point "B" of Fig. 5.11(c).

Reference to Figs. 5.10 and 5.12 shows that the firing angle of the thyratrons is delayed when the plate current of the 12AT7 is increased. Conversely, the firing angle of the thyratron is advanced when the plate current of the 12AT7 is decreased.

The plate current of the 12AT7 is a function of the voltage E applied to the grid. The grid input voltage E is furnished by a comparator circuit which will be discussed in section 5.6.

5.6 COMPARATOR

Fig. 5.13(a) shows a difference amplifier circuit proposed by Millman and Taub.[5.4] In this circuit a signal R is applied directly to the grid of tube T_2 and a second signal B is applied to the cathode through the cathode follower T_1. Both R and B are voltage signals.

Fig. 5.13(b) shows the equivalent circuit diagram where each tube has been replaced by its equivalent impedance looking back into the cathode. The output voltage E_o is I_2R_7. The presence of R_8 may be entirely neglected if $(u + 1) R_8 \gg r_p$. For a 12AU7-A triode $(u + 1) \cong 20$ and $r_p \cong 10$ K ohms. If R_8 is large then reference to Fig. 5.13(b) shows $I_1 = I_2$. The output is exactly proportional to the difference (B - R). The

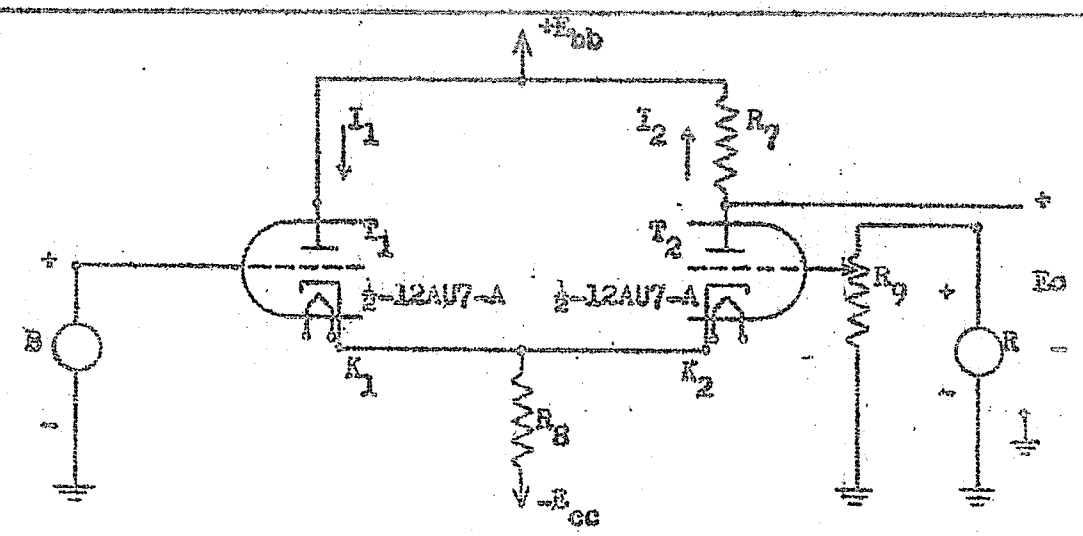

FIGURE 5.13(a) DIFFERENCE AMPLIFIER

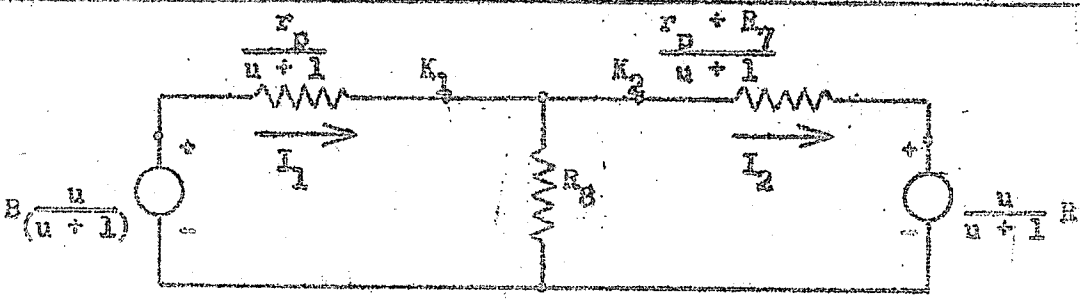

FIGURE 5.13 (b) EQUIVALENT CIRCUIT OF DIFFERENCE AMPLIFIER

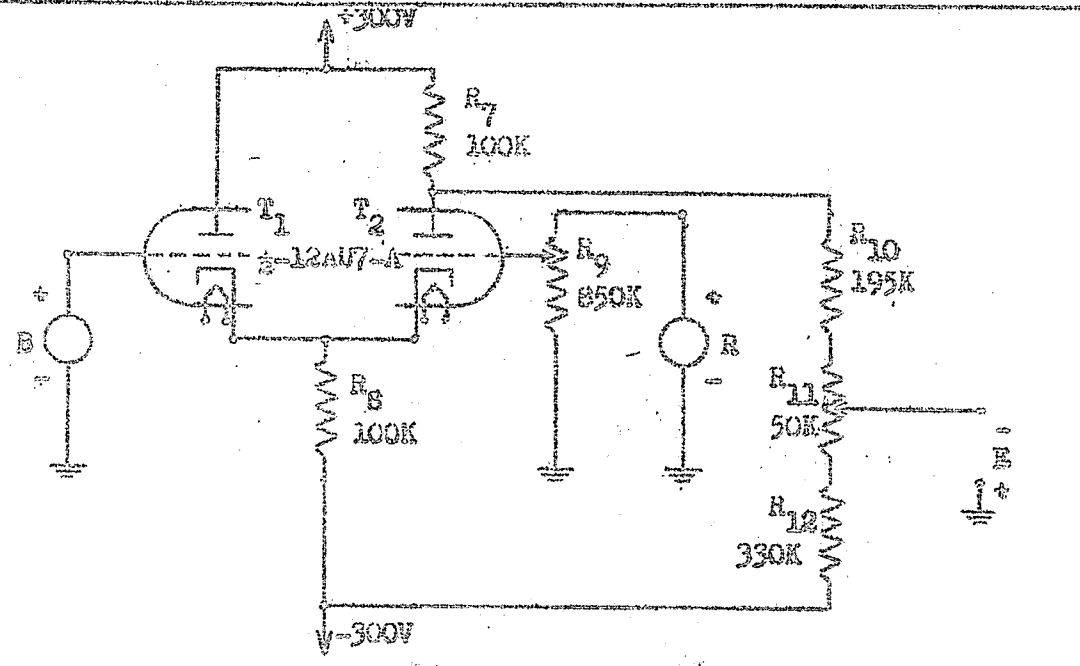

FIGURE 5.13 (c) MODIFIED DIFFERENCE AMPLIFIER

output voltage E_o is given by:[5.4]

$$E_o = \frac{u R_L (B - R)}{(2r_p + R_L)}$$

If R is an applied reference voltage, and B is a voltage which is proportional to the speed of the drive, then E_o can be varied by varying R. If R changes, E_o will also change.

The circuit of Fig. 5.13(a) is modified as shown in Fig. 5.13(c). An adjustable voltage E is available at the output of the circuit, and is applied to the input of the amplifier circuit shown in Fig. 5.12. The potentiometer R_{11} may be adjusted so that the output voltage E varies within the prescribed range estimated in Appendix B.5.

The voltage R was chosen variable within the range 0 to 2 volts, and B was variable within the range 0 to .5 volts. The adjustment of E was left to be made under actual closed-loop operation of the drive.

The circuit parameters are a variation of those proposed by Millman and Taub.[5.4] Iterative procedure led to a choice of parameters as shown in Fig. 5.13(c). The circuit was tested and found to operate satisfactorily.

5.7 ANTI-HUNT CIRCUIT.

Sustained oscillations which occur in a high-gain closed-loop system are referred to as hunting. If system amplification is high, over-shoot may result, and sustained oscillations may develop. A damping or "anti-hunt" arrangement must then be used to stabilise the system. A damping system

should respond to the rate of change of one of the quantities involved in such a manner that a change in that quantity will create a transient damping force acting in the direction opposite to that of the restoring force.

An anti-hunt circuit was built into the system. The design of the circuit is given in Appendix B.6. The effect of the circuit on thyratron operation will be discussed in section 5.8.

5.8 CONTROL CIRCUIT OPERATION

Fig. 5.14 shows the circuit that controls the power modulator. If the action of the anti-hunting circuit is neglected for the moment, it is seen that a slight decrease in motor speed (i.e. a decrease in B) will cause the output E of the comparator circuit to become more negative. Consequently, the amplifier tube current will decrease and the potential of point "B" will increase with respect to point "A". The angle of thyratron ignition will be advanced causing an increase of control current to the power modulator. The power modulator will then supply additional power to the 3-phase motor, so as to oppose the change in motor speed.

The anti-hunting circuit consists of a current transformer T_4, a 6H6 rectifier, resistors R_{13}, R_{14}, R_{15}, and condenser C_6. A direct voltage proportional to power modulator control current appears across R_{14}. Capacitor C_6 blocks any d.c. voltage component from appearing in the grid circuit of the amplifier. Under unstable conditions the system will tend to oscillate and the current through the power modulator control-coil

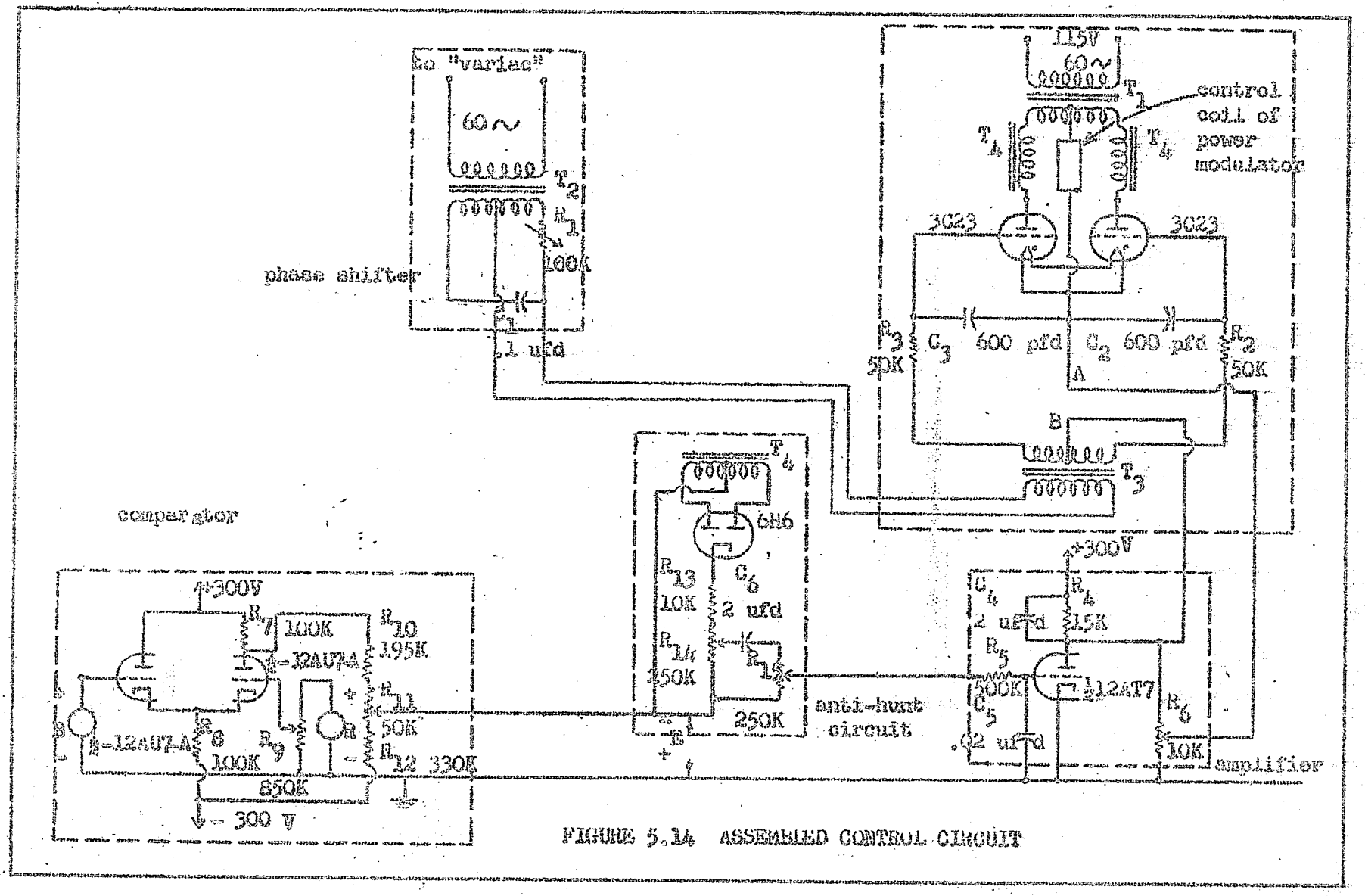

FIGURE 5.14 ASSEMBLED CONTROL CIRCUIT

will be subject to a rapid change. This change in current is reflected through the current transformer T_4, and results in a change in voltage across R_{14}. Capacitor C_6 will cause a transient current to flow in the circuit consisting of C_6, R_{14}, and R_{15}. Capacitor C_6 will either charge or discharge, depending on the sign of the rate of change of the voltage across R_{14}. The magnitude of the rate of change of the voltage across R_{14} is dependent upon the magnitude of the rate of change of current through the power modulator control coil. During the duration of this transient a damping voltage will appear across R_{15}. If, say, the control current to the power modulator is increasing, it is seen that the voltage across R_{14} will increase in the same way. This will cause a transient current to flow through C_6, R_{15}, and R_{14} in that order. Momentary positive voltage will appear in the grid circuit of the amplifier, the magnitude of this voltage being dependent upon the setting of R_{15}. An increase of amplifier tube current will occur, delaying the angle of ignition of the thyratrons momentarily, and thus damping the system.

CHAPTER VI

PERFORMANCE OF THE DRIVE

6.1 INTRODUCTION

The functions of the various elements and the idealized performance of the drive have been discussed through Chapters I to V.

The drive was assembled, and experimental results were obtained. Fig. 6.1 shows the assembled drive in block diagram form.

6.2 OPEN-LOOP MOTOR SPEED-TORQUE CHARACTERISTICS

The system loop was opened, and the three phase induction motor was tested on a dynamometer. Speed-torque characteristics were determined for the following motor secondary connections:

(a) The three rotor phases were wye connected.

(b) A rotor network was inserted into each phase of the motor secondary, and the networks were then wye connected.

In both cases, the induction motor stator circuit was supplied from a balanced three phase source. Due to dynamometer limitations, the motor stator voltage supply was limited to approximately 50% of rated stator terminal voltage.

Results obtained from tests (a) and (b) are tabulated in Tables 6.1 and 6.2.

The dynamometer scale was marked in pounds with scale subdivisions of .1 pounds. Since the weighing arm was 6 inches

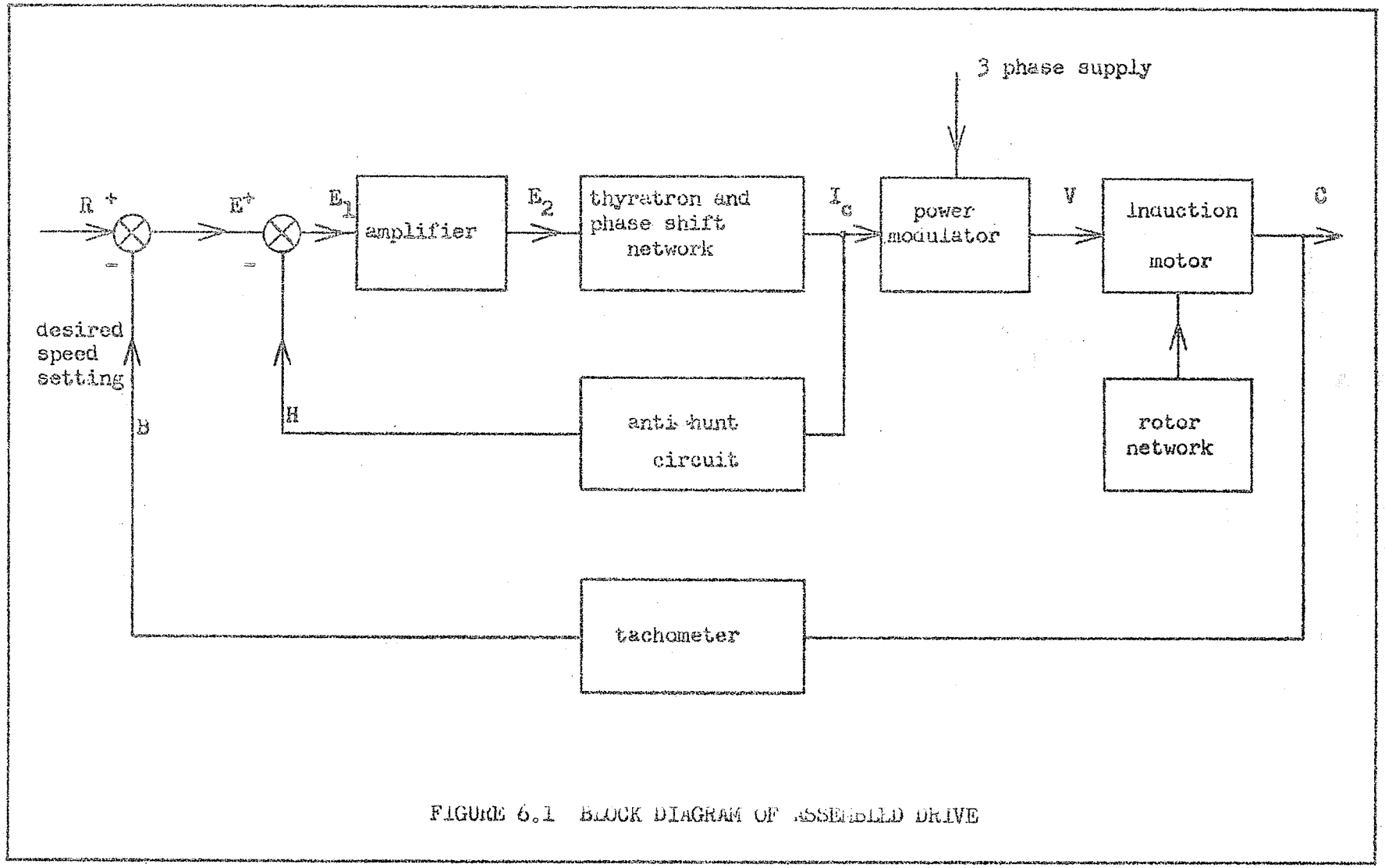

FIGURE 6.1 BLOCK DIAGRAM OF ASSEMBLED DRIVE

long, the torque in foot-pounds was obtained by dividing the scale reading by 2. The stator voltage supply was 50 volts line to line. The torque measured on the dynamometer was corrected to the value which would have been measured if the motor had been supplied with rated terminal voltage, neglecting saturation. The correction was applied as follows:

Let V_m be the applied stator line to line voltage.

Let V_r be the rated stator line to line voltage.

Let T_m be the total 3 phase torque measured on the dynamometer.

Let T_r be the total 3 phase shaft-torque at rated stator line to line voltage.

Then

$$T_r = T_m \left[\frac{V_r}{V_m}\right]^2 \qquad 6.1$$

Equation 6.1 is only exact if T_r and T_m are the internal electromagnetic developed torques. Since, T_m is measured at the motor shaft, T_r will not vary exactly as $\left[\frac{V_r}{V_m}\right]^2$. However, the discrepancy is small, and was neglected. The following is a sample calculation based on information found in Table 6.1:

Motor speed 1055 rpm.

Dynamometer scale reading 2.0 pounds.

Motor stator terminal volts 50 volts line to line.

Whence, the corrected torque is $2 \times \frac{1}{2} \times \left[\frac{110}{50}\right]^2 = 4.84$ ft.-lbs.

Table 6.1

Motor Speed-Torque Characteristics

(rotor network out)

Stator voltage - 50 volts line to line

Motor speed r.p.m.	Dynamometer Scale Rdg. lbs.	Motor Shaft-Torque ft. - lbs.	Corrected Motor Shaft-Torque ft. - lbs
1140	0.00	0.00	0.00
1130	0.75	0.375	1.82
1120	1.00	0.500	2.42
1100	1.25	0.625	3.03
1080	1.50	0.750	3.64
1070	1.75	0.875	4.25
1055	2.00	1.00	4.84
1030	2.25	1.13	5.46
1010	2.50	1.25	6.05
940	3.00	1.50	7.25
850	3.25	1.63	7.90
800	3.30	1.65	8.00
	unstable region		
- 810	2.50	1.25	6.05
-1000	2.45	1.23	5.85
-1200	2.35	1.17	5.65
-1300	2.30	1.15	5.55

Table 6.2

Motor Speed-Torque Characteristics

(rotor network in)

Stator volts - 50 volts line to line

Motor speed r.p.m.	Dynamometer Scale Rdg. lbs.	Motor Shaft-Torque ft. - lbs.	Corrected Motor Shaft-Torque ft. - lbs
1140	0.00	0.00	0.00
1090	0.50	0.25	1.21
1050	0.75	0.375	1.82
1010	1.00	0.500	2.42
980	1.25	0.625	3.20
900	1.50	0.750	3.62
660	1.75	0.875	4.24
110	2.00	1.00	4.84
0	2.25	1.13	5.42
- 40	2.55	1.28	6.28
- 100	2.60	1.30	6.30
- 220	2.65	1.33	6.45
- 660	2.70	1.35	6.54
- 800	2.70	1.35	6.54
-1000	2.75	1.38	6.65
-1100	2.75	1.38	6.65
-1400	2.80	1.40	6.78

Examination of Table 6.1 shows that an unstable operating region exists between approximately +800 and -800 r.p.m. Subsequently, no steady-state, speed-torque characteristic could be obtained in this region. The motor speed-torque data found in Table 6.1 are plotted in Fig. 6.2 and referred to as curve (1). The region of curve (1) between +800 and -800 r.p.m. has been estimated.

If stable motor operation had been obtainable through the region of zero speed, a discontinuity would have occured at zero speed. This discontinuity is due to dynamometer losses and to "stiction" (nonlinear friction). For induction motor speeds greater than zero, the shaft output torque read from the dynamometer

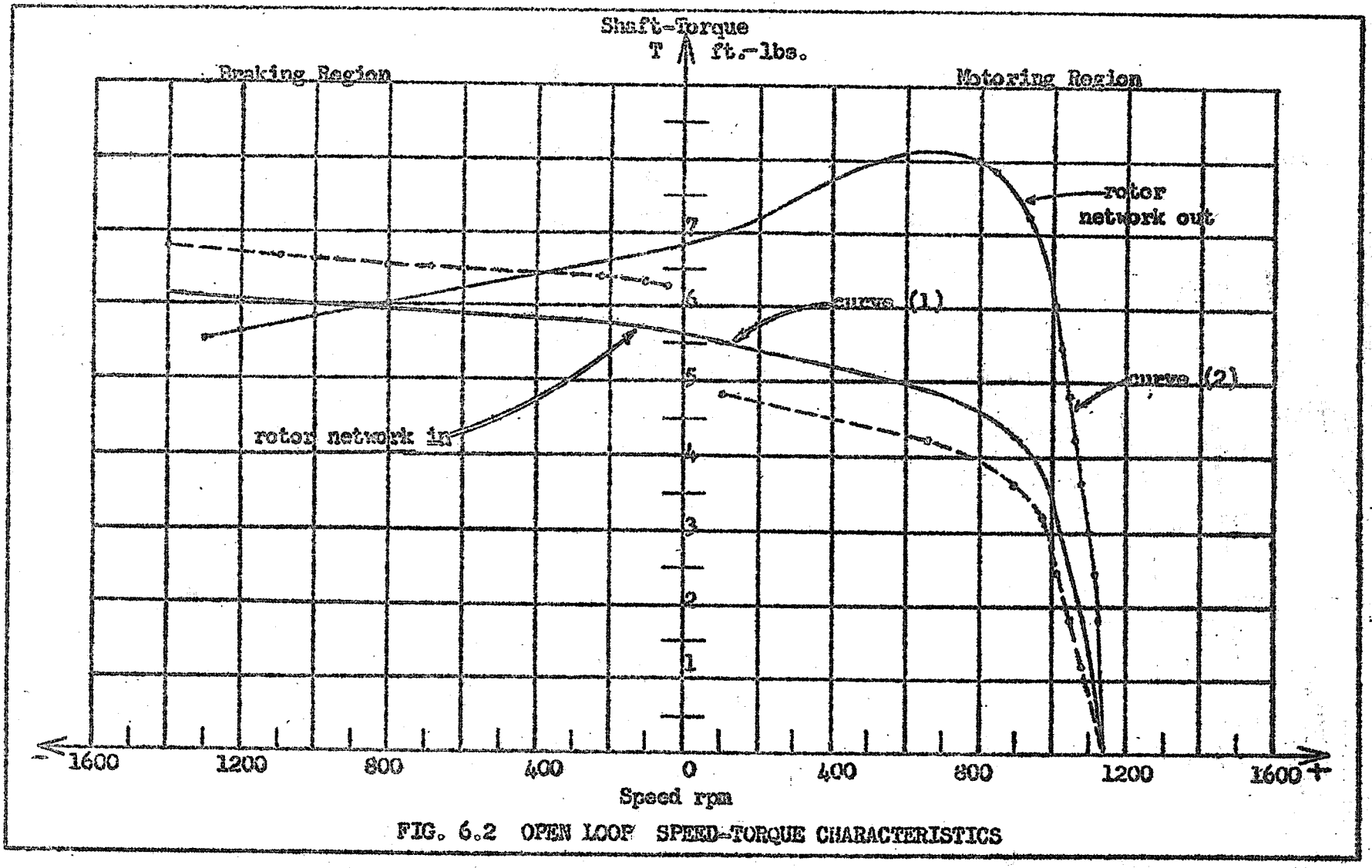

FIG. 6.2 OPEN LOOP SPEED-TORQUE CHARACTERISTICS

scale will be low by the amount of the losses incurred in the braking motor. When the induction motor behaves as a brake (i.e. the reverse speed region), the shaft-torque read from the dynamometer scale will be high by the amount of the losses incurred in the dynamometer. Since, the region between +800 and -800 r.p.m. has been approximated, curve (1) will not be corrected.

Data obtained from Table 6.2 are plotted as the broken line characteristic in Fig. 6.2. As predicted in Chapter III, the motor speed-torque characteristic exhibits a rising negative slope, and permits stable operation at any motor speed throughout both the driving range and the counter-torque range. As discussed earlier, there is a discontinuity in the speed-torque characteristic at zero speed. If the negative segment of the speed-torque characteristic is extrapolated to zero speed, the torque discontinuity may be approximated.

Half the torque discontinuity at zero speed was subtracted from each ordinate plotted for the negative segment of the speed-torque characteristic. Conversely, the same amount of torque was added to each ordinate plotted for the positive segment of the speed-torque characteristic. The resultant, curve (2) is continuous through zero speed and has a rising negative slope.

For speeds in excess of approximately 70% synchronous speed, comparison of curves (1) and (2) of Fig. 6.2 shows that the motor develops a greater shaft-torque in the absence of the rotor network. For speeds less than approximately 70% synchronous speed, the motor exhibits unstable operation if no compensation is introduced into the rotor circuit. Although the rotor network

ensures open loop stability through both the driving and counter-torque range, examination of Fig. 6.2 shows that the available shaft-torque has been decreased by approximately 50% for speeds in excess of 70% synchronous speed.

6.3 CLOSED-LOOP MOTOR SPEED-TORQUE CHARACTERISTICS

The system loop was closed, and the anti-hunt circuit was adjusted to a limiting setting, beyond which motor oscillations occurred. This adjustment was carried out under no-load conditions. Since the system was stable under no-load conditions, then it would certainly be stable under loaded conditions since some of the components in the system would operate at greater saturation.

The drive was then tested on a dynamometer with various settings of speed and initial torque load. Tests were performed for both the driving and counter-torque regions.

A brief description of the method of testing in the driving region is as follows. The drive was adjusted to deliver an initial torque at a chosen speed. The torque load was then increased to a new value. Subsequent to this change in torque, the drive experienced a speed transient. The new steady-state speed was then measured. An increased value of torque load was then applied, and the procedure was repeated until the torque limit of the drive was reached. Any attempt to increase the torque load beyond this point led to a decrease in drive speed to zero and ultimate drive reversal. Once the torque limit of the drive had been reached, the drive speed was readjusted to the speed and torque load chosen initially in the test. The torque load was then

reduced and the steady-state speed for each step in torque reduction was recorded. Several tests for various conditions of initial torque and speed were conducted in the driving region. Similar tests were conducted in the braking region. These tests differed only from those in the driving region in that the induction motor was now supplying braking torque rather than motoring torque.

Results obtained in the driving range and counter-torque range are recorded in Table 6.3. Values of initially chosen torque load and speed are denoted by a raised asterisk.

Table 6.3

Steady-State Speed Versus Torque Characteristics of Complete Drive for Various Settings of Desired Speed and Torque.

Motor Speed r.p.m.	Motor Shaft-Torque ft.-lbs.
1100*	1.00*
1090	1.50
1060	2.00
1010	2.50
940	3.00
850	3.25
1120	0.75
1140	0.50
1000*	2.00*
980	2.50
900	3.00
820	3.25
1020	1.50
1040	1.00
1140	0.50

Table 6.3 (continued)

Motor Speed r.p.m.	Motor Shaft-Torque ft.-lbs.
800*	2.00*
790	2.50
730	3.00
650	3.25
800	1.50
880	1.00
700*	1.50*
690	2.00
660	2.50
600	3.00
500	3.25
740	1.00
800	0.75
1140	0.50
500*	1.75*
490	2.00
460	2.50
410	3.00
340	3.25
510	1.50
600	1.00
1140	0.50
400*	2.00*
380	2.50
370	2.75
330	3.00
250	3.25
410	1.75
420	1.50
500	1.00
200*	1.75*
200	2.00
200	2.50
180	2.75
150	3.00
100	3.25
200	1.50
240	1.00

Table 6.3 (continued)

Motor Speed r.p.m.	Motor Shaft-Torque ft.-lbs.
-1000*	2.00*
-1020	2.50
-1040	3.00
-1060	3.25
-1080	3.38
-1140	3.50
- 980	1.75
- 950	1.50
- 900	1.25
- 800*	2.00*
- 820	2.50
- 910	3.00
- 950	3.25
- 970	3.38
-1040	3.50
- 750	1.50
- 600	1.00
- 600*	2.00*
- 610	2.50
- 620	3.00
- 640	3.25
- 700	3.50
- 580	1.75
- 550	1.50
- 400*	2.00*
- 410	2.50
- 430	3.00
- 470	3.25
- 530	3.50
- 350	1.50
- 300	1.25
- 200*	2.00*
- 210	2.50
- 220	3.00
- 300	3.50
- 150	1.50

Steady-state speed versus torque characteristics of the drive for various settings of desired speed and torque are shown in Fig. 6.3. The initial speed and torque setting on a given

characteristic is denoted by a cross.

Examination of Fig. 6.3 shows that load torques of less than .50 foot-pounds were not plotted. As the torque load was decreased, the system regulated motor speed by decreasing reactor control current. When torque load was decreased to approximately .5 foot-pounds, the reactor control current became negligibly small, and the motor reverted to single-phase operation. This behaviour had been predicted in section 4.5 of Chapter IV. Further system regulation was not possible beyond this point, and motor speed approached synchronous speed if the machine was initially operating in the driving region. Consequently, the speed torque characteristics in the driving region were projected to rated no-load motor speed. The motor reverted to single-phase operation for small values of torque in the braking region. Again, system regulation was not possible beyond this point and motor speed decreased. Moreover, the final speed of the motor could not be predetermined. It was possible for the motor to stall at zero speed or continue on to reversed speed, ultimately approaching synchronous speed in the driving region. As a result of this, the speed-torque characteristics measured in the braking region were not projected to ultimate values.

A review of section 6.2 will show that the ordinates of the measured values shown in Fig. 6.3 are low in the motoring region and high in the braking region. Correction of the speed-torque characteristics would produce the following results: in the motoring region, the speed-torque characteristics would exhibit a steeper slope for torques greater than the initial torque, while the

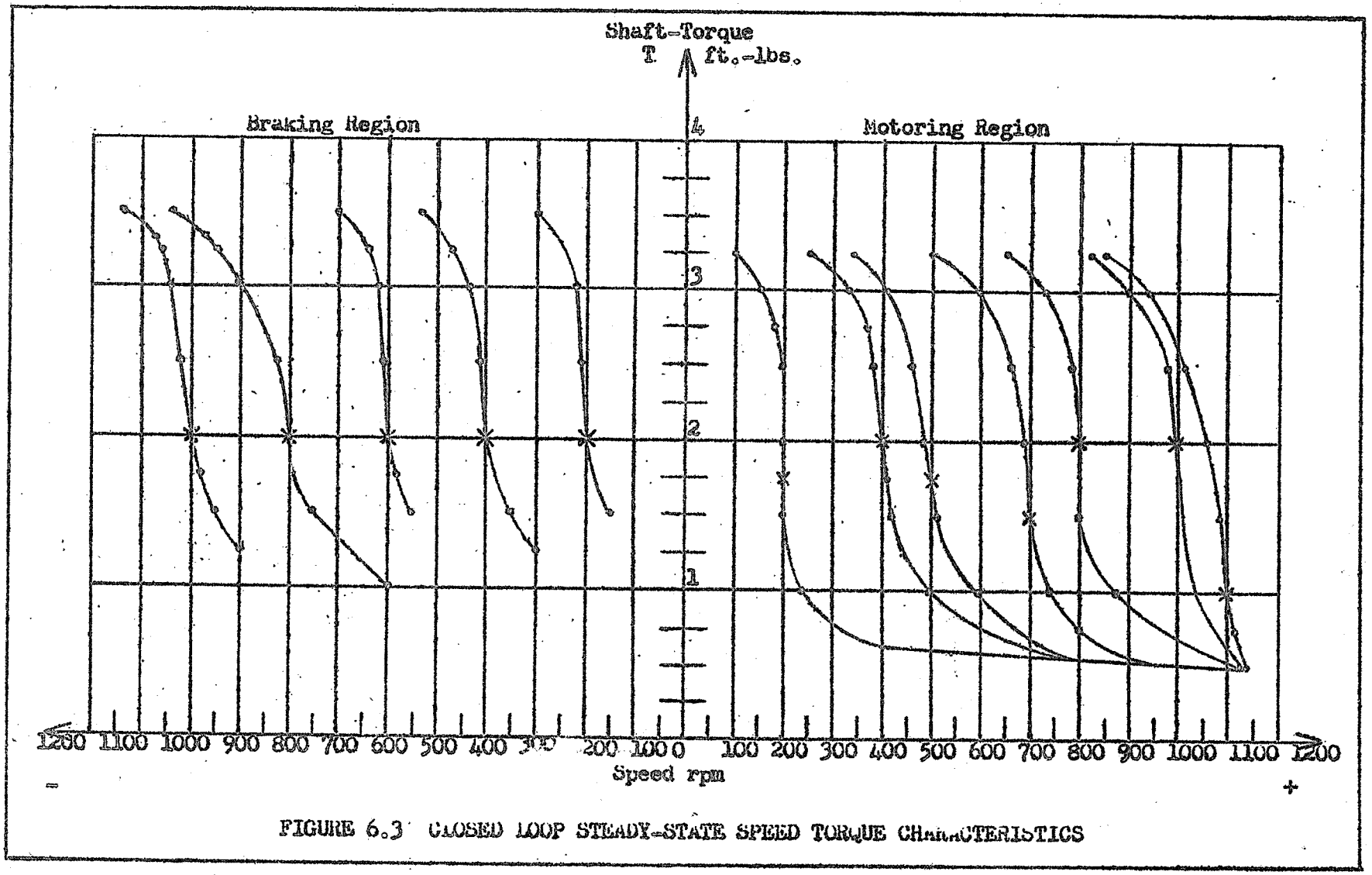

FIGURE 6.3 CLOSED LOOP STEADY-STATE SPEED TORQUE CHARACTERISTICS

slope would decrease for values of torque less than the initial value. In the braking region, the speed-torque characteristics would exhibit a steeper slope for torques less than the initial torque, while the slope would increasefor values of torque greater than the initial torque. In order to preserve the actual results obtained, the characteristics were not adjusted.

Examination of the characteristics of Fig. 6.3 shows that the speed regulation for torques ranging between 1 and 3 foot-pounds approaches an average of approximately 15%. This average neglects the presence of the characteristic drawn for an initial braking torque of 2 foot-pounds at a speed of -800 r.p.m. The shape of this characteristic suggests than an error was made in recording the results.

The speed regulation might have been decreased by the use of higher amplifier gain. The apparatus was required to be dismantled and the laboratory space vacated before this could be done.

6.4 TRANSIENT RESPONSE OF THE CLOSED-LOOP SYSTEM.

A number of tests were performed to assess the transient performance of the drive connected to a dynamometer load. A Sanborn 150 multi-channel recorder was used to obtain a permanent record of the test results.

Briefly, with reference to Fig. 6.1, the test procedure was as follows: the reference voltage R was set so that the drive operated at a given speed for a chosen value of torque load. The magnitudes of reference voltage R, tachometer feedback voltage B, and error signal E_1 were simultaneously recorded on a strip chart. Tachometer feedback voltage B was proportional to tachometer speed

as shown in Fig. C.1 of Appendix C.1.

The reference voltage R was then "stepped", and the transient behaviour of B and E_1 were simultaneously recorded. The tachometer feedback voltage B had a small superimposed generator noise voltage. This in itself did not affect the operation of the drive, but made the interpretation of the results difficult. The filter network shown in Fig. C.2 of Appendix C.2 was installed between the recording unit and the tachometer.

The transient speed response of the drive for a sudden change of reference voltage R is shown in Fig. 6.4. Inspection of Fig. 6.4 shows that the rise time of the speed characteristic is much greater than the time required to increase R to its final value. Consequently, the change in the value of R will be referred to as a "step change".

Extensive tests were conducted in order to evaluate the transient response of the drive. Due to lack of facilities, it was not possible to test the transient response of the drive for a step change in torque load. Figures 6.4, 5, 6, 7, 8, 9, 10, and 6.11 show the system transient response for a step change in reference voltage R.

Examination of Fig. 6.4 shows that the speed response of the drive is oscillatory in nature, and decays to a steady-state value after a finite time. Although, the system under discussion is non-linear, the system oscillatory speed response in a small region about a point exhibits the type of behaviour expected of a second-order linear system. Data obtained from the aforementioned figures

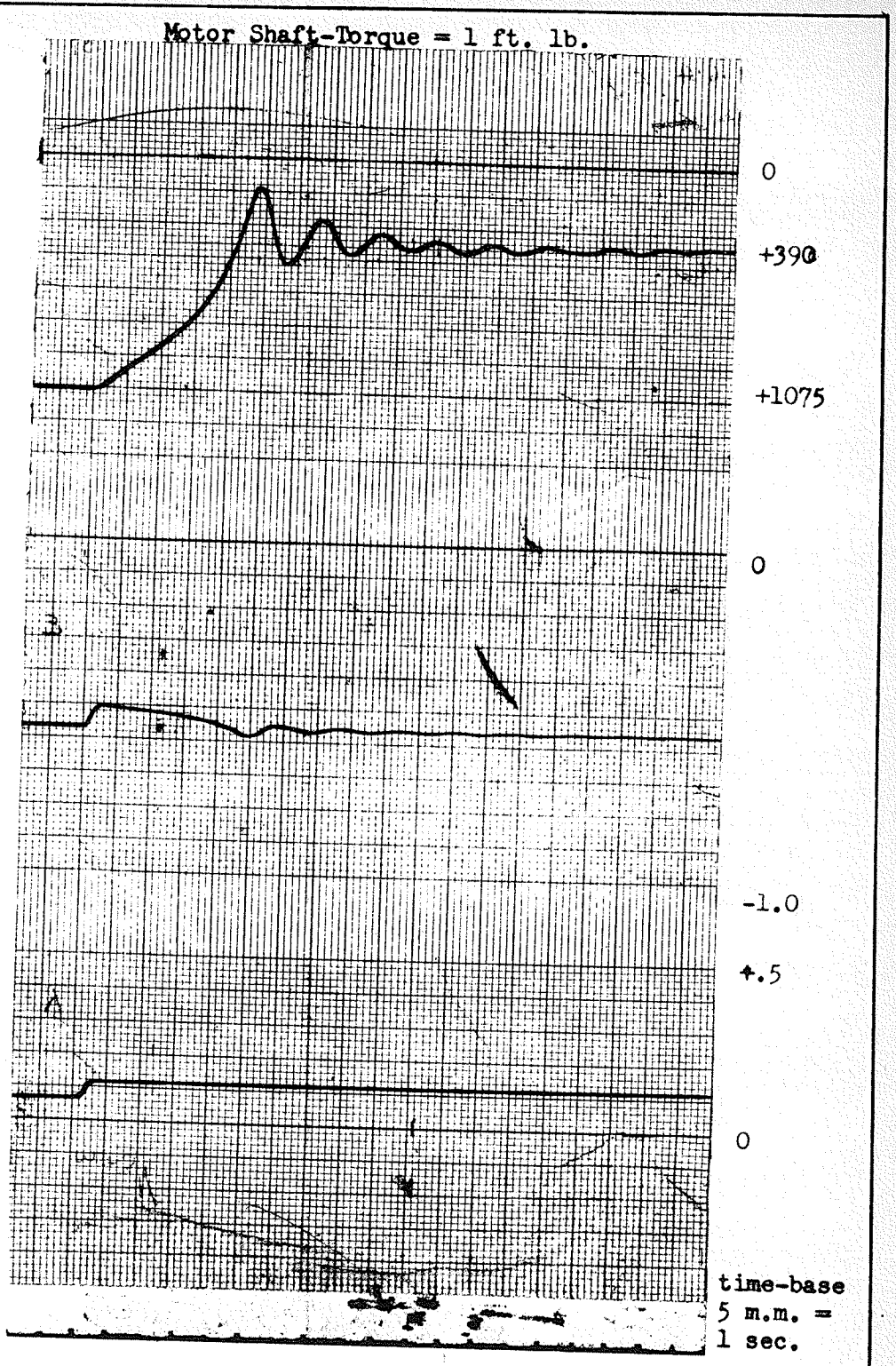

Fig. 6.4 SYSTEM TRANSIENT RESPONSE FOR STEP CHANGE IN REFERENCE VOLTAGE
(T_L=1 ft. lb., $I_{s.s.}$ =1075 r.p.m.)

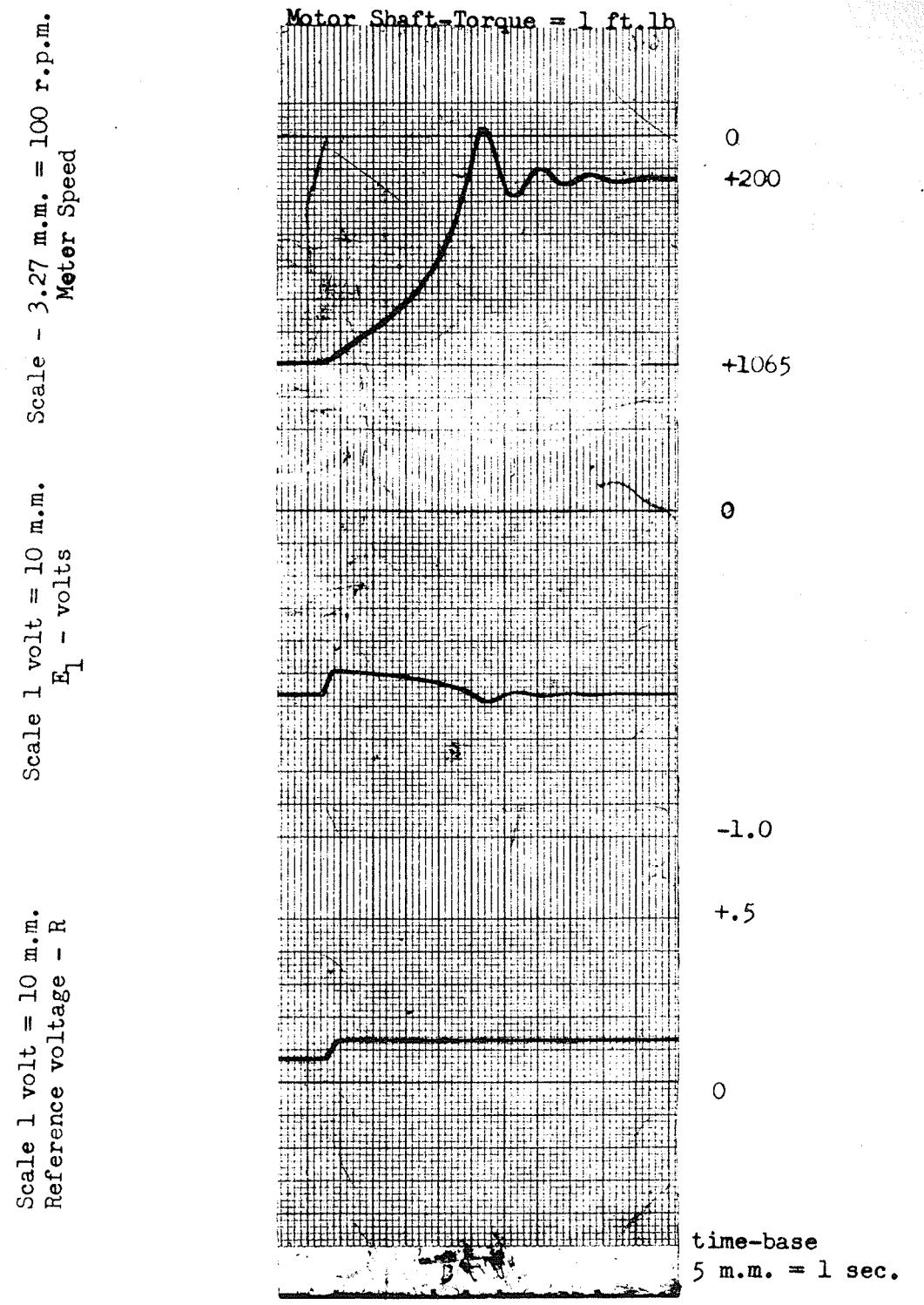

Fig. 6.5 SYSTEM TRANSIENT RESPONSE FOR STEP CHANGE IN REFERENCE VOLTAGE
(T.L.=1 ft. lb., I.s.s. = 1065 r.p.m.)

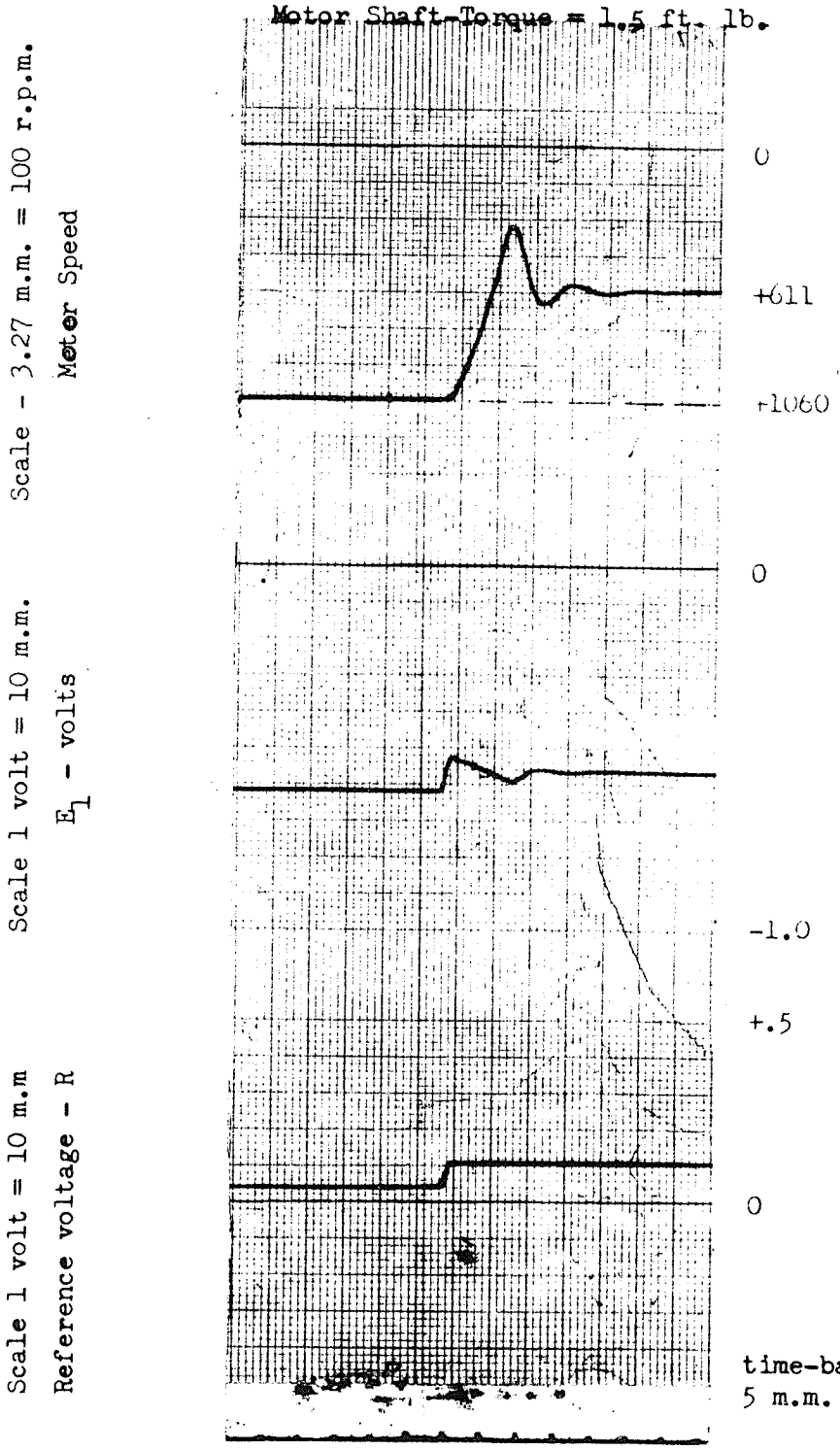

Fig. 6.6 SYSTEM TRANSIENT RESPONSE FOR STEP CHANGE IN REFERENCE VOLTAGE (T_L = 1.5 ft. lb., $I_{s.s.}$ = 1060 r.p.m.)

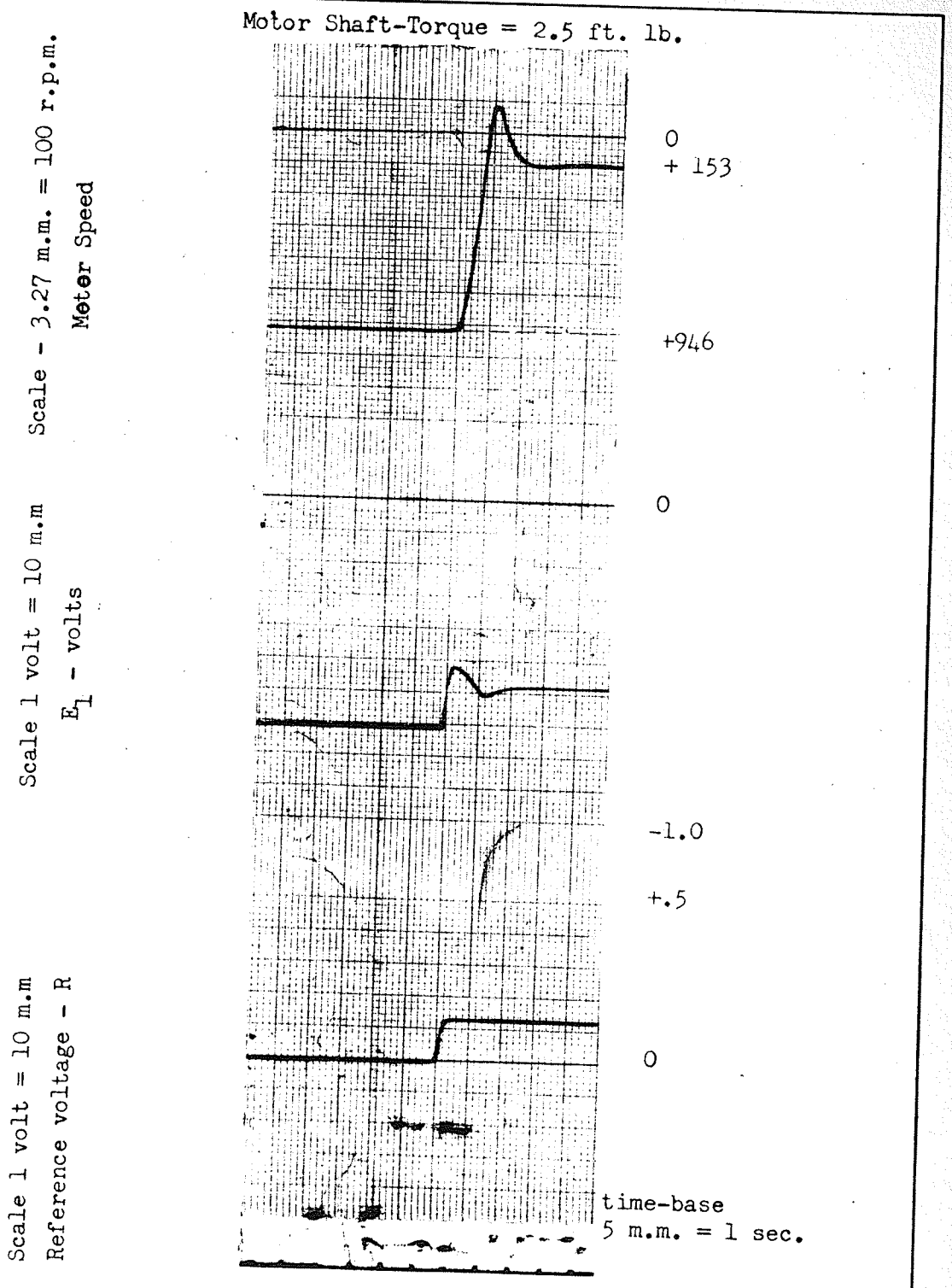

Fig. 6.7 SYSTEM TRANSIENT RESPONSE FOR STEP CHANGE IN REFERENCE VOLTAGE ($T.L.=2.5$ ft. lb., $I_{s.s.}=946$ r.p.m.)

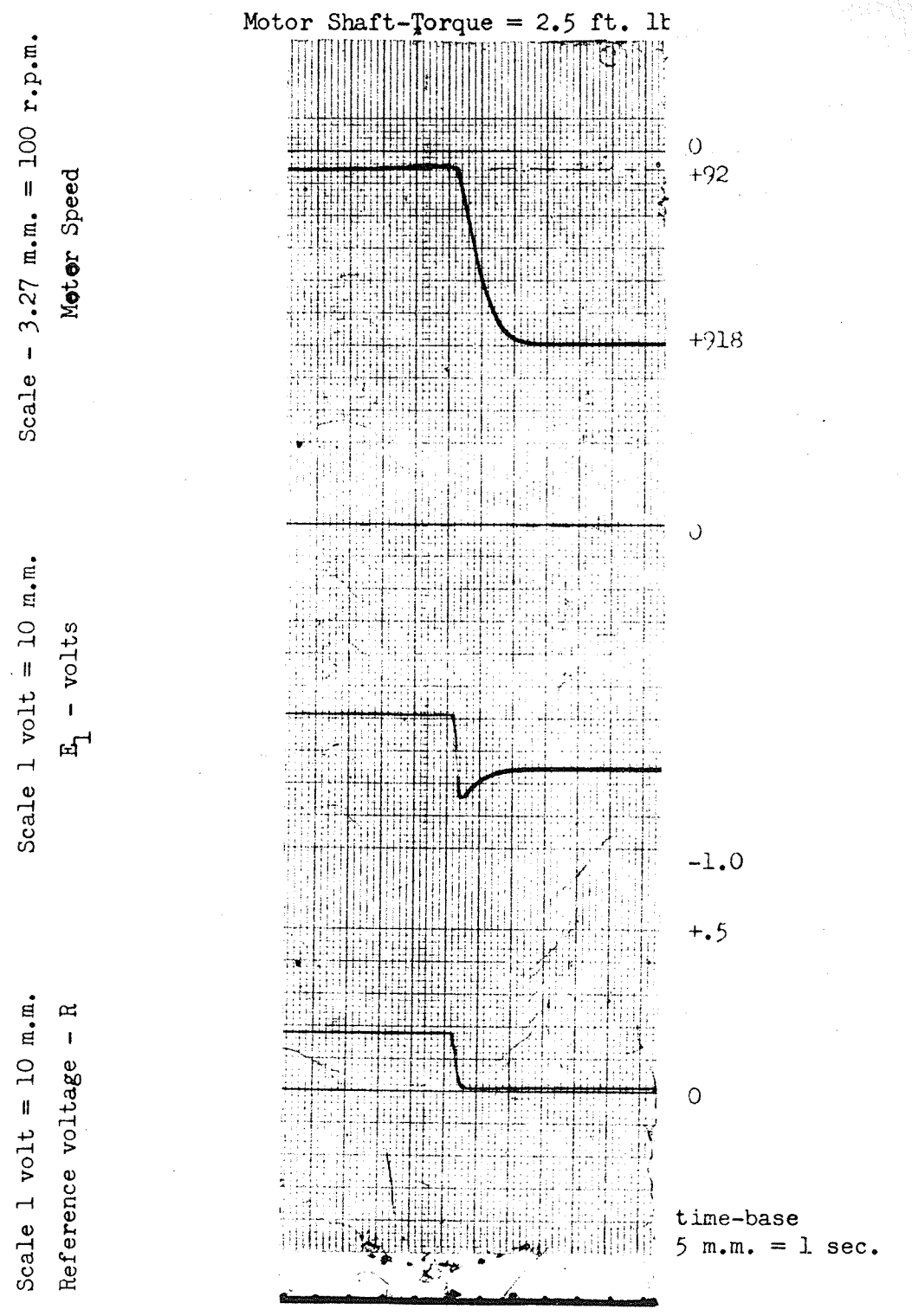

Fig. 68 SYSTEM TRANSIENT RESPONSE FOR STEP CHANGE IN REFERENCE VOLTAGE (T_L = 2.5 ft. lb., $\omega_{s.s.}$ = 92 r.p.m.)

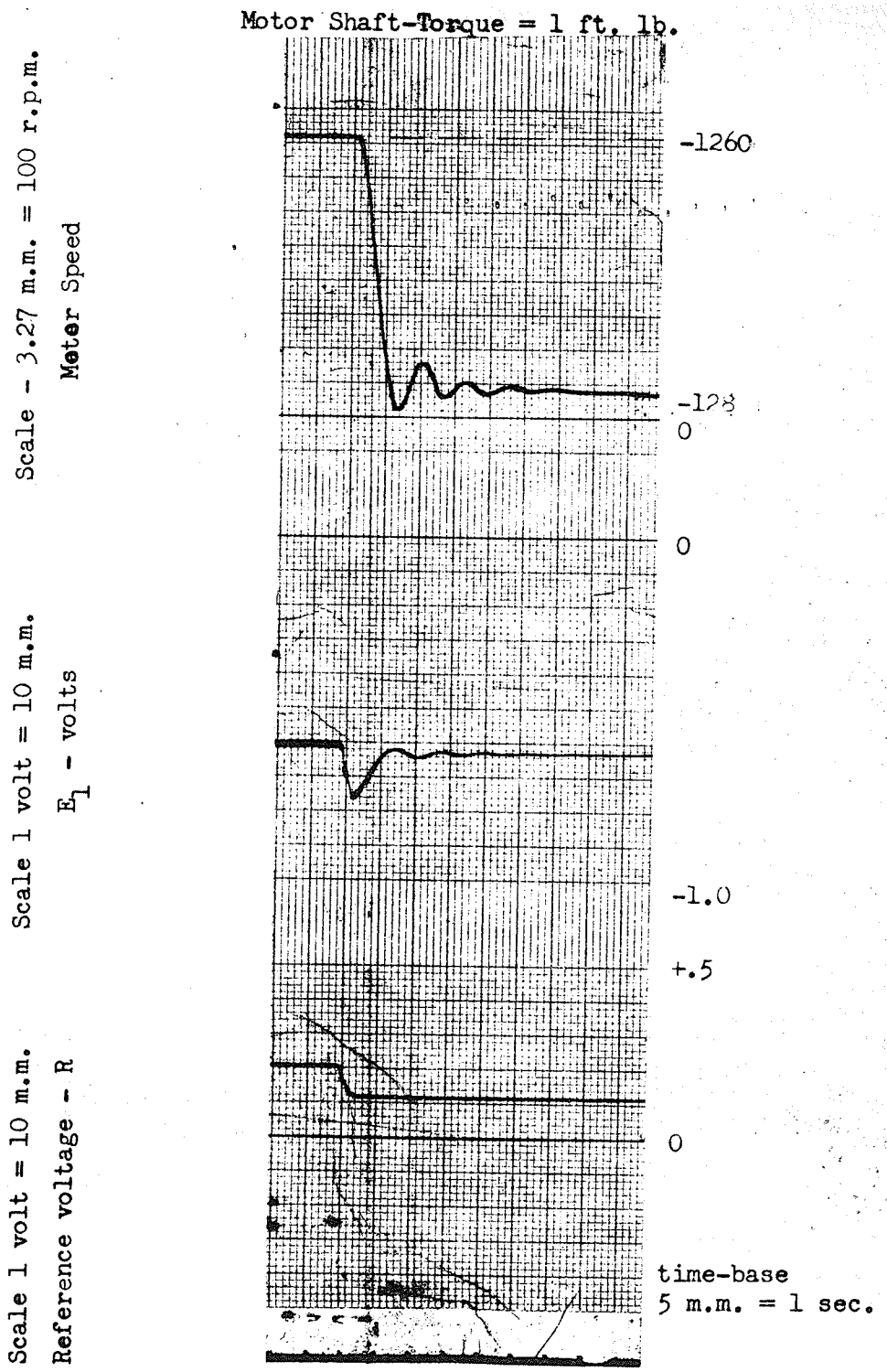

Fig. 6.9 SYSTEM TRANSIENT RESPONSE FOR STEP CHANGE IN REFERENCE VOLTAGE
(T_L=1 ft. lb., $I_{s.s.}$ = - 1260 r.p.m.)

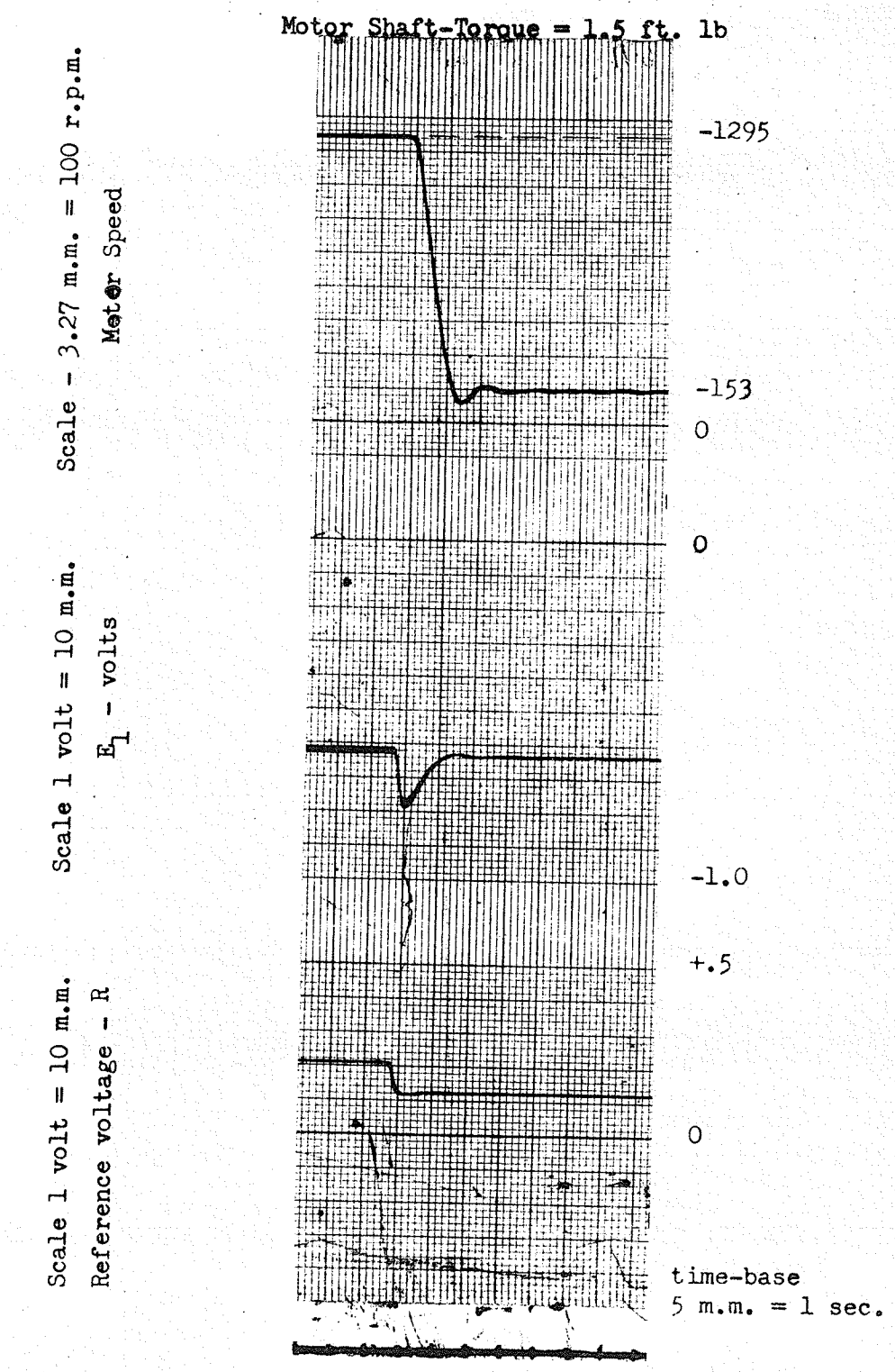

Fig. 6.10 SYSTEM TRANSIENT RESPONSE FOR STEP CHANGE IN REFERENCE VOLTAGE (T_L=1.5 ft. lb., $n_{s.s.}$=-1295 r.p.m.)

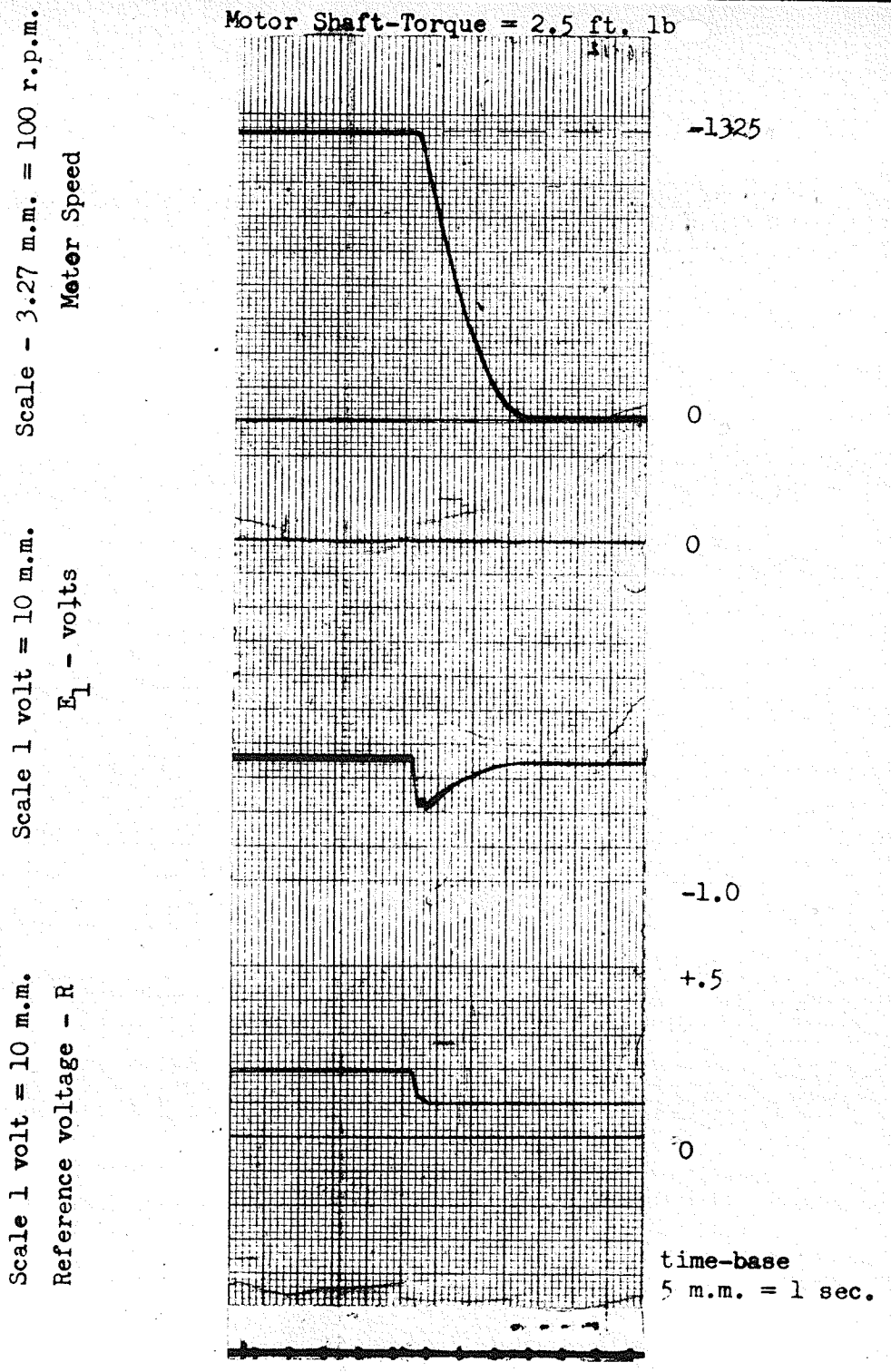

Fig. 6.11 SYSTEM TRANSIENT RESPONSE FOR STEP CHANGE IN REFERENCE VOLTAGE (T.L.=2.5 ft. lb., $I_{s.s}$=-1325 r.p.m.)

are presented in Table 6.4 as follows:

Table 6.4

System Transient Response for a Step Change in Reference Voltage.

Fig.	T.L. ft. lbs.	I.s.s. r.p.m.	F.s.s. r.p.m.	T seconds	γ seconds
6.4	1.0	1075	390	1.9	18.8
6.5	1.0	1065	200	1.8	10.0
6.6	1.5	1060	611	1.8	5.3
6.7	2.5	946	153	- -	1.8
6.8	2.5	92	918	- -	2.8
6.9	1.0	-1260	-120	1.4	5.8
6.10	1.5	-1295	-153	1.4	4.0
6.11	2.5	-1325	0	- -	3.0

where

T.L. is the motor shaft torque.

$I_{s.s.}$ is the initial motor steady-state speed.

$F_{s.s.}$ is the final motor steady-state speed.

T is the period of the motor-speed oscillation.

γ is the settling time of the drive.

The variable γ was not computed, but approximated from the figures. Settling time was taken to be the time lapse from the instant the reference voltage was "stepped" until such time as the drive approached 5% of its final steady-state speed. It is seen that the settling time γ is small for large shaft-torques. This may be attributed to the fact that the drive components are operating under conditions nearing saturation.

Reference to Table 6.4 indicates a difference in the period of motor speed oscillation for the driving and braking regions.

The characteristics which furnished the data represented in Table 6.4 are representative of drive operation. More test results were recorded than have been shown, many indicating better drive performance than some of those shown.

CHAPTER VII

CONCLUSIONS

An attempt has been made to construct a reactor-controlled, reversible, induction motor drive. A simplified analysis of a reversible reactor-control scheme has been presented. The principles of the reactor-control operation have been presented and the motor operation has been compared on the basis of symmetrical and asymmetrical operation.

The results suggest that a criterion for machine heating due to current asymmetry must be considered if the power modulator is to be useful in control of the induction motor. It would be instructive to perform the corresponding calculations for different saturable reactor connections. Such a computation would require the use of computing machines.

The insertion of an external rotor network into the rotor circuit of the motor decreased the available shaft-torque to approximately 50% rated motor torque. Capacitive compensation might be employed to increase the available shaft-torque.[7.1] This may be done by connecting capacitors at the motor terminals for power factor correction. Use of the rotor network ensures open-loop stability which is not available throughout the driving and counter-torque range for a machine with a short-circuited rotor.

Under conditions of closed-loop operation, the speed regulation for torques ranging between 1 and 3 foot-pounds approached an average of approximately 15%. It was found that the speed regulation increased very rapidly for small torque loads due

to single phasing motor operation. The circuit configuration of the power modulator made this an unavoidable condition.

Tests were performed to determine the speed transient response (at constant load) to large step inputs. Experimental results have been presented as evidence of the good transient response which can be obtained by the use of reactor-controlled induction motors.

BIBLIOGRAPHY

BIBLIOGRAPHY

1.1 Leonhard, Werner. "Elements of Reactor-Controlled Reversible Induction-Motor Drives", Transactions of The American Institute of Electrical Engineers, vol. 78 (May, 1959), pp. 106-113.

1.2 Butler, O. I., and V. Ahmed. "A New Form of Crane-Hoist Control Using a 3:1 Pole-Changing Induction Motor", The Proceedings of the Institution of Electrical Engineers, vol 108, part A June, 1961), pp. 215-221.

1.3 Butler, O. I. "Stopping Time and Energy Loss of A.C. Motors With D.C. Braking", The Transactions of the American Institute of Electrical Engineers, vol. 76 part III (1957), p. 285.

1.4 Schmitz, N. L. "Control of Slip Ring Motors by Means of Unbalanced Primary Voltages", The Transactions of the American Institute of Electrical Engineers, vol. 66 (1947), p. 1103.

1.5 Butler, O. I., and V. Ahmad, "A.C. Dynamic Braking of Induction Motors," Engineering, vol. 187 (1959), p. 590.

1.6 Van Niekerk, A. "Single-Phase Braking of Three-Phase Induction Motors", Electrical Journal, vol. 33 (1936), p. 121.

1.7 Brown, J. E., and O. I. Butler. "A General Method of Analysis of Three-Phase Induction Motors with Asymmetrical Primary Connections", The Proceedings of the Institution of Electrical Engineers, vol. 100 part 2 (February, 1953), p. 25.

1.8 Wickerham, W. R. "Variable Unbalanced Voltage Cont. l", The Transactions of the American Institute of Electrical Engineers, vol. 64 (1945), p. 98.

1.9 Scott, Lawrence. Revcon Control System for Cranes, Electromotors Ltd., Publication No. 125 (1958).

1.10 Pyle, C. M., "Twin Motor A.C. Crane Hoist Control", Metropolitan-Vickers Gazette, vol. 30 (1959), p. 76.

1.11 Bolt, M. H., Simeon, A., and Shepherd, W. "Variable Three-Phase Reversible Voltage Sources Using Saturable Reactors," The American Institute of Electrical Engineers, Paper No. 61-37 (November 21, 1960).

1.12 Zollinger, H. A. "Application of Reactor Control to A.C. Motors," Westinghouse Engineer, vol. 19 (September, 1959), pp. 156-160.

1.13 Foote, L. R. "Adjustable Speed Control of A.C. Motors", Electrical Engineering, vol. 78 (August, 1959), pp 840-843.

1.14 Hausen, G., Beringer, P. P. , and Slemon, G. R. "A Variable-Speed Reversible Drive Using an Induction Motor," The American Institute of Electrical Engineers, paper no. 59-976 (June 2, 1959).

2.1 Nyquist, H. "Regeneration Theory", Bell System Technical Journal, vol. 11 (January, 1932), p. 126.

3.1 Fitzgerald, A. E. and Charles Kingsley, Electric Machinery, (The McGraw-Hill Book Co. Inc., 1952), pp.392-433.

3.2 Ibid., p. 397.

3.3 Ibid., p. 402.

3.4 Ouchstein, Lloyd, and Conrad. Alternating Current Machines, (John Wiley and Sons, Inc., 1954), Chapt. 25, p. 318.

3.5 Fitzgerald, A. E. and Charles Kingsley. op. cit., p. 403.

3.6 Shepherd, W. and G. R. Slemon. "Rotor Impedance Control of the Wound Rotor Induction Motor," The American Institute of Electrical Engineers, paper no. 59-138 (November 3, 1958).

3.7 Ibid.

4.1 Wagner and Evans. Symmetrical Components, (The McGraw-Hill Book Co. Inc., 1933), p. 21.

4.2 Ibid.

4.3 Ibid., p. 375.

4.4 Ibid., p. 349.

4.5 Langsdorf, A.S. Theory of Alternating Current Machinery, (The McGraw-Hill Book Co., Inc., 1955), Chapt. 9, p. 363.

4.6 Quanza, S. "Speed Control of Induction Motors Using Saturable Reactors", Automatic and Remote Control, vol. IV, (Proceedings of the Moscow Conference, 1961).

5.1 Davis and Weed. Industrial Electronic Engineering, (Prentice-Hall Inc., 1953), Chapt. III, p. 112.

5.2 Ibid., p. 114.

5.3 Ibid., p. 101

5.4 Millman, Jacob, and Herbert Taub. Pulse and Digital Circuits, (The McGraw-Hill Book Co., Inc., 1956), p. 20.

7.1 Hausen, G., Beringer, P. P., and Slemon, G. R., op. cit. p.417.

A.1 Puchstein, Lloyd, and Conrad. op. cit. pp. 284-288.

A.2 Fitzgerald and Kingsley, op. cit. p. 417.

B.1 Puchlowski, K. P. "An Electronic Drive for Windup Reels", The American Institute of Electrical Engineers paper no. 46-125 (May 3, 1946).

APPENDIX

APPENDIX A

MACHINE CONSTANTS

A.1 DETERMINATION OF THE INDUCTION MOTOR PARAMETERS

Nameplate of Induction Motor.

ASEA	Mot. 3 phase 60 cycle
MKD 11	Serial No. 4236081
1 h.p.	1140 r.p.m.

Primary wye connected

110 volts	Secondary 70 volts
5.3 amps	7 amps.

Measurement of Stator and Rotor Resistances.

The stator circuit was connected to a d.c. supply as shown in Fig. A.1. It was assumed that the stator windings had equal d.c. resistance. The d.c. voltage source V shown in Fig. A.1 was increased until the ammeter indicated rated stator current.* The stator was allowed to heat, adjustments of V being made to hold the stator current I constant. The results were as follows:

$V = 4.80$ volts d.c.

$I = 5.10$ amps d.c.

Stator d.c. resistances per phase were found with the aid of Fig. A.1 to be as follows:

$5.1R + 2.55R = 4.8$

$R_{d.c.} = .627$ ohms/phase.

---

* This measurement was inadvertently performed at a current other than the rated stator current.

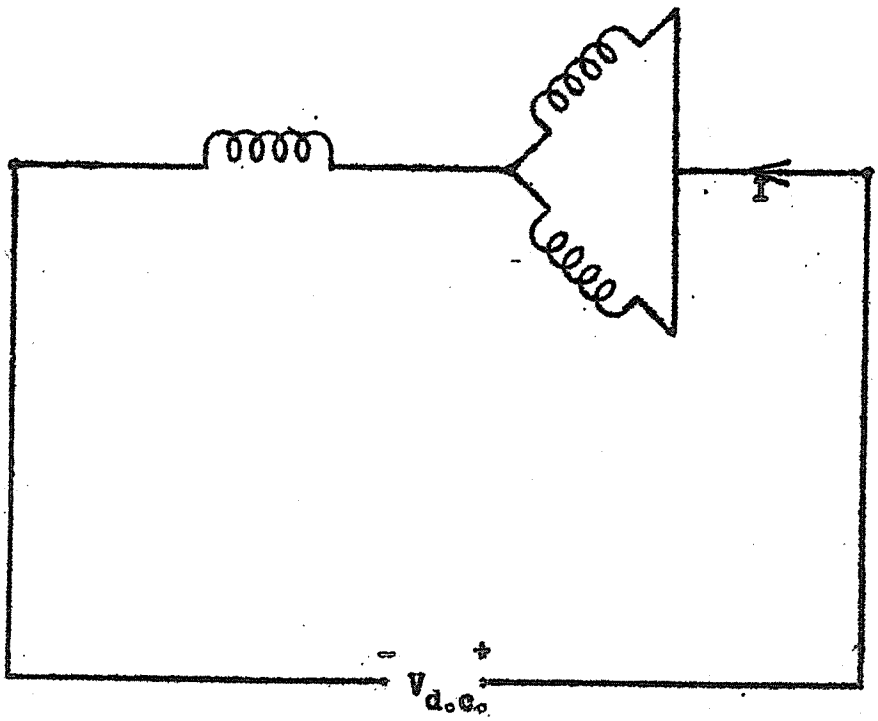

FIGURE A.1

TEST CONNECTION OF MOTOR PRIMARY AND SECONDARY TO DETERMINE r_1 & r_2

It is generally accepted that the a.c. resistance $R_{a.c.}$ of a motor winding may be expressed as 1.15 $R_{d.c.}$ at 60 cycles. Thus, it follows that $R_{a.c.} = 1.15 \times .627 = .720$ ohms per phase.

The results of a similar test of the rotor circuit were as follows:

V = 5 volts d.c.

I = 7.1 amps a.c.*

$R_{d.c.} = .469$ ohms per phase

$R_{a.c.} = 1.15 \times .469 = .540$ ohms per phase

Open and short circuit tests were carried out as described by Puchstein, Lloyd, and Conrad[A.1]. Results are tabulated in Tables A.1 and A.2 as follows:

Table A.1 Open Circuit Test

Stator Volts L/L	Stator Line Current	Power Input Watts	Rotor Open Circuit Volts
110	3.7	65	70

Table A.2 Short Circuit Test

Stator Volts L/L	Stator Line Current	Power Input Watts	In Phase Component of Short Circuit Current
17.0	3.00	50	1.70
29.5	5.30	138	2.71
33.0	6.00	170	2.98
38.5	7.00	233	3.50
44.0	8.00	305	4.03
49.5	9.00	380	4.43

* This measurement was inadvertently performed at a current other than the rated rotor current.

Fig. A.2 shows a plot of line current versus line to line stator terminal volts.

From the open circuit test $Z_{\text{no load}} = \frac{110}{\sqrt{3} \times 3.7} = 17.2\ \Omega$ per phase.

$R_{\text{no load}} = \frac{65}{3 \times (3.7)^2} = 1.58\ \Omega$ per phase

$X_{\text{no load}} = \sqrt{Z^2_{\text{no load}} - R^2_{\text{no load}}} = \sqrt{296 - 2.5} = 17.1\ \Omega$ per phase.

From Fig. A.2, the blocked motor impedance Z_{bl} at rated voltage is

$$Z_{bl} = \frac{110}{\sqrt{3} \times 20} = 3.18\ \Omega \text{ per phase.}$$

The blocked motor resistance is

$$R_{bl} = \frac{10.2}{20} \times 3.18 = 1.62\ \Omega \text{ per phase.}$$

Hence, the blocked motor reactance is

$$X_{nl} = \sqrt{(3.18)^2 - (1.62)^2} = 2.74\ \Omega \text{ per phase.}$$

From table (9-1) Fitzgerald and Kingsley[A.2]

$$x_{\text{stator}} = a^2 x_{\text{rotor}} = .5\, X_{bl} = .5 \times 2.74 = 1.37\ \Omega \text{ per phase}$$

where "a" is the turns ratio.

$$x_m = X_{nl} - x_{\text{stator}} = 17.1 - 1.37 = 15.7\ \Omega \text{ per phase.}$$

In order to find the correct ratio of transformation "a", it was necessary to eliminate error owing to differential leakage flux between stator and rotor turns. The method is that given in reference A.1. When the stator windings were connected to their rated line to line voltage V, the rotor line to line voltage E_2 was found. The stator winding was then disconnected and a voltage E'_2 was impressed on the rotor. The induced stator line to line voltage V' was read. The correct ratio of transformation is given by[A.1]:

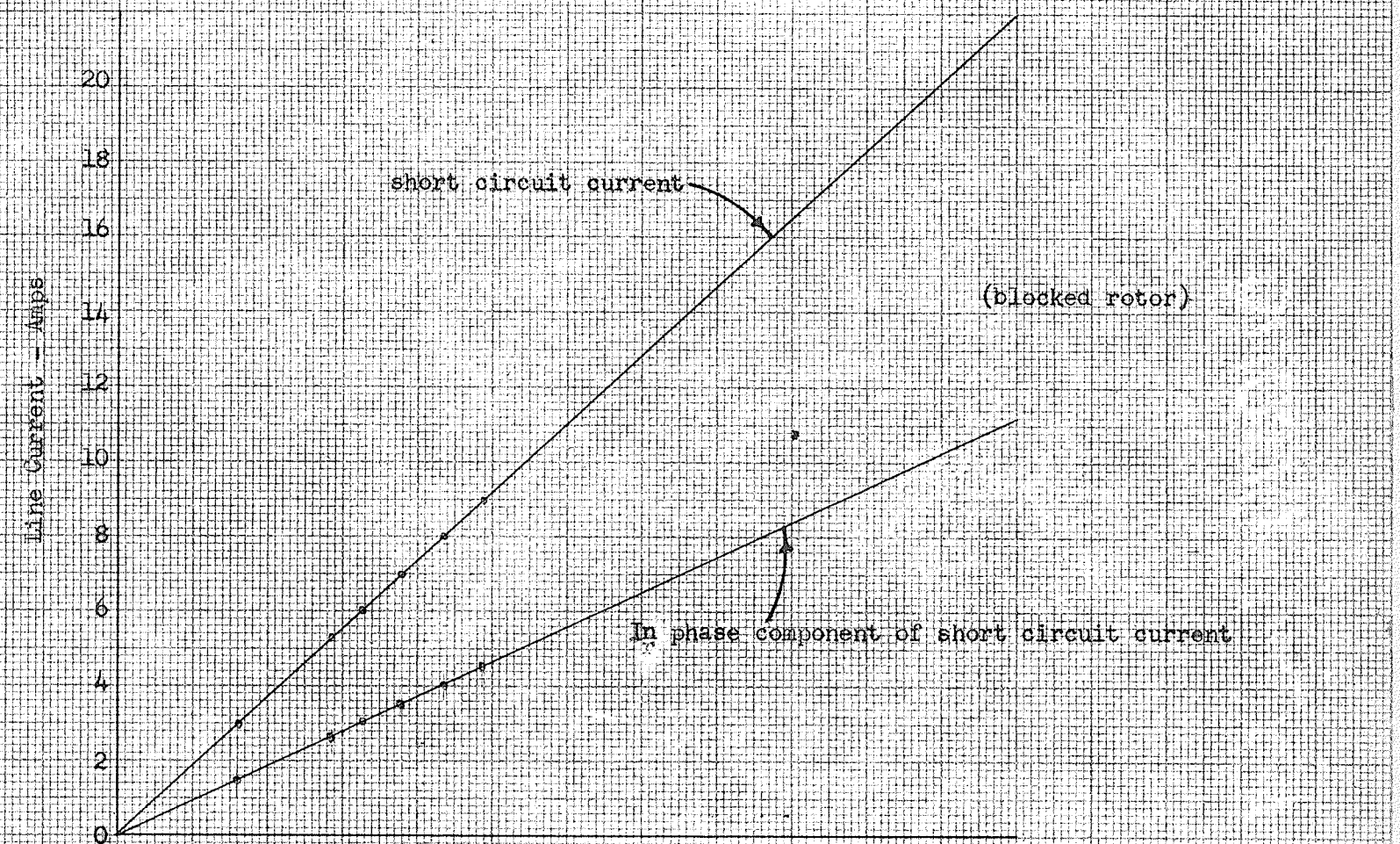

FIGURE A.2 SHORT CIRCUIT TEST OF INDUCTION MOTOR

$$a = \frac{V}{E_2}\sqrt{\frac{V\,E'_2}{V'E_2}}$$

Results:

$V = 100$ volts $\qquad V' = 93.0$ volts

$E_2 = 70$ volts $\qquad E_2' = 40$ volts.

$a = 1.29$

The machine parameters may be tabulated as follows:

Primary resistance $r_1 = .720$ ohms/phase.

Secondary resistance $r_2 = .540$ ohms/phase.

Primary reactance $x_1 = 1.37$ ohms/phase @ 60 cycles.

Secondary reactance $x_2 = .825$ ohms/phase @ 60 cycles.

Magnetizing reactance $x_m = 15.7$ ohms/phase @ 60 cycles.

Ratio of transformation $a = 1.29$.

It is more convenient to refer the machine quantities to the stator on a per unit basis.

Motor Constants referred to the stator are:

$r_1 = .720$ ohms/phase.

$r_2 = .54\ (1.29)^2 = .90$ ohms/phase.

$x_1 = 1.37$ ohms/phase @ 60 cycles.

$x_2 = (.825)(1.29)^2 = 1.37$ ohms/phase @ 60 cycles.

$x_m = 15.7$ ohms/phase @ 60 cycles.

base voltage per phase $= \frac{110}{\sqrt{3}}$ volts.

base current per phase $= 5.3$ amps.

Thus the base impedance $Z_{base} = \frac{110}{\sqrt{3} \times 5.3} = 12$ ohms/phase.

The machine parameters on a p.u. basis referred to the stator are as follows:

$$r_1 = \frac{.720}{12} = .060 \text{ p.u./phase.}$$

$$r_2 = \frac{.90}{12} = .075 \text{ p.u./phase.}$$

$$x_1 = \frac{1.37}{12} = .114 \text{ p.u./phase.}$$

$$x_2 = \frac{1.37}{12} = .114 \text{ p.u./phase.}$$

$$x_m = \frac{15.7}{12} = 1.31 \text{ p.u./phase.}$$

APPENDIX B

THYRATRON CIRCUIT AND ASSOCIATED EQUIPMENT DESIGN

B.1 THYRATRON PLATE-SUPPLY TRANSFORMER

It was pointed out in section 5.3 of Chapter V that a plate transformer which had a secondary capacity of 110 VA and a secondary voltage rating of 445 volts centre-tapped was required for the plate supply of the thyratrons. In order to be conservative it was decided to use a transformer of at least 200 VA secondary rating. Such a transformer was not available, and since the installation was to be temporary, use was made of large identical transformers available in the A.C. Lab. The transformers had the following name plate data:

Name Plate Data of Transformers:

Westinghouse	KVA 3
Style 582677	Impedance 3.4%
Voltages 220, 110 to 220, 110	Serial No.'s 1887548
60 cycles	1887550

It was found that the output voltage of the transformers connected as shown in Fig. B.1 was slightly higher than required. The discrepancy was thought to be small enough to be neglected.

B.2 DESIGN OF THE PHASE SHIFTING CIRCUIT

The schematic circuit diagram and the vector diagram of the phase shifting circuit are shown in Figs. B.2(a) and (b). With reference to these Figures, circuit considerations show that

$$\frac{Xc_1}{R_1} = \tan\frac{\phi}{2} \qquad \text{B. 1}$$

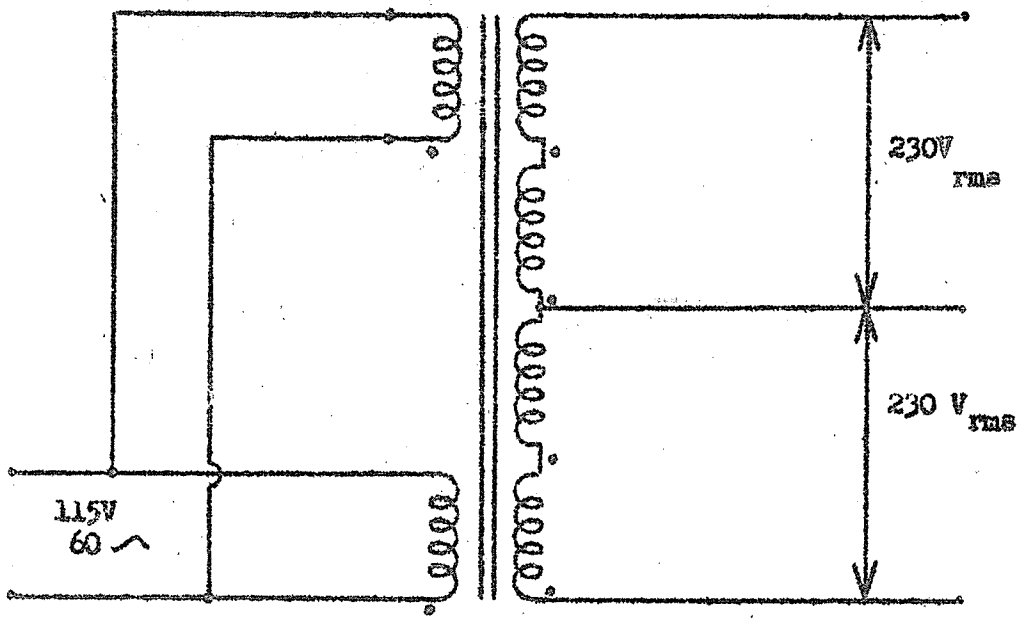

FIGURE B.1 ARRANGEMENT OF THYRATRON PLATE-SUPPLY TRANSFORMERS

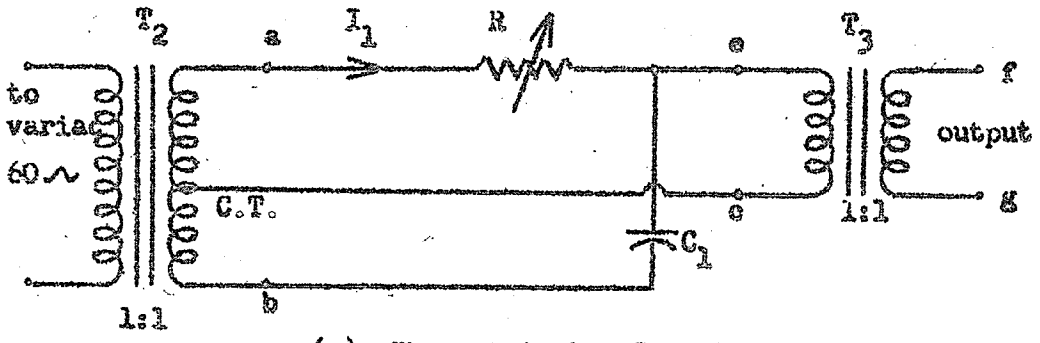

(a) Phase Shifting Circuit

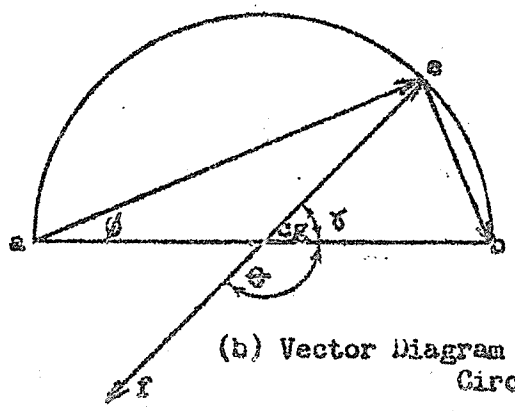

(b) Vector Diagram of Phase Shifting Circuit

FIGURE B.2 PHASE SHIFTING NETWORK

where γ is as shown in Fig. B.2(b)

The circuit was designed so that voltage V_{fg} would lag V_{ab} by 135°. This required an angle γ such that $\gamma = 45°$. A .1 ufd. capacitor was chosen for C_1. From equation B.1, R_1 was determined as follows:

$$R_1 = \frac{Xc_1}{\tan \frac{\gamma}{2}}$$

where $$Xc_1 = \frac{1}{wC_1}$$

$$w = 377 \text{ radians/sec}$$

$$R_1 \cong \frac{1}{\frac{377 \times .1 \times 10^{-6}}{\tan \frac{45°}{2}}}$$

$$R_1 = 64 \text{ K ohms.}$$

In order to insure easy circuit adjustment, a potentiometer variable in the range 0 to 100 K ohms was chosen for R_1.

The transformers T_2 and T_3 had no nameplate data stamped on them. Tests on these transformers showed that each had a unity turns-ratio.

Tests also showed that if the input of the phase shift circuit was a voltage at 60 cps, the output voltage waveform suffered negligible distortion. The current in the circuit was limited by the high series impedance of Xc_1 and R_1.

An examination of Fig. 5.10(b) of Chapter V shows that thyratron tube current can be closely controlled because the angle of intersection between the critical grid characteristic and the phase shifted grid voltage is large. A small change in

magnitude of alternating component of grid voltage has little effect on tube current, provided the alternating component itself has sufficient magnitude.

It was decided to make the magnitude of the output of the phase shifting circuit 15 volts peak to peak. This was about three times the maximum critical grid voltage of the thyratrons. A "variac" was placed at the input of the circuit and adjusted so that the output phase shifted voltage was 15 volts peak to peak. The potentiometer R_1 was adjusted so that the proper phase shift was obtained. Fig. B3 shows an oscillogram of voltages V_{ab} and V_{fg} displaced 135° in phase.

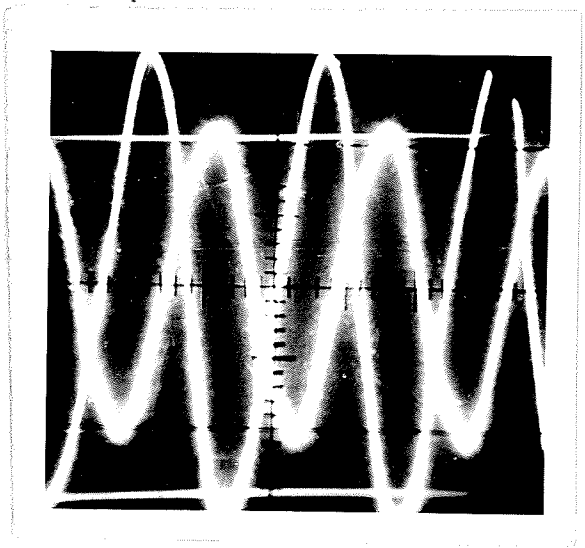

FIGURE B.3
PHASE SHIFT BETWEEN A.C. THYRATRON PLATE AND GRID VOLTAGE*

B.3 CRITICAL GRID CHARACTERISTIC OF 3C23 THYRATRON

In order to determine the critical grid characteristic of the 3C23 thyratrons the circuit shown in Fig. B.4 was set up. With reference to Fig. B.4 it is seen that the 1 megohm resistor in the plate circuit served to limit the tube current when the tube

*Note: Thyratron plate voltage is the larger waveform.

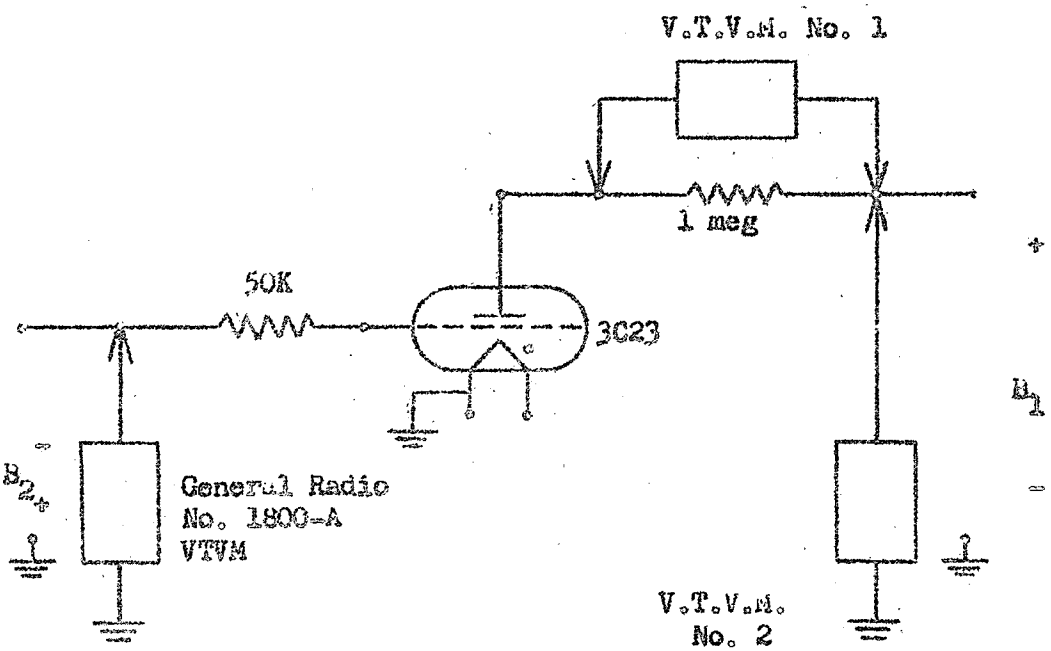

FIGURE B.4

CIRCUIT USED TO DETERMINE CRITICAL GRID CHARACTERISTIC OF 3C23.

fired.

Grid voltage E_2 was held sufficiently negative to prevent the tube from firing when voltage E_1 was several hundred volts. Voltage E_1 was then adjusted to a fixed value and read on VTVM No. 2. Grid voltage E_2 was then allowed to become more positive until the tube fired. At the instant of firing VTVM No. 1 indicated a sharp rise in potential. The grid voltage E_2 was read on a "General Radio Meter" type 1800-A just before the tube fired:

Test Results:

D.C. Grid Volts	D.C. Plate Volts
-2.15	30
-3.40	50
-3.70	75
-4.08	100
-4.34	125
-4.51	150
-4.71	175
-4.86	200
-5.04	225
-5.20	250
-5.40	275
-5.58	300
-5.76	325

B.4 CONTROL OF THYRATRON OUTPUT

The critical grid characteristic of a type 3C23 thyratron is plotted in Fig. B.5 with the information obtained from section B.3. It was pointed out in section B. 1 that the secondary voltage for half the winding of the plate transformer was 230 volts r.m.s. Subsequently, the critical grid characteristic in Fig. B.5 was drawn for a sinusoid having a peak voltage of $230 \times \sqrt{2} = 325$ volts.

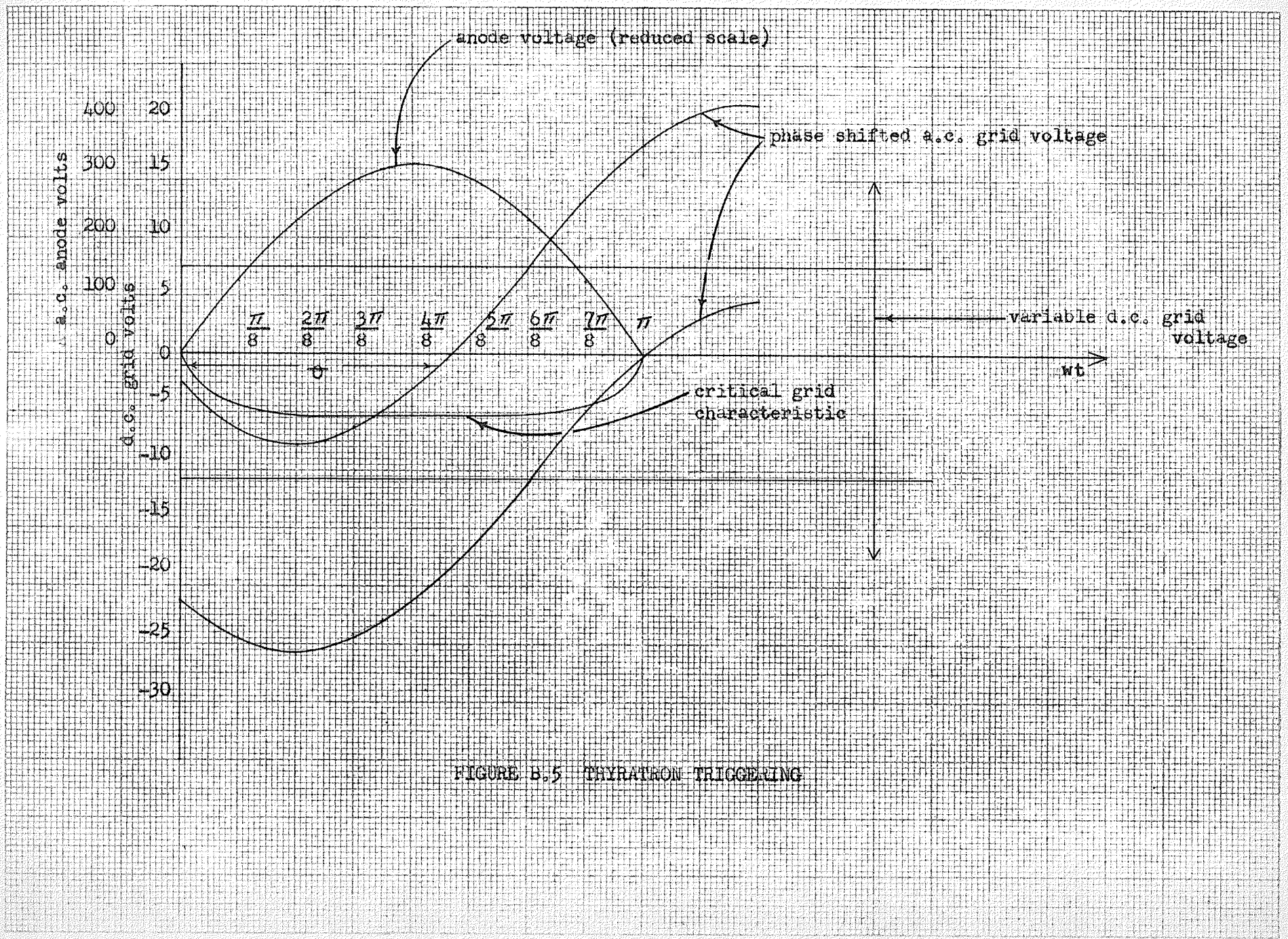

FIGURE B.5 THYRATRON TRIGGERING

It is apparent from Fig. B.5 that control of the thyratron is available in the range $\frac{3\pi}{8} < wt \leq \pi$. For $wt \leq \frac{3\pi}{8}$ the thyratron fires over its whole range. This was a glaring error in design. Apparently the phase shifting network should have been designed for $\Theta = 90^{\circ}$, where Θ is the angle indicated in Fig. B.5.

However, tests showed that the thyratron power supply would supply load current in excess of 1000 ma for a firing range $\frac{3\pi}{8} < wt \leq \pi$ and thus met load current specifications.

An inspection of Fig. B.5 will show that the d.c. control voltage to the thyratron grid must not exceed +8 volts, otherwise the thyratron will fire over the whole range $0 \leq wt \leq \pi$.

Examination of Fig. B.5 shows that a d.c. control voltage of -15 volts applied to the grid will assure extinction of the thyratron.

The circuit of Fig. 5.11(c) was tested, and the control voltage was applied to points "A" and "B" as shown on the figure. Point "B" was allowed to range in potential from -15 to +8 volts with reference to point "A". The resulting load current varied within specifications.

B.5 DESIGN OF THE AMPLIFIER

The operation and purpose of the amplifier shown in Fig. B.6 was discussed in section 5.5 of Chapter V.

Design centred around a 12AT7 duo-triode for reasons stated in section 5.5 of Chapter V. The plate voltage supply was chosen to be 300 volts and the load resistor R_4 in the plate

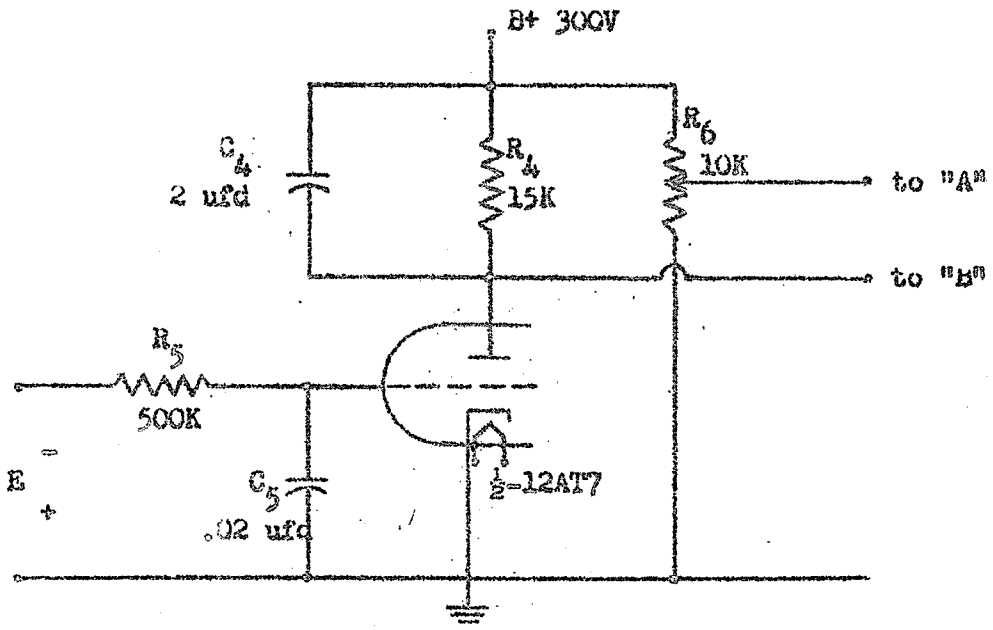

FIGURE B.6 AMPLIFIER CIRCUIT

circuit was chosen as 15K ohms.

The plate characteristics for a 12AT7 tube are reproduced in Fig. B.7. The load line may be plotted on these characteristics as follows:

When $i_b = 0$, $e_b = E_{bb} = 300$ v.

and $$ib = \frac{E_{bb}}{R_4} = \frac{300}{15} = 20 \text{ ma}, \quad e_b = 0.$$

It was pointed out in section B.4 that point "B" was allowed to range in potential from -15 to +8 volts with reference to point "A". As pointed out in section 5.5, the voltage applied to point "B" is a variable negative voltage dependent upon the amplifier tube current. The amplifier tube current is controlled by a variable negative voltage E applied to the grid circuit as shown in Fig. B.6. The amplifier was designed so that the potential of point "B" varied from -15 to +8 volts when the grid voltage E varied so that $-3 \geq E \geq -4$ volts.

Examination of Fig. B.7 indicates that when the grid voltage is -4 volts, the voltage drop across R_4 is approximately 35 volts. That is to say, the potential of point "B" is approximately 35 volts below the B+ supply. As discussed previously in section 5.5, the firing angle of the thyratrons is advanced as the grid of the amplifier in Fig. B.6 is made more negative. Since the potential of point "B" should not exceed the potential of point "A" by more than +8 volts, R_6 is tapped at a point where the potential of "A" is 43 volts below the potential of the B+ supply. If the grid voltage of the amplifier in Fig. B.6 is allowed to increase to -3 volts, the potential of point "B" is

12AT7 (Cont'd)

AVERAGE PLATE CHARACTERISTICS

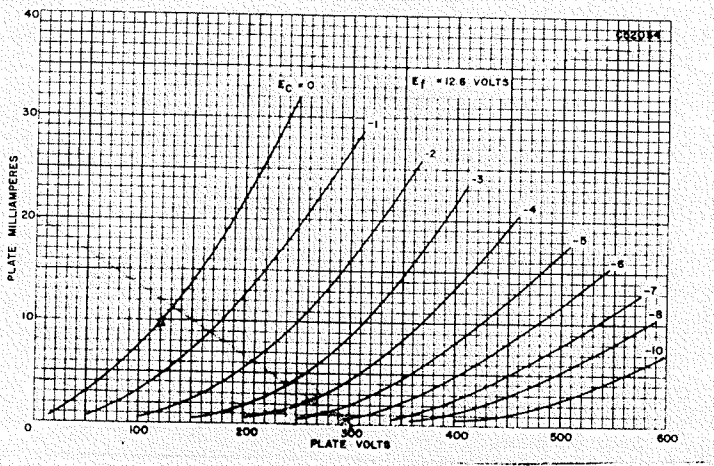

FIGURE B.7

AVERAGE PLATE CHARACTERISTICS OF A 12AT7

approximately 60 volts below the potential of the B+ supply. Hence, point "B" is approximately 17 volts below the potential of point "A", which insures that the thyratrons will not fire.

Variable resistor R_6 should be large enough to avoid loading the B+ supply and small enough to permit a fine adjustment. A 10 watt, 10 K ohm resistor was chosen. With a calculated dissipation of 9 watts, a 10 watt Ohmite wire-wound resistor was considered sufficient.

Capacitor C_4 bypasses R_4. Since the lowest ripple-frequency expected was 60 cycles a 2 ufd. capacitor was used. This corresponds to approximately 1300 ohms impedance at 60 cps and thus serves to bypass 60 cycle or higher ripple frequencies.

Grid resistor R_5 was chosen to be 500K ohms which is a standard value. The grid bypass capacitor C_5 serves to bypass any extraneous a.c. signals present in the circuit. Capacitor C_5 was chosen so that an a.c. signal of 15 cps was down 3 db at the grid terminal. All higher frequencies would be attenuated at the rate of 6 db/octave.

$$2\pi f R_5 C_5 = 1$$

$$C_5 = \frac{1}{2 \times 15 \times 500 \times 10^3}$$

$$C_5 = .0212 \text{ ufd.}$$

A .02 ufd. capacitor was chosen for C_5.

The circuit was tested and the operation behaved as anticipated. It was found that if the B+ voltage and the tap on R_6 were varied and then held constant, the required output between points "A" and "B" could be obtained for different ranges

of grid voltage input E'.

B.6 ANTI HUNTING CIRCUIT

The anti-hunt circuit is a variation of a circuit proposed by K. P. Puchlowski [B.1]. Operation of the circuit is discussed in section 5.7.

Fig. B.6 is a schematic of the circuit used. A 6H6 rectifier was chosen as having sufficient current carrying capacity. The current transformer T_4 had its primaries connected as shown in Fig. 5.14.

A spare saturable transformer was available, and was chosen to act as the current transformer T_4. The saturable transformer was the same as the type described in Chapter IV. Each of the three windings had 4 taps available which allowed different portions of the windings to be used. The primary winnings were connected as shown in Fig. 5.14 and taps were chosen so that approximately 100 volts appeared across the secondary of T_4 when the load was drawing maximum current. Resistor R_{13} served as a current limiting resistor.

It was decided to use a 10K resistor for R_{13}, subject to change if necessary under actual operating conditions. Resistors R_{14}, R_{15}, and condenser C_6 determine the time constant of the anti-hunt circuit. Since, it was not known at what frequency the system would hunt, resistors R_{14} and R_{15} were made variable. R_{14} and R_{15} were chosen as 250 K ohms each, and the condenser C_6 was so chosen that for a maximum time constant of 1 second

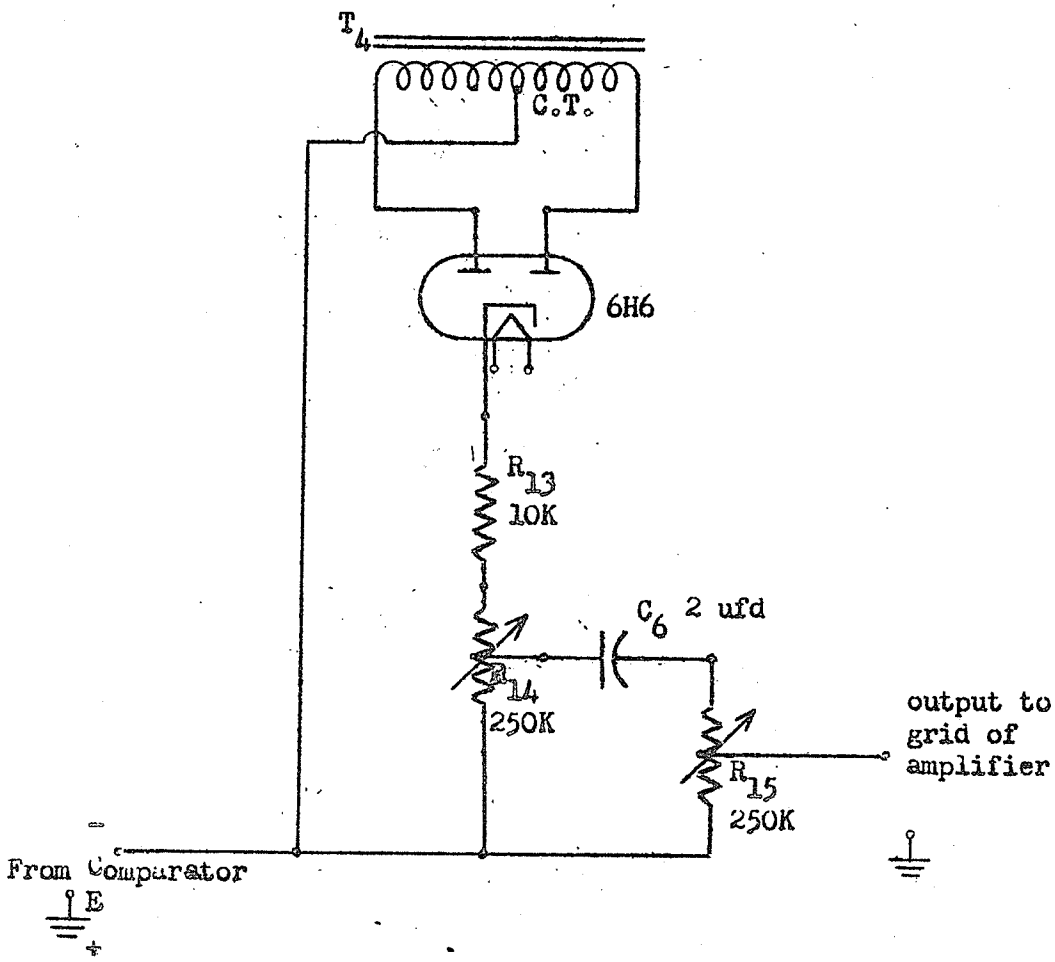

FIGURE B.8 ANTI-HUNT CIRCUIT

$$RC = 1$$

$$\therefore\ C_6 = \frac{1}{500 \times 10^3} = 2 \text{ ufd.}$$

Under operating conditions R_{14} was adjusted to an appropriate level to provide anti-hunting action (as determined by experiment) and R_{15} was adjusted to provide a proper level of damping voltage to the grid of the amplifier.

APPENDIX C

TACHOMETER CHARACTERISTICS

C.1 TACHOMETER OUTPUT CHARACTERISTICS

Nameplate of Tachometer.

The Electric Tachometer Co.,

Philadelphia, P. A., U. S. A.,

No. 00704

Max. Speed = 2000 r.p.m.

The tachometer was tested and its output voltage was found to vary speed as shown in Table C.1:

Table C.1

Tachometer Output Voltage vs Speed

Volts	Speed r.p.m.
.580	1760
.515	1580
.425	1310
.310	960
.170	520
.070	220
.050	160
.040	130
.020	60

Fig. C.1 shows that the tachometer output voltage varies almost linearly with speed.

The tachometer time constant was much smaller than the mechanical time constant of the induction motor. It was assumed that the tachometer time constant had a negligible effect on system operation.

FIGURE 6.1

TACHOMETER OUTPUT VOLTAGE vs. SPEED

C.2 FILTER NETWORK

The tachometer output voltage was found to contain a small amount of "hash". While, this did not effect system performance, it made interpretation of the strip-chart obtained from the Sanborn recorder difficult.

The filter circuit shown in Fig. C.2 was inserted between the output of the tachometer and the recording unit.

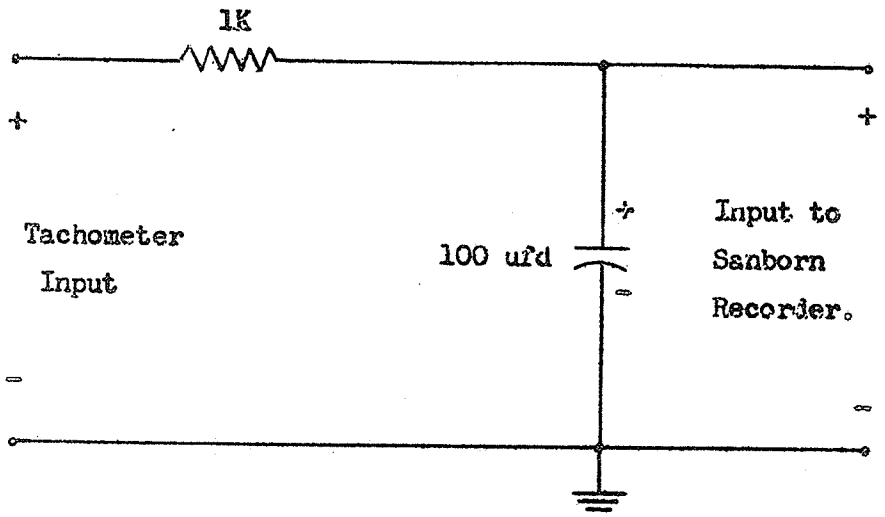

FIGURE C.2

TACHOMETER OUTPUT FILTER